Aus der Klinik für Strahlentherapie und Radioonkologie
der Medizinischen Fakultät Mannheim
(Kommissarischer Direktor: Dr. med. Michael Ehmann)

Second cancer risk after intensity-modulated and conventional radiotherapy in a small animal model

INAUGURALDISSERTATION

zur Erlangung des Doktorgrades

Doctor scientiarum humanarum (Dr. sc. hum.)

der

Medizinischen Fakultät Mannheim

der Ruprecht-Karls-Universität zu Heidelberg

vorgelegt von

Kaga Gomarteli

aus

Tiflis

2020

Dekan: Prof. Dr. med. Sergij Goerdt

Referent: Prof. Dr. med. Frederik Wenz

CONTENT

LIST OF TABLES

LIST OF FIGURES

GLOSSARY

RT	Radiation therapy (radiotherapy)
EBRT	External beam radiotherapy
LINAC	Linear accelerator
IR	Ionizing radiation
SC	Second cancer
SCR	Second cancer risk
HL	Hodgkin's Lymphoma
Gy	Gray (Joule · kg^{-1})
3D-CRT	Three-dimensional-conformal radiotherapy
CT	Computed tomography
IMRT	Intensity-modulated radiotherapy
PTV	Planning target volume
VMAT	Volumetric-modulated arc therapy
IGRT	Image-guided radiotherapy
CBCT	Cone-beam computed tomography
DRR	Dose-response relationship
ABS	Atomic bomb survivors
RR	Relative risk
TTT	Time to tumor
eV / keV / MeV	Electron Volts / kilo-eV (10^3 eV) / Mega-eV (10^6 eV)
LET	Linear energy transfer
DSBs	Double-strand breaks
HRR	Homologous recombination repair
NHEJ	Non-homologous end-joining repair
ATM	*Ataxia telangiectasia mutated*
Tp53	*Tumor protein 53*
P53	Protein 53
LFS	Li-Fraumeni syndrome
LOH	Loss of heterozygosity
AP/PA	Anterior-posterior/posterior-anterior
C273	Cysteine codon 273
XX/XY	Female/male
F1/2	Filial generation 1 and 2
L1 – L11	Litters 1 – 11
DVR	Dose to volume relationship
DVH	Dose to volume histogram
HDV	High dose volume
BHDV	Bordering high dose volume
LDV	Low dose volume
NIRV	Non-irradiated volume
FFPE	Formalin-fixed paraffin-embedded
H&E	Hematoxylin and eosin
gDNA	Genomic DNA
PCR	Polymerase chain reaction
bp	Base pair
Gapdh	*Glyceraldehyde-3-phosphate-dehydrogenase*
kb	Kilo-bases (10^3 bases)

1 INTRODUCTION

1.1 Second cancer risk after radiation therapy

Radiation therapy (radiotherapy, RT), an essential component of cancer treatment in more than half of all oncological cases, significantly improves patient survival [1-3]. The most frequently used treatment method in radiation oncology is external beam RT (EBRT), in which high-energy x-rays, emitted by a clinical linear accelerator (LINAC), specifically hit a target tumor volume. EBRT is indeed indispensable as a single treatment method, especially for tumors poorly treated by surgery or chemotherapy. Unfortunately, in some cancer survivors, ionizing radiation (IR) may promote the development of new, radiation-induced primary malignant neoplasms [4]. However, not all second-primary tumors, called second cancer (SC), are radiation-induced. Several non-iatrogenic reasons such as age at first cancer diagnosis, genetic susceptibilities to cancer development [5-8], population-specific traits as well as obesity [9] or consumption of alcohol [10,11] and tobacco [12,13] can trigger SC. Cancer chemotherapy may also promote SC development. For example, a four-fold increased second breast cancer risk have been reported in childhood cancer survivors treated with high-dose alkylating agent and anthracycline chemotherapy, compared with the general population [14]. Nevertheless, an increase in SC risk (SCR) in childhood cancer survivors has long been associated with RT used as a single treatment modality or in combination with chemotherapy against first cancer [15-19]. Thus, children with Hodgkin lymphoma (HL) receiving no RT have a substantially lower SCR than those treated with RT (5% vs. 25%) [20]. Therefore, minimizing the risk of radiation-associated SC is important, especially for young patients [21].

According to global cancer statistics, approximately 8% – 18% of all cancer survivors develop SC at all [22,23], which is the most common reason for the mortality of first cancer survivors, irrespective of gender [24]. An analysis of epidemiological studies on adult cancer patients estimates that only about 0.67% (3266 of 485481 persons) of all SC cases could be associated with radiation after 15 years follow-up of the first cancer treated with RT alone [25]. While the radiation-related SCR appears to be low in adult cancer survivors, it is expected to be higher in long-term survivors of childhood and early adolescence cancer treated with RT [26]. Thus, the risk for second and continuing new malignancies increases over time in childhood cancer survivors, especially for former patients with HL, a disease, which incidence rates peaks in children and adolescents [15,19,22,27-32]. For example, after 30 years of follow-up, the estimated

cumulative incidence of SC among European childhood cancer survivors treated with RT for leukemia, HL, and non-HL, was 2.43%, 12.7%, and 2.5% respectively [33].

Notably, the SCR after RT of HL patients is much higher in long-term survivors of childhood diseases than in adults [12,18,34,35]. Nevertheless, the advantages of RT in treatment of HL outweigh the possible disadvantages of IR. Thus, more than 90% of HL patients are cured successfully and their life expectancy increases since year 2000 due to improvements in oncology, and particularly in RT, which is often used as a single treatment approach for early stage I and II diseases [36-40].

Since the risk of developing radiation-associated cardiac and pulmonary abnormalities rises with increased minimum threshold doses, especially in pediatric HL patients [41], a limited field- and dose- RT for thoracic HL treatment recommended, as a reliable risk mitigating solution [42-46]. On the other hand, analysis of long-term complications after HL-therapy showed a doubled cumulative mortality due to SC compared to cardiac and other causes [47].

1.2 Radiation dose to volume relationships and SC development

Since the development of a radiation-induced SC depends on the distribution of the radiation dose within the body volumes planned for radiation (irradiated volume), it is associated with RT planning and RT delivery technology. Radiation dose describes a quantity of energy absorbed per unit of mass expressed by a dose-unit Gray (Gy, Joule · kg^{-1}) named in honor of the British physicist and founder of radiobiology, Louis Harold Gray. Thus, the dose distribution in RT means how much energy is ultimately absorbed from the irradiated volume. The precision of irradiation correlates with better clinical outcome and, therefore, is of great importance. Modern RT planning systems enable to perform highly personalized therapy plans for each patient individually. Personalized RT today considered as being the most sensible strategy for efficient treatment of cancer and protection of normal tissues from undesirable radiation dose toxicity.

The implementation of a three-dimensional- conformal RT (3D-CRT), after the adoption of computed tomography (CT) into daily RT practice in the 1990s [48], was a big step towards advanced RT. The 3D-CRT techniques shape the radiation beams to include the 3D anatomic configuration of the target tissue volume, for precise delivering of therapeutic doses, while sparing surrounded normal tissues from undesirable higher doses. During the following years, 3D-CRT has become increasingly important and continuously developed to a highly conformal RT-technique called intensity-modulated radiotherapy (IMRT). IMRT precisely concentrates

therapeutic doses to the planning target volume (PTV) and protects healthy (normal) tissues from high-dose-toxicity at the expense of increasing the volume receiving low- and moderate-radiation doses [49]. Its advanced rotational variant volumetric-modulated arc therapy (VMAT) covers the PTV with the highest doses in sub-millimeter accuracy while substantially reducing unwanted doses to a minimal level by expanding low-dose exposed volume [50-53]. Thus, IMRT and VMAT generate a so-called "low-dose bath" within the normal tissue while 3D-CRT burdens the normal tissue with substantial higher doses due to fewer beam directions.

A long-standing dogma in radiation oncology postulates that IMRT can increase (almost double) SCR compared to conventional 3D-CRT owing to more beam directions and enlarged healthy tissue volumes receiving low doses [54-58]. Therefore, 3D-CRT has established as a conventional technique for the treatment of mediastinal HL, especially for young patients. However, which of the two dose-distribution patterns, 'a little to a lot vs. a lot to a little' (IMRT vs. 3D-CRT), carries the greater risk of SCs remains undecided [46].

Besides the improvements in modern radiation planning systems, the volumetric accuracy in advanced RT has been additionally improved by the implementation of image-guided RT (IGRT) [59], such as e. g., in modern RT of prostate cancer [60-63]. The image-guidance is performed with a low-energy x-ray-based cone-beam CT (CBCT), delivering very low doses to the tissues during rotational scanning of the RT-planning body region before a patient receives a next RT fraction. The use of specific software matching a CBCT with an irradiation plan results in correct patient-couch-position for highly precise irradiation of the target and protection of normal tissues. Little is known whether CBCT can increase SCR. However, calculations based on the organ absorbed doses estimate an additional 3% to 3.5% increase in SCR when using 25 to 30 CBCT fractions to the chest [64], probably due to an underlying 3% to 5% increase in mutagenic risk [65]. It should be noted here that no preclinical study has yet shown the disadvantage of additional very lower doses compared to higher doses in terms of the increase in SCR.

1.3 Dose-response-relationships for radiation-induced cancer

The opinion that lower doses may increase the risk of SC compared to high doses, is explained by the assumption that irradiated cells may survive the low-grade DNA damage caused by low radiation doses, while being killed by high doses [66]. Based on this still acceptable assumption, established prediction models estimate increased SCR after low compared to high dose [67-74].

Because the tumor cells carry substantial genomic alterations and proliferate more rapidly than the normal cells, radiation kills tumor cells more efficiently. It is expected that only a part (about one-third) of exposed cells could be killed with approximately 2 Gy, which is the most common fraction dose in fractionated RT. In more details, this is a highly complex scenario of killing and repopulation events of huge cell cohorts along the tracks of radiation paths. The response of human cells to a fractionated radiation exposure is therefore determined based on the relationship between cell killing and cell repopulation events and is given by the ratio of α/β tissue-specific factors, according to the linear-quadratic model [74,75]. This model helps to determine the therapeutic window for fractionated total doses, as it is described in the manuals for radiotherapists [71,76]. Furthermore, the mechanistic model for predicting cancer induction after fractionated RT bases on the same linear-quadratic response model [77].

Reflecting the cell repopulation kinetics, the risk prediction models consider an increase in dose-response relationship (DRR) for radiation-induced SC after cumulatively received doses below 1 Gy, an exponential elevation at a dose range of 1 Gy to 2.5 Gy, and either an increase, reaching a plateau or even a decrease at doses above 2.5 Gy [73]. However, all of these models may contain significant uncertainties in predicting the dose-response relationship at very low doses and at very high doses (lower than 0.5 Gy and higher than 10 Gy) because no *in vivo* results exist. Thus, all known SCR models are based on the same and unique epidemiological lifespan data of Japanese atomic bomb survivors (ABS) from Hiroshima and Nagasaki [70,78,79]. However, it is to note that the uncontrolled whole-body exposure of ABS to radiation doses lower than 2.5 Gy is not fully comparable to a locally applied fractionated RT performed in cancer patients. The whole-body response to low doses of ABS differs additionally from the response to local RT doses because the organ-specific sensitivities to the radiation dose, determines the risk of radiation carcinogenesis [70]. The relative excess risk per Gy among ABS at age of 70 years was increased linearly with estimated received dose to the lungs and female breast while it was decreased for stomach and thyroid cancers or reached a plateau for rectal, pancreatic, colon, bladder, and brain tumors [21]. For the exposure to high-dose fractionated local RT, a linear increase in relative risk (RR) was associated with breast cancer and brain tumors, whereas a plateau estimated for colon, rectal and stomach cancers, and a decrease observed only for thyroid and pancreatic tumors [80]. Interestingly, evidence for decreased second lung cancer risk after lower compared to higher integral dose expositions was recognized in female patients treated with whole-breast RT [81].

Whereas there are some uncertainties in dose-response below 1 Gy in patients treated for their childhood cancer with RT alone, certain linearity in the increase of second bone and soft tissue

sarcoma incidences were registered after exposure to estimated integral doses of above 10 Gy [80,82,83]. Thus, the results calculated from 28 retrospective studies, including sixteen childhood cancer studies, a linear dose-response relationship observed for several SCs developed after HL treatment with RT. An exception was second thyroid cancer, showing an increased risk up to maximum received dose of about 20 Gy and then either a downturn or an enrichment to a plateau at higher doses. The combined risk for all SCs was 5 to 10 times higher for patients receiving doses of above 40 Gy, compared with those receiving very low or no radiation doses [80].

Most importantly, several retrospective clinical studies indicate secondary sarcomas and carcinomas mostly within the PTV or closely adjacent normal tissues exposed to the highest doses during RT [84,85]. All the dose-response facts mentioned above more likely indicate higher toxicity of high doses compared to low doses that contradicts the assumed disadvantages of low doses vs. high doses.

1.4 Dose to latency relationships for radiogenic tumor development

There is reported evidence for association of specific latency times with distinct entities of radiation-induced tumors among Japanese ABS who received survivable whole-body doses. According to the information of the radiation effects research foundation, the earliest most neoplastic disease detected after two to six years of exposure to atomic bomb radiation was leukemia. In contrast, an increased risk of solid tumors was not observed during the first decade after exposure. However, the increase in incidence rates of solid tumors was discovered in 1956 first, shortly after the tumor-registries were established in Japan. In a continuing retrospective life span study on ABS published in 2003, the relative lifetime-attributable risk of radiation-associated solid tumors appeared at least four times lower compared to second leukemia, but it was still more than five times increased compared to non-exposed populations [86].

The time from irradiation of a patient to the occurrence of a second malignancy can be considered as the latency time to tumor (TTT). There are differences observed between the times of occurrence of different SCs in patients who received chemotherapy, RT, or ‘chemoradiotherapy’ [87]. Thus, the prevalent development of second leukemia after chemotherapy alone and second solid cancers after RT alone or ‘chemoradiotherapy’ has been observed in childhood HL survivors. Therefore, the latency of second solid tumors can certainly be associated with expected tumor entities in former RT patients, as shown in the literature [12,28,34,35,38,88]. Accordingly, second lymphomas mostly arise during the first decades of HL

follow up, however, relatively earlier than lung carcinomas, to which the approximated TTT takes up to two decades. Most solid SCs of esophagus, connective tissue, stomach, thyroid, and female breast appear commonly after two to more than three decades of follow up, whereby the rate of solid tumors exceeds the rate of leukemia.
The relationship of RT doses to the latency of radiation-induced different tumors remains largely unexplored on an experimental level.

1.5 Characteristics and effects of ionizing radiation

Ionization means the process of the ejections of electrons from the atoms. There are two main types of IR, particle radiation (electrons, protons, α particles, and heavy ions) and electromagnetic (photon) radiation (x-rays and γ rays).
Medical x-rays are produced by the acceleration of electrons in an x-ray tube of a LINAC and their deceleration by the collision with the target of gold or tungsten resulting in photon streams called 'bremsstrahlung' – an original term of x-ray radiation, coined by its discoverer, the German engineer Wilhelm Conrad Röntgen in 1895.
During the generation of x-rays, a fraction of kinetic energy of accelerated fast electrons is converted into streams of highly energetic photon packets (quants) with a wavelength ranging from 0.01 to 10 nm. The energy of the x-rays is inversely proportional to the wavelength expressed by the equation $E_x = h \cdot c/\lambda$ (where h is Planck's constant ($6.62607015 \cdot 10^{-34}$ Joule · seconds), c is the velocity of light, and λ is the wavelength of radiation. This energy is commonly given in electron Volts (eV) so that the x-rays with the wavelength of 0.1 nm have the energy of about 124 kilo-electron Volts (keV, 10^3 eV) while 1 eV = $1.602176638 \cdot 10^{-19}$ Joule. X-rays belong thus a type of IR that can be controlled by choosing the most favorable acceleration energies for certain plans. While corpuscular radiation species typically can only penetrate about a centimeter deep into the mater, an increase in energy for the acceleration of the electrons proportionally increases the depth of maximum doses within the living mater. The higher this energy, the deeper the highest dose in the substrate (dose depth). The ability to control the dose depth prerequisites the basis for the conformality of photon beam RT. For example, x-rays with six Mega-electron Volt (MeV, 10^6 eV) acceleration energy have an approximated maximum dose-depth of about 1.5 cm in water or in the human or animal body.
A descriptive specification of the penetrating nature of radiation energy is referred to as radiation quality – ionization density. A measure of the average energy rate directly transmitted along the track of photons or particles per unit distance is defined as linear energy transfer

(LET, expressed as keV/µm). The sparsely ionizing x-rays (≈ 0.3 keV/µm), as well as γ-rays and electrons, are characterized by a low LET in contrast to densely ionizing high-LET-radiation types such as e. g. α particles (≈ 100 keV/µm). Therefore, high LET radiation species are biologically more effective than low LET radiation. While particles ionize the molecules directly, x-rays and γ-rays damage the living matter indirectly, via radiolysis of water and generation of H_2O^+ interacting with the neighboring water molecule and generating H_3O^+ and free reactive hydroxyl radicals [OH·]. Approximately two thirds of the tissue damages irradiated with x-rays are caused by indirect actions of photons with water. There are two well-studied ionization mechanisms of x-rays known. While the photoelectric effect appears to be relevant for radiological low-energy x-rays, the Compton effect, that is the elastic collision of a photon with an electron, dominates in RT. This accelerated electron leaves its path and ionizes the neighboring atom. Thus, Compton's effect multiplies the damage of the atoms along the tracks of high energetic photons.

The time scale of radiation effects on the living system comprises three main phases: the physical phase of ionization lasting up to approximately 10^{-18} seconds, followed by a chemical phase of the breakage of chemical bonds (10^{-3} seconds), and a subsequent biological phase from DNA repair to the early and late adverse effects lasting from few seconds to many years and sometimes even lifelong [71,76].

The relative biological effectiveness, which is determined experimentally, bases on the effects of different types of radiation on the survival rates of different organisms, differs between electromagnetic and corpuscular radiation species owing to their specific LET. The international atomic energy agency for radiation protection differentiates between deterministic (not accidental) and stochastic (random) radiation effects. The deterministic radiation damage has a threshold dose below which no damage can expected. After exceeding this threshold, the damage increases strongly with increased dose. By contrast, no threshold dose assumed for stochastic damage. The most critical adverse effect is radiation carcinogenesis, which is dependent on absorbed radiation doses. Thus, radiation protection considered two main dose concepts. The organ equivalent dose (organ dose) is defined as an absorbed cumulative dose in an organ, multiplied by the specific radiation weighting factors that determine the effectiveness of one type of radiation in comparison with reference effects of x-rays and γ-rays (assumed as 1). The high LET radiation types having a weighting factor of 2 for protons or 20 for the α-particles and heavy ions. In addition to the equivalent dose, which already involves the weighting factors of the different types of radiation, the effective dose also takes into account the different sensitivity of the organs and it is calculated by a multiplying the organ equivalent

doses with the organ-weighting factors. The international commission on radiological protection – ICRP, recommends factor 0.4 for bladder, esophagus, liver and thyroid gland, 0.01 for the skin, bone surface, brain and salivary glands, and 0.12 for the bone marrow, lungs, female breast, stomach, colon and all other organs and tissues that together make 1.0 [89].

Taken together, biological effects of radiation depend on radiation quality, LET, the different sensitivity of irradiated organs to doses, temporal dose rate, homogeneity of received doses, and so on, but also on factors associated with the individual person.

1.6 Somatic context of radiation carcinogenesis

Radiation biology provides an understanding of biological mechanisms of the early responses of neoplastic and normal tissues such as DNA damage, tumor cell killing and repopulation, hypoxia, re-oxygenation but also long-term effects including non-neoplastic adverse alterations of normal tissues as well as the development of SCs.

The highly reactive free radicals damage biomolecules, including DNA, by the uptake of missed electrons from affected molecules. DNA is the most important target for radiation-induced damage in exposed cells. A radiation dose of about 1 Gy may cause approximately 10000 ionizations per cell, and consequently about 1000 DNA single-strand breaks and 20 – 40 DNA double-strand breaks (DSBs).

Radiation is also able to induce large deletions and multiple rearrangements within the genome, such as several DNA-DNA or DNA-protein cross-links.

DNA-damage is followed by a biochemical phase of the repair taking approximately 0.5 to 1.5 hours in most human cells.

In response to radiation-induced DNA damage, animal cells activate various specific cellular mechanisms for the cell cycle-arrest and DNA repair processes. DSBs are the most difficult damage for irradiated cells that must be repaired by two alternative mechanisms: a homologous recombination repair (HRR) either or a non-homologous end-joining (NHEJ) repair. HRR is only available if a homologous allele (sister chromatid) is intact for the use as a template for the error-free repair. However, due to the high complexity of radiation-induced chromosome aberrations, which increases with increasing radiation doses, mammalian cells preferably use the NHEJ repair mechanism which is unable for an error-free repair of processing ends of the broken DNA strand.

Recent radiobiological findings show that in response to radiation-induced DNA damage, an exposed cell, either repairs the radiation-damaged DNA, undergoes apoptosis, or retains a

mutation and passes it on to progeny. It is believed that radiation-associated cancer is induced due to unrepaired or residual DNA-damage in a single exposed cell that proliferates to the clonal cell populations. However, several further mutations are required in the cell, to form rapidly proliferating aggressive tumor cell populations with persistently increasing genomic instability based on the step by step accumulated alterations or completely lost mechanisms such as e.g. molecular controlling of cell cycle checkpoints [71,76].

Mutations occur also spontaneously over time, but radiation may specifically increase the likelihood of DNA alterations. However, only specific driver mutations, some of that described below, may promote the carcinogenesis, while the silence passenger mutations may not. The driver mutations in different genes may predispose humans to the development of tumors, including radiation-induced SC. For example, the risk of SC increases with increasing RT doses to patients with inactivated tumor suppressor genes *Breast Cancer 1* and *2* (*BRCA1/2*) [6,90,91]. SCR also increases in breast cancer patients with mutated *Ataxia Telangiectasia Mutated* (*ATM*) gene [5], acting as a key sensor and signal transducer for DNA-DSB repair [92]. Downstream of the serine/threonine kinase activity in *ATM*, a key signal transducer to cell cycle arrest for DNA repair is mediated by a transcription factor for several effector genes, the major tumor-suppressor gene *Tumor Protein 53* (*TP53*) encoding tumor suppressor protein 53 (p53) [93]. Loss of p53 in tumor cells is a prerequisite for the onset and progression of malignity because of loss of cell-cycle regulation and initiation of programed cell death (apoptosis) [94]. Hereditary heterozygous mutation in one allele of the human *TP53* gene causes Li-Fraumeni syndrome (LFS), which dramatically increases the risk for spontaneous [95,96] and radiation-induced [97,98] tumor development.

Most notably, radiation may promote genome-wide alterations in aggressive second bone sarcomas and soft tissue sarcomas in pediatric RT patients [99]. The loss of second intact *Tp53* allele in heterozygous mutants, loss of heterozygosity (LOH), have been equally observed in many tumor types in humans [98-105], and also in experimental small animals [106-110]. Whether the aggressiveness of the radiation-induced SC could be specifically shaped by radiation-induced *Tp53*-LOH remained clarified insufficiently.

1.7 Research question and experimental system

As mentioned previously, there is an experimentally unproven assumption that IMRT will increase SCR compared to conventional 3D-CRT in the body volume exposed to low and moderate doses, especially in childhood and adolescent cancer survivors. Therefore, radiation

physicians are currently advised against IMRT applications for young HL patients who are irradiated with the less dose-sparing 3D techniques such as e.g. two opposite anterior-posterior/posterior-anterior (AP/PA) beam irradiation. However, under consideration of above-mentioned retrospective data about the relationships of high-doses to SC development, the predicted doubling of SCR from low-dose exposure during IMRT may not hold true in clinical practice. Moreover, the theory of disadvantages of IMRT owing to enlarged low-dose volume compared to 3D-CRT appears less plausible because it was never been confirmed or refuted by *in vivo* experiments.

A cancer-prone *Tp53* functional knockout line of Wistar-rats, established by a target selected mutagenesis driven nonsense mutation in the cysteine codon 273 (C273) of the *Tp53* gene [108,110-112], in which the *Tp53*-mediated tumor-suppression is impaired, seemed to be a suitable experimental model for radiation-induced cancer research. In this heterozygous ($Tp53^{+/C273X}$) rat model, the gene defect is not the trigger but an 'enhancer' of tumor development, similar to the mutation of *TP53* in patients with LFS.

1.8 Purpose

The main purpose of the study was to compare radiation-associated tumor induction after mediastinal irradiation with VMAT (rotational IMRT) and AP/PA irradiation in cancer-prone $Tp53^{+/C273X}$ rats, simulating mediastinal RT in HL patients. Thus, the study aimed to provide a biological rationale to the clinical practice about the justification of withholding IMRT from young patients. The main uncertainty – 'a little to a lot or a lot to a little' – had to be investigated by testing the possible disadvantages of IMRT compared to conventional 3D CRT in rats.

In order to meet the challenge, the following objectives were pursued:

- development of a suitable study design and establish the heterozygous $Tp53^{+/C273X}$ rat model to demonstrate the development of radiation-induced cancer,
- comparison of the rates of tumors in rats irradiated with different radiation doses and techniques and between the body-volumes exposed to different doses,
- further analyzes of the life span in differently exposed animal groups and the measurements of the TTT from the time point of irradiation, and
- Determination of the properties of tumors on a pathological and molecular level.

Thus, this is the first experimental preclinical study of its kind to test the hypothesis of the increased carcinogenicity of modern IMRT compared to older 3D-CRT techniques in living animals.

2 MATERIALS AND METHODS

2.1 MATERIALS

2.1.1 Animal husbandry and handling

Rat standard 1500 cm^2 cage	Tecniplast, Hohenpeissenberg, DE
Rat 1500 cm^2 IVC cage	Tecniplast, Hohenpeissenberg, DE
SUMC 501 cm^2 filter hood IVC	Tecniplast, Hohenpeissenberg, DE
SSNIFF grain-based regular diet	SSNIFF Spezialdiäten, Soest, DE
Rollenpflaster FL TRA 10 m × 2.5 cm	Gothaplast, Gotha, DE
RS-Müllkompressen 5×5 cm, 7.5×7.5 cm	TZMO Deutschland, Biesenthal, DE
F.S.T. Finger Loop Ear Punch (1 mm)	Fine Science Tools, Heidelberg, DE
Small animal isoflurane vaporizer	AbbVie Deutschland, Wiesbaden, DE
Polycarbonate narcosis box with sliding lid	Orthopedics laboratory UMM, Mannheim, DE
Injekt disposable syringes 2 ml, 5 ml	B. Braun, Melsungen, DE
Tuberculin syringes with 0.01 ml graduation	Dieckhoff & Ratschow, Longuich, DE
Neoject cannulas: 22G, 18G, 20G, 25G	Dispomed Witt, Gelnhausen, DE
CLiP neo safety catheter, 26G (0.6×19 mm)	Vygon - Vigmed, Aachen, DE
Combi stopper PE closing cones	B. Braun, Melsungen, DE
Luer-lock connector/adaptor, m/m, f/m	Shop.lowcostexperiments.de
PORTEX® PE hose tubes (0.58/0.96 mm)	A. Hartenstein, Würzburg, DE

2.1.2 Radiation delivery and CT

LINAC Versa HD/Agility MLC	Elekta AB, Stockholm, SWE
Philips Brilliance Big Bore	Philips GmbH Market DACH, Hamburg, DE

SOMATOM force	Siemens Healthcare Diagnostics, Eschborn, DE
Micro-CT Y.FOX	YXLON GmbH, Hamburg, DE

2.1.3 Pharmaceuticals and chemicals

Bepanthen® Augen- und Nasensalbe	GP Produktions, Grenzach-Wyhlen, DE
Isotonic saline solution 0.9% 500 ml	B. Braun, Melsungen, DE
Midazolam-ratiopharm® 15 mg/3 ml	Ratiopharm, Ulm, DE
Domitor® (medetomidin 1 mg/ml)	Orion Corporation, Espoo, FIN
Fentanyl-Janssen® 0.1 mg	Janssen-Cilag, Neuss, DE
Naloxon-Actavis® (naloxon 0.4 mg/ml)	Actavis, München-Riem, DE
Anexate® (flumazenil 0.5 mg/5 ml)	Roche Pharma, Grenzach-Wyhlen, DE
Antisedan® (atipamezol 5 mg/ml)	Orion Corporation, Espoo, FIN
FORENE® (isoflurane 100% V/V)	AbbVie Deutschland, Wiesbaden, DE
Imeron®-300	Bracco Imaging, Konstanz, DE

2.1.4 Histology

Devices:

LEICA HistoCore Arcadia H	Leica Biosystems, Nussloch, DE
LEICA RM2245 Microtome	Leica Biosystems, Nussloch, DE
LEICA EG 1150 C	Leica Biosystems, Nussloch, DE
LEICA HI1210	Leica Biosystems, Nussloch, DE
LEICA Autostainer XL	Leica Biosystems, Nussloch, DE
LEICA CM3050 S – Cryostat	Leica Biosystems, Nussloch, DE
Prutscher S/TA/120/1297	Prutscher Laboratory Systems, Neudörfl, DE

HERAsafe® KSP12	Thermo Elictron LED, Langenselbold, DE
Panasonic MDF-DU700VH Freezer	PHC Europe, Etten-Leur, NL
Heraeus® drying cupboard	Thermo Scientific Heraeus, Dreieich, DE
LEICA DMBRE upright light microscope	Leica Mikrosysteme, Wetzlar, DE
Leica DFC 450	Leica Mikrosysteme, Wetzlar, DE

Supplies:

MaiMed absorbent pads	MaiMed, Neuenkirchen, DE
30×30 cm Rotilabo®-Presskork-Untersetzer	Karl Roth, Karlsruhe, DE
ROTIPURAN® 37% formaldehyde solution	Carl Roth, Karlsruhe, DE
Dulbecco's phosphate buffered saline (PBS)	Merck KGaA, Darmstadt, DE
NeoLab Embadding cassettes	NeoLab Migge, Heidelberg, DE
Tissue-Tek® O.C.T.™ Compound	Sakura Finetek, Alphen, NL
Decalcifier soft	Carl Roth, Karlsruhe, DE
Roti®-Histokitt mounting medium	Carl Roth, Karlsruhe, DE
Microscope object slides, 76×26×1 mm	Fisher Scientific, Schwerte, DE
Microscope Cover Glasses 15H 24×50 mm	Fisher Scientific, Schwerte, DE
FEATHER carbon steel blades C35	Feather safety Razor, Osaka, JPN
FEATHER stainless steel blades R35	Feather safety Razor, Osaka, JPN
Sample beakers, with screw cap 100 ml	Carl Roth, Karlsruhe, DE
Fine brushes (#1 and #3)	Science Services, München, DE
Surgical disposable scalpels	B. Braun, Melsungen, DE
Fine scissor - sharp/blunt, 22×900 mm	Fine Science Tools, Heidelberg, DE
Strabismus scissors, 23×115 mm	Fine Science Tools, Heidelberg, DE
Scissors straight, sharp/blunt,14.5 cm	Medicon, Tuttlingen, DE
Tissue forceps - 1×2 teeth, 2×1.5×145 mm	Fine Science Tools, Heidelberg, DE

Dumont #5 forceps, 0.1×0.06×110 mm	Fine Science Tools, Heidelberg, DE
Standard pattern forceps 2.8×1.4×130 mm	Fine Science Tools, Heidelberg, DE
Cover Glass forceps, 4×0.6×105 mm	Fine Science Tools, Heidelberg, DE

2.1.5 Molecular biology

Equipment:

Reference PhysioCare concept pipets	Eppendorf, Hamburg, DE
Agarose gel electrophoresis chamber	Biozym, Landgraaf, NL
Owl™ EC-105 compact power supply	Thermo Fisher Scientific, Langenselbold, DE
INTAS Gel iX20 imager	Intas Science Imaging, Gottingen, DE
Microbalance scale BP301 S	Sartorius, Göttingen, DE
Accuracy scale LP 620 S	Sartorius, Göttingen, DE
Eppendorf® Bio photometer	Eppendorf, Hamburg, DE
Eppendorf® Thermomixer Compact	Eppendorf, Hamburg, DE
Heraeus Biofuge Pico	Heraeus Deutschland, Hanau, DE
Heraeus MEGAFUGE 8 centrifuge	Thermo Fisher Scientific, Langenselbold, DE
Eppendorf centrifuge 5810 R	Eppendorf, Hamburg, DE
Ice maker machine	Manitowoc Deutschland, Herborn, DE

Supplies:

KAPA Express Extract Kit	Merck, Darmstadt, DE
mi-PCR50 Purification Kit	Metabion, Planegg/Steinkirchen, DE
Rapid PCR Cleanup Enzyme Set	New England BioLabs, Frankfurt, DE
KAPA2G™ Fast PCR Kit	VWR International, Darmstadt, DE

GoTag®Long PCR Master Mix	Promega Deutschland, Mannheim, DE
GoTaq® colorless PCR Master Mix	Promega Deutschland, Mannheim, DE
2-Log DNA Ladder	New England BioLabs, Frankfurt, DE
Agarose Roti®garose Low Melt	Carl Roth, Karlsruhe, DE
Loading Dye 6× Purple	New England BioLabs, Frankfurt, DE
Gel Red	INTAS, Göttingen, DE
TRIS ≥ 99.9 %;121,14 g/mol	Carl Roth, Karlsruhe, DE
Acetic acid ≥ 95.9 %; 60,05 g/mol	Carl Roth, Karlsruhe, DE
EDTA ≥ 99 %; 292.25 g/mol	Carl Roth, Karlsruhe, DE
LightRun® Barcodes	Eurofins GATC Biotech, Konstanz, DE

Primer

Description	**5´- 3´ direction**
Rat-Tp53-for1	GCTGAGTATCTGGACGACAGG
Rat-Tp53-for2	GTACCGTATGAGCCACCTGAG
Rat-Tp53-for3	CGGCCCATCCTTACCATCATC
Rat-Tp53-rev2	AGAAACCACAGCCTCAGAGC
Rat-Tp53-rev3	TGCGCTCTGACGATAATGTCATAG
Rat-Tp53-rev4	GAGAGGAGCTTGTGCTGGTG
Rat-Chr10-for	CTTCGGTCTCTTCTCTGACT
Rat-Chr10-rev	CAACTGACCGGATAGGATTT
Rat-Gapdh-for	GGTGAAGGTCGGTGTGAACGG
Rat-Gapdh-rev	CCACTTCCAGCCACACTTGCC

***Tp53/TP53* reference sequences:**

*R. norvegicus*_strain mixed ch.10, Rnor_6.0_NC_005109.4_8531-9606_bp

R. norvegicus strain BN chromosome 10 CRA_213000034379661

*R. norvegicus*_p53_X2, mRNA_XM_006246595.2

H. sapiens Tumor Protein 53 (TP53), Ref. Seq. Gene (LRG_321) on chromosome 17, NG_017013.2. NCBI GenBank

2.1.6 Software

Intas capture software	INTAS Science Imaging, Göttingen, DE
A plasmid Editor (ApE); v2.0.49	University of Utah, Salt Lake City, UT, USA
GraphPad Prism 6.0	GraphPad Software, San Diego, CA, USA
Monaco® version 5.0	ELEKTA AB, Stockholm, SWE
MOSAIQ®	ELEKTA AB, Stockholm, SWE
Syngo.via	Siemens Healthcare, Erlangen, DE
RadiAnt DICOM viewer	Medixant, Poznan, POL
Microsoft Office®	Microsoft, Redmond, WA, USA

2.1.7 Data repository

WD Server (4 TB) #WCC4E2NJO3Y6	WD® NL B. V. Hoofddorp, NL

2.2 METHODS

2.2.1 Cancer-prone rat model and experimental design

The experiment was carried out after approval by the regional ethics board (Regierungspräsidium Karlsruhe) and following the legal guidelines of the federation of european laboratory animal science associations – FELASA.

Heterozygous *Tp53*$^{+/C273X}$ rats (Crl:WI(UL)-Tp53$^{m1/Hubr}$) were kindly provided by colleagues from Hubrecht institute for developmental biology and stem cell research, department of biomedical genetics, Utrecht, the Netherlands.

The main 'roadmap' of the experiment is shown schematically in **Figure M1**.

Figure M1

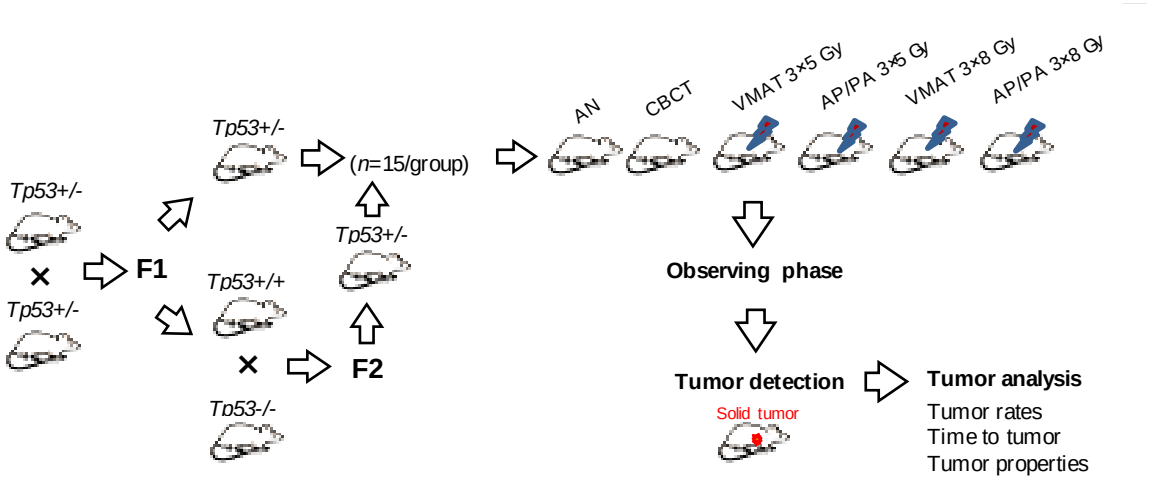

Schematic overview of work-steps. Heterozygous rats (*n* = 90), derived from both heterozygous or heterozygous and homozygous parents (F1 and F2 respectively) were distributed into the two control groups (AN or CBCT only) and four groups for irradiation with different radiation techniques (VMAT or AP/PA) and doses (3×5 Gy or 3×8 Gy). Animals were followed up and sacrificed when a solid tumor was detectable. The material and data obtained were used to compare tumor rates, latency time to tumors, and tumor properties of irradiated and non-irradiated groups of rats and between body volumes exposed to different doses.

Abbreviations: *Tp53*$^{+/-}$, heterozygous for tumor protein 53 gene; F1/2, filial generation 1 and 2; AN, anesthesia only control group; CBCT, cone-beam computed tomography controls; VMAT, volumetric-modulated arc therapy; AP/PA, anterior-posterior/posterior-anterior; CT, computed tomography; Gy, Gray; 3×5 Gy or 3×8 Gy, three fractions of 5 or 8 Gy; TTT, time to tumor.

Two control groups were formed: one for the treatment with anesthesia only (AN group) and another for additional positioning scanning with CBCT (CBCT group). Rats belonging to further four radiation treatment groups were aimed to receive, additionally to anesthesia and CBCT, either 15 Gy or 24 Gy total doses divided into three equal fractions and delivered every other day with VMAT or AP/PA irradiation techniques: 3×5 Gy VMAT, 3×5 Gy AP/PA, 3×8 Gy VMAT, 3×8 Gy AP/PA. Each group consisted of $n = 15$ rats.

Animals were followed up until they showed tumor-associated symptoms and a tumor was detectable. Rats were euthanized for the further standardized autopsy to prepare tumors and normal tissue samples for subsequent pathological and molecular characterizations.

2.2.2 Animal housing

Rats were housed in conventional rat cages, (rat standard 1500 cm^2 cage, Tecniplast, Hohenpeissenberg, Germany) in the animal facility of the medical research center of the medical faculty Mannheim of Heidelberg University, under controlled conditions (12-hour light/dark cycle, room temperature 22 ± 2°C, 45% ± 5% relative humidity).

Animals were supplied by a grain-based regular diet (SSNIFF Spezialdiäten) and water (*ad libitum*).

The results of the quarterly hygienic screenings were always negative for any new pathogens for the entire breeding and living period of animals. This was made to excludes possible influences of infections on the standardization of the experimental model and thus on the experimental results.

2.2.3 Animal breeding

The accurately performed genotyping-guided breeding method, daily monitoring, and controlled environmental conditions provide an optimal basis for lifespan experiments with p53-insufficient rats.

Local breeding was carried out to produce experimental $Tp53^{+/C273X}$ rats. Breeding animals were placed into the individually ventilated cages (Rat 1500 cm^2 IVC cage) under controlled conditions: temperature 22 ± 2°C, humidity 45% ± 5%, ventilation 10 – 15 air changes per hour, and a lighting cycle of 12 hours light/dark. The offspring (aged 4 weeks) were separated from the mother before the weaned animals received their identities (**Table A1**). From this time on

rats were housed in sex-separated groups of maximal four animals per standard 1500 cm^2 rat cage.

Due to an expected accumulation of spontaneous mutations in *Tp53* knockout rats, the mating age was kept as low as possible: median 110 days for females (XX) and 89 days for males (XY), with a 75% confidence interval of [86 – 160] and [76.8 – 160] for XX and XY respectively.

Heterozygous n = 37 rats of filial generation 1 (F1) belonging to litters 1 – 3 (L1 – L3) were derived from 2 male and 3 female parents with the same heterozygous $Tp53^{+/C273X}$ genotype. The F2 rats (n = 53) of L4 – L11 were provided from homozygous ($Tp53^{C273X/C273X}$) males (n = 8) and wild type ($Tp53^{C273/C273}$) females (n = 7) of F1 generation. Taken together, only five ancestral knockout allele variants are drifted among all experimental animals of F1 and F2 generations (**Table M1**, **Table A1** and **Table A2**).

The outbreeding trend was maintained.

Table M1

Recruitment of rats to experimental groups. $Tp53^{+/C273X}$ rat litters (L1-L11) of the F1 and F2 generations were randomized in order to balance the ancestral background. The numbers indicate the rats.

Rats per litter and group	F1			F2								Total
	L1	L2	L3	L4	L5	L6	L7	L8	L9	L10	L11	
AN	4	-	5	2	0	0	0	0	4	0	0	15
CBCT	5	1	4	3	0	0	2	0	0	0	0	15
VMAT 3×5 Gy	6	-	3	1	0	0	4	0	1	0	0	15
AP/PA 3×5 Gy	5	1	3	4	0	0	1	0	1	0	0	15
VMAT 3×8 Gy	0	0	0	0	1	4	0	3	0	4	3	15
AP/PA 3×8 Gy	0	0	0	0	1	5	0	2	0	2	5	15
Total	20	2	15	10	2	9	7	5	6	6	8	90

Abbreviations: F1 and F2, filial generation 1 and 2; L1 – L11, litters L1 – L11; AN, anesthesia only group; CBCT, cone-beam CT only; VMAT, volumetric-modulated arc therapy; AP/PA, anterior-posterior/posterior-anterior irradiation; Gy, Gray; 3×5 Gy or 3×8 Gy, three fractions of 5 or 8 Gy.

The weight of animals at the treatment was well-balanced by the gender-balanced distribution of rats among treatment groups, however, with some insignificant variability, as shown in **Table M2**.

Table M2

Weight and age of female and male rats at treatment. The median values (with minimum to maximum intervals) of the weight of female and male rats per group are arranged separately and those of the age are combined.

Parameters per group and sex	**Weight (gram)**		**Age (days)**
	XX	**XY**	**XX/XY combined**
	median [min. – max.]	**median [min. – max.]**	**median [min. – max.]**
AN	162.5 [150 – 190], *n* = 6	205.0 [175 – 305], *n* = 7	82.0 [63 – 108], *n* = 13
CBCT	182.5 [155 – 200], *n* = 8	272.5 [175 – 295], *n* = 6	69.0 [64 – 96], *n* = 14
VMAT 3×5 Gy	180.0 [170 – 185], *n* = 7	242.5 [225 – 280], *n* = 8	68.0 [58 – 85], *n* = 15
AP/PA 3×5 Gy	185.0 [155 – 225], *n* = 9	250.0 [225 – 285], *n* = 5	68.0 [58 – 85], *n* = 14
VMAT 3×8 Gy	215.0 [185 – 225], *n* = 7	287.5 [220 – 335], *n* = 6	106.0 [81 – 124], *n* = 13
AP/PA 3×8 Gy	205.0 [180 – 215], *n* = 7	285.0 [215 – 330], *n* = 8	106.0 [81 – 116], *n* = 15

Abbreviations: XX, female; XY, male; *n*, number; AN, anesthesia only; CBCT, cone-beam CT only; VMAT, volumetric-modulated arc therapy; AP/PA, anterior-posterior/posterior-anterior irradiation; Gy, Gray; 3×5 Gy or 3×8 Gy, three fractions of 5 or 8 Gy.

The median age (gender-mixed) was 37.5 days higher for the 3×8 Gy irradiated groups compared to all other groups (106 [81 – 124] vs. 68.5 [58 – 108] days, respectively). The possible impact of the age variability on treatment outcomes is discussed below in section 4.6. Taken together, these preparations helped to standardize the experimental model for comparison of experimentally obtained data between groups containing subjects with relatively similar risk factors.

2.2.4 Identification of animals

For identification of animals an ear marking method was used. The incidental tissue sample was used for subsequent genotyping. Therefore, an animal was placed in a polycarbonate narcosis box (made by the orthopedics laboratory of the university medical center Mannheim) saturated with isoflurane using a small animal vaporizer device. Prior to the ear punching rats received short (< 1 minute) inhalation anesthesia (isoflurane, FORENE® 100% V/V). An ear punch tool (Fine Science Tools) was used for earmarking making samples with a diameter of 2 mm. The earmarking scheme, according to Ackert-Bicknell [113], is shown below in **Figure M2**.

Figure M2

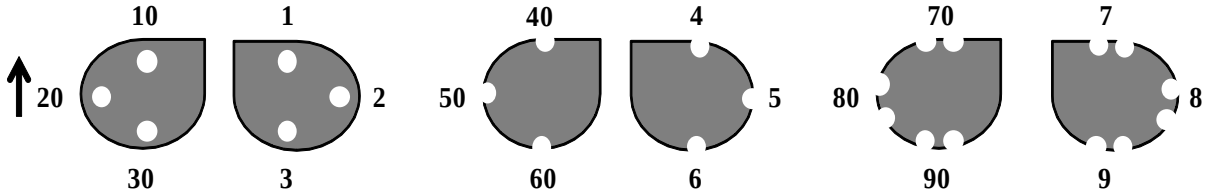

Earmarking. A combination of the ear punches represents the identity. The arrow directed from the caudal to the cranial direction (dorsal view).

2.2.5 Preparation of animals for CT and RT

Prior to irradiation and CT scanning, rats underwent continuous narcosis to sleep over the whole procedure duration, which was in the range of about 1 hour for a foursome group of animals. For this purpose, the initial sedation was made by a short inhalation of FORENE®, as mentioned in section 2.2.4. Subsequently, rats received a subcutaneous injection of an anesthesia mixture of 0.15 mg medetomidine (Domitor®), 2.0 mg midazolam (Midazolam-ratiopharm® 15 mg/3 ml) and 0.005 mg fentanyl (Fentanyl-Janssen® 0.1 mg) per kg body mass.

For transportation of an anesthetized rat, a single use individually ventilated transport cage (SUMC, 501 cm^2) was used, which is equipped with a microfiber filter hood protecting animals from pathogens (**Figure M3**).

Figure M3

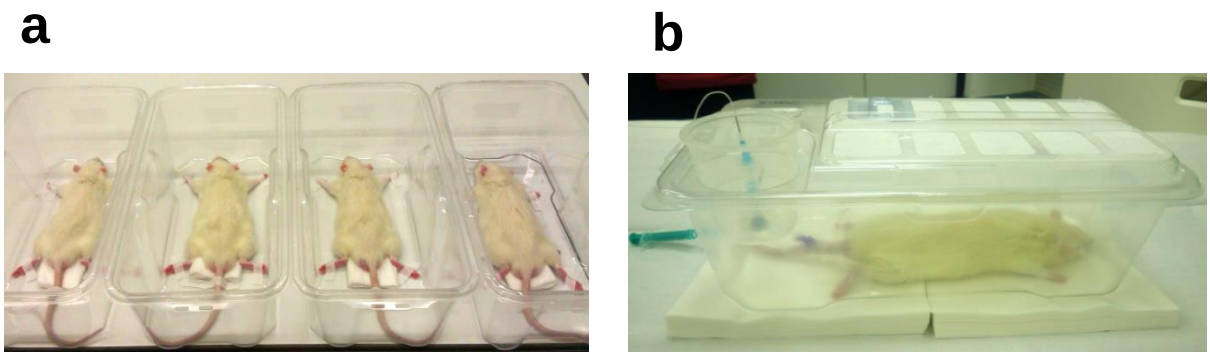

Preparation of rats for irradiation and CT. (**a**) Shown is a foursome group of narcotized male rats fixed in disposable cage for transportation. (**b**) An anesthetized female rat with an inserted tail vein catheter for the infusion.

Narcotized rats were placed in the cages and secured to the bottom of the cage by tapping the extremities and tails using tape (Rollenpflaster).

To absorb anesthesia-related urinary urgency, 3 – 4 compresses (RS-Mullkompressen 7.5×7.5 cm) were put underneath the animals.

An eye ointment (Bepanthen® Augen- und Nasensalbe) was applied to rats to prevent the cornea from drying out during the narcosis.

For rehydration, narcotized animals received subcutaneous depot-injection of 2 ml 0.9% isotonic saline solution per 250 g of their body mass using 22G Neoject cannulas and 2 ml or 5 ml single use syringes (Injekt Disposable Syringes).

The cages with narcotized and fixed rats were closed with filter hoods remaining over the whole transport and radiation procedure period, for the pathogen-safety.

After experimental procedures were finished, to antagonize the residual anesthetics, sleeping rats received a subcutaneous injection of 0.3 mg naloxon (Naloxon Actavis® 0.4 mg/ml), 0.5 mg flumazenil (Anexate® 0.5 mg/5ml), and 2.5 mg atipamezole (Antisedan® 5 mg/ml).
Shortly prior to CT examination, a contrast agent was injected intravenously using a self-constructed catheter system consisting of a 26 g CLiP® neo safety intravenous catheter (Vygon - Vigmed), which was connected to a flexible polyethylene tube (PORTEX® PE with 0.58/0.96 mm inner/outer diameter) with luer-lock connectors, and was terminated by a closing cone (Combi stopper PE closing cone). The catheter was inserted into a tail vein of an animal (**Figure M2b**). The catheter was charged with isotonic saline solution to avoid the impermeability of the tubes during the transportation. The contrast media applied via the catheter using tuberculin syringes.

2.2.6 Radiation planning and dose delivery

Two template CTs for radiation planning were taken from 250 g male (large) and 170 g female (small) rats using a routine clinical planning CT device (Philips Brilliance Big Bore,120 kV). For the contouring of the body structures for irradiation planning a Monaco® (version 5.0) treatment planning system from ELEKTA was used.
The whole-body (‘patient’) volume of the rat and organ-structures at radiation risk were contoured separately on each of two planning CTs (small and large): head, brain, heart, diaphragm, thymus, sternum, neck, spine, liver, stomach, colon and bladder as well as the right and left lungs, chest walls, axilla, forelimbs, dorsal muscles and kidneys. Representative dose to volume relationships (DVR) for these structures at risk of 3×5 Gy delivered with small or large VMAT and AP/PA plans are given in **Table A4**.
A cylindrical 296 mm^3 PTV with an approximated radius of 0.5 mm and a high of 10 mm within the mediastinum of the rat, was similarly defined on both planning CTs.
Based on these two planning CT datasets, the plans for the dose delivering techniques (360° arc VMAT and two opposing AP/PA beams) were constructed separately for each body masses (plan size).
Recruitment of n = 30 female and n = 27 male rats to each treatment plan size (small, ≤ 215 g or large, ≥ 220 g), the total doses (3×5 Gy or 3×8 Gy), and irradiation techniques (VMAT or AP/PA) is given in **Table M3**.

Table M3

Recruitment of female and male rats to particular radiation plan size. Given are applied irradiation plans (large or small), dose delivering technique (VMAT or AP/PA), and prescribed doses (3×5 Gy or 3×8 Gy). The numbers indicate rats without dropout animals.

Plan size for XX and XY rats per treatment group	**XX**		**XY**
	large plan	**small plan**	**large plan**
VMAT 3×5 Gy	0	7	8
AP/PA 3×5 Gy	1	8	5
VMAT 3×8 Gy	3	4	6
AP/PA 3×8 Gy	0	7	8
Total	4	26	27

Abbreviations: XX, female; XY, male; VMAT, volumetric-modulated arc therapy; AP/PA, anterior-posterior/ posterior-anterior irradiation; Gy, Gray; 3×5 Gy or 3×8 Gy, three fractions of 5 or 8 Gy.

The fraction dose to the PTV was defined as 5 Gy for 3×5 Gy and 8 Gy for 3×8 Gy irradiation. The beam on time of the delivery of 5 Gy to the PTV was approximately 45 seconds for full arc VMAT and 30 seconds for AP/PA. These were expanded to 60 seconds and 45 seconds for the delivery of 8 Gy respectively VMAT and AP/PA. Thus, the estimated dose rate (Gy/minute) for VMAT was higher than for AP/PA. The dose rates were not affected by the different treatment plan sizes (small or large).

Representative images of contoured organs (structures) at radiation risk and the PTV, as well as DVRs and dose-volume histograms (DVHs) in a rat thorax irradiated with VMAT or AP/PA beams, shown in **Figure M4**.

For the irradiation accuracy, an image-guided irradiation method performed using CBCT. For this procedure, rats in transport cages were initially positioned using laser beams (**Figure M5a**). CBCT was taken from each rat before each treatment fraction to match it with prescribed treatment plans and to correct the position of the PTV as precisely as possible using positioning software MOSAIQ® (**Figure M5b – c**). The deviations in each of the three-dimensional directions between treatment plans and CBCT were scarcely different between animals, as exemplarily shown in **Figure M5c**.

Figure M4

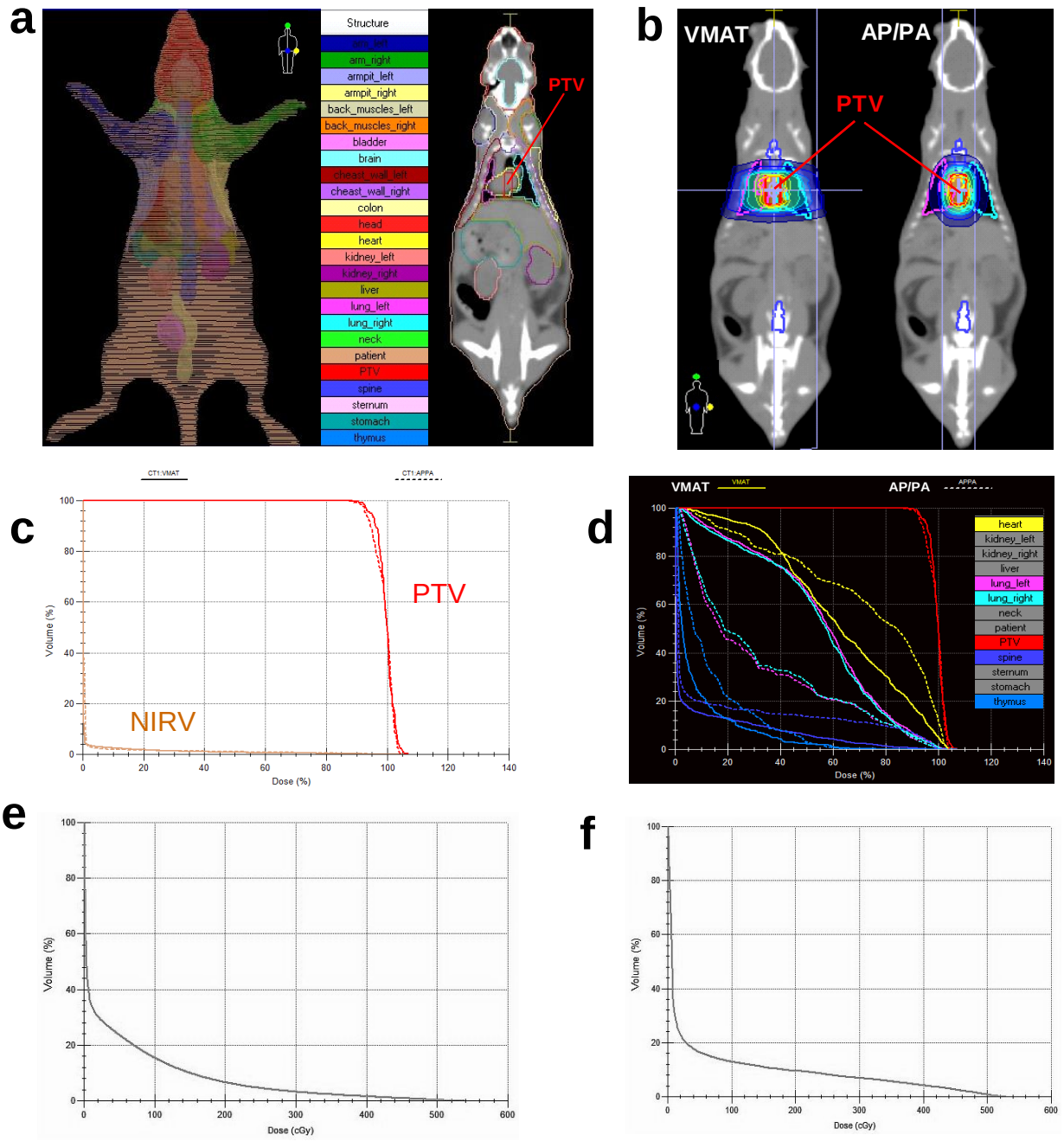

Radiation planning for VMAT and AP/PA. (**a**) Contouring of the 'structures' at radiation risk (color panel) and the PTV (red) in the mediastinum of the rat (coronal view). (**b**) Radiation dose distribution for VMAT and AP/PA techniques (colored area). (**c**) The DVHs for the PTV, and integral dose ('patient') for VMAT or AP/PA irradiation (permanent and dashed, respectively). (**d**) DVHs for selected thoracic organs at risk and the PTV for VMAT and AP/PA. (**e** – **f**) Total DVHs of 5 Gy fraction delivered with (**e**) VMAT or (**f**) AP/PA. Screenshots are from the small treatment plans.

Abbreviations: PTV, planning target volume; VMAT, volumetric-modulated arc therapy; AP/PA, anterior-posterior/ posterior-anterior; Gy, Gray; DVRs, dose to volume relationships; DVHs, dose to volume histograms; NIRV, non-irradiated volume.

Figure M5

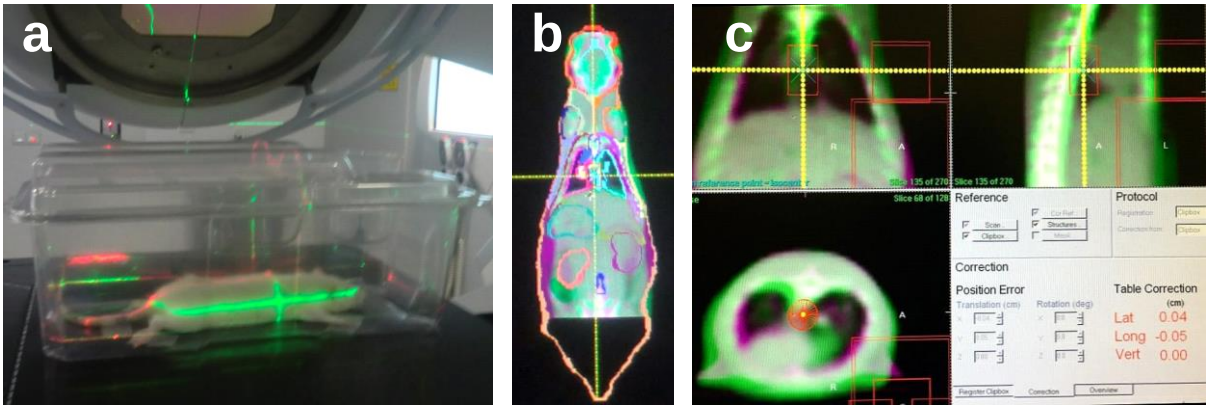

Positioning for image-guided irradiation. (**a**) An anesthetized rat located under the gantry of the LINAC using positioning laser beams (green); (**b** – **c**) CBCT matching with the planning CT scan (magenta/green) and correction of the couch position for irradiation accuracy.

Abbreviations: LINAC, linear accelerator; CBCT, cone-beam computed tomography; CT, computed tomography.

2.2.7 Observation phase

During the entire follow-up period (median 254 [91 – 431] days), rats were monitored daily to detect typical signs of a sickness such as rough hair coat, porphyrin staining, apathy, abnormal breathing, orbital tightening, limb paralysis, or a visible tumor mass.

From the age of four weeks all rats underwent weekly weight controls to collect individual growth data and to define a progressive weight loss of more than 10% – 20% of the attained body weight. Obtained growth data was documented, ordered by various parameters, and assembled in **Table A1C – F**.

2.2.8 Tumor detection using high-resolution low-dose CT

In addition to regular health checks, animals were examined with a high-resolution ultra-low dose (spatial resolution 0.24 mm, < 50% compared to conventional systems) CT scanner SOMATOM Force®. This dual-source CT system was aimed to deliver high-quality images even at very fast respiratory and cardiac activities in rats (60 – 170 breaths per minute and 300

– 500 heartbeats per minute, respectively). It has also been supposed that these parameters could decrease substantially due to narcosis.

An iodinated contrast agent (Imeron®-300) was applied by intravenous administration via a catheter inserted in a tail vein (2 – 4 µl per gram body mass). The contrast media was not used in some cases, in which the scans could not be assisted by the contrast agent due to technical errors (the catheter was impermeable or it was lost from a vein).

During the entire follow up period most rats (n = 77) were examined by SOMATOM Force CT. Out of remaining n = 57 rats, n = 45 were examined repeatedly (final CT) as most of that appeared to be ill. A list of SOMATOM Force data is compiled in **Table A6**. The analysis of the CT-reconstructions (total body and thorax windows), for an improved image display, was performed using versatile imaging software (Syngo.via,). RadiAnt DICOM Viewer was also used to visualize the DICOM (digital imaging and communications in medicine) data. Representative images are shown below, in **Figure M6a**.

For technical reasons, it was not possible to perform final Force CT scans of six rats with tumors. However, one of these rats, which had a mediastinal tumor, and another - an axillary tumor - were scanned with a micro-CT modified for preclinical applications (Y. FOX) [114,115]. But these micro-CT scans resulted in images of unsatisfactory quality. Out of the remaining four animals, two rats had mediastinal solid tumors located exactly within the HDV, one had a bone tumor on the sacral vertebra, and an additional small tumor on a rib. The last one was affected by a solid tumor sitting on the right scapula. Thus, these last four malignancies were identified during the necropsy and assigned to corresponding predefined volumes.

2.2.9 Euthanasia

All rats were euthanized using CO_2 overdoses. Therefore, animals were placed in a standard rat cage with a flat Plexiglas® top connected to the CO_2 source with a flexible tubule. The gas was delivered during 10 – 15 minutes, with very low pressure with a barely audible flow, until the signs of death were identified (cardiac and respiratory arrest).

2.2.10 Assessment of detected tumors to different dose-volumes

For the assessment of tumors to initially received radiation dose, tumor positions on the final CTs were compared with radiation plans using RadiAnt DICOM Viewer and the volumes of tumors were visually assigned to the corresponding isodose levels of the radiation plan used.

The assignment of tumors to related dose-volume by adjusting the Monaco® treatment plans with SOMATOM force® CT images is represented in **Figure M6a**.

Figure M6

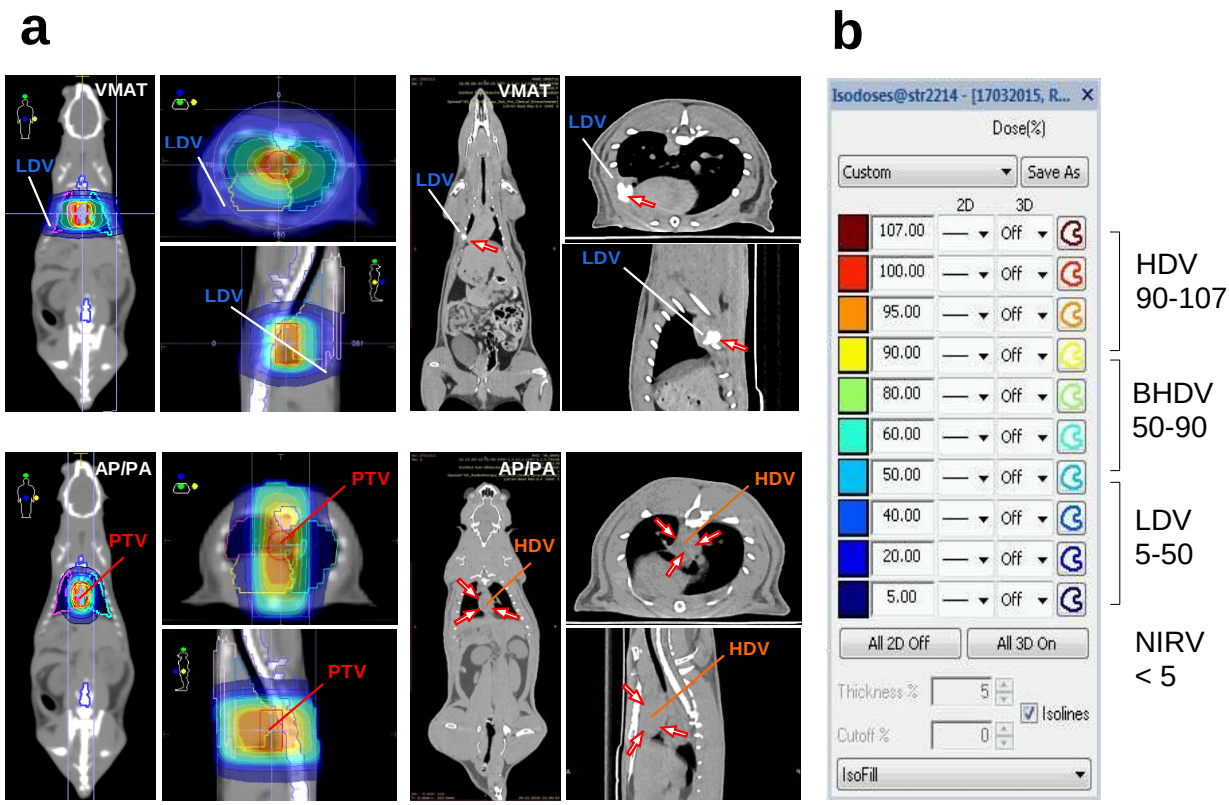

Allocation of tumor positions to different dose volumes. (**a**) Representative VMAT plan and final SOMATOM force CT images of the rat developing rib bone sarcoma within the LDV (upper left and right, respectively) and AP/PA plan and final CT with mediastinal lymphoma in the HDV (lower left and right). Both are native CTs without contrast media injection. Arrows show the positions of tumors. (**b**) A scale (Monaco®) of the dose distribution in the irradiated volume and assignment of the isodoses to the predefined HDV (90 – 107% of the prescribed dose), BHDV (50 – 90%), LDV (5 – 50%), and NIRV (< 5%) volumes.

Abbreviations: VMAT, volumetric-modulated arc therapy; AP/PA, anterior-posterior/posterior-anterior; CT, computed tomography; PTV, planning target volume; HDV, high-dose volume; BHDV, bordering high-dose volume; LDV, low-dose volume; NIRV, non-irradiated volume.

Based on estimated dose-volume relationships for tumor-affected volumes, isodoses were assigned to three predefined dose-volume levels at risk of radiation-induced tumor development: high-dose volume (HDV) exposed to at least 90% of the total target doses (3×5 Gy or 3×8 Gy), bordering high-dose volume (BHDV) receiving 50% – 90%, and low-dose volume (LDV) receiving 5% – 50% of total doses (**Figure M6b**).

Tumors outside these dose-volumes were assigned to the non-irradiated volume (NIRV) at risk of < 5% of the doses.

Based on Monaco® statistics, the HDV, BHDV, and LDV comprised approximately 0.8 cm^3, 3.9 cm^3, and 22.2 cm^3 for the large VMAT-plan while for the large AP/PA-plan 2.5 cm^3, 4.3 cm^3 and 12.0 cm^3 were measured respectively. For smaller animals (plan size small), the volumes to the HDV, BHDV, and LDV were about 0.7 cm^3, 2.9 cm^3, and 12.4 cm^3 for VMAT and 1.3 cm^3, 3.4 cm^3, and 7.4 cm^3 for AP/PA.

The DVRs of tumors, corresponding to different body volumes receiving different doses or no doses before tumors arose, are given in **Table A3E – H** and **Table A4**.

2.2.11 Necropsy

Sacrificed rats were fixated on a dissection cork plate (30×30 cm Rotilabo®-Presskork-Untersetzer), covered with a pulp-made pad (20×40 cm MaiMed Absorbent Pads), and moistened with 70% ethanol.

First the skin was incised across the inguinal-pelvic area and cut up to the mandible, prior to open abdominal and thoracic cavities using strabismus scissors and tissue forceps. The thorax and the abdomen were then opened for visual inspection by making a longitudinal incision along the length axis.

All visible organs in the abdominal and thoracic cavities, head, neck, and extremities were visually examined for abnormalities such as swelling, changes in the consistency of the tissue surfaces, fluid accumulation, differences in size and displacements of the organs, and, especially for additional tissue.

An example of a rat dissection is shown in **Figure M7a**.

Figure M7

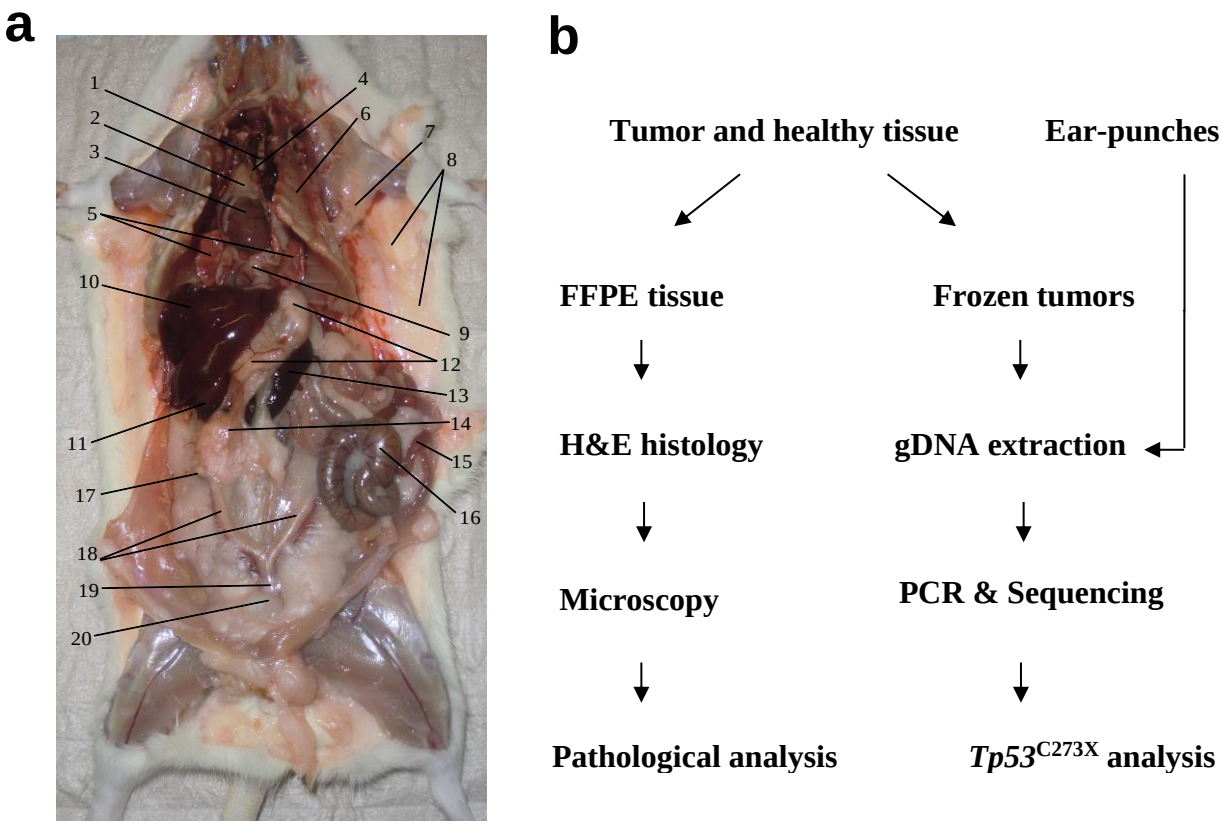

Gross necropsy and tissue sampling. (**a**) Representative autopsy of a female rat: (1) trachea, (2) thymus, (3) heart, (4) aortic arch, (5) lungs, (6) ribs, (7) lymph node, (8) mamma, (9) diaphragm, (10) liver, (11) right kidney, (12) stomach, (13) spleen, (14) pancreas, (15) colon, (16) cecum, (17) right ovary, (18) oviduct, (19) uterus, and (20) bladder. (**b**) Schematic workflow of tissue analyses.

Abbreviations: FFPE, formalin-fixed paraffin-embedded; H&E, hematoxylin and eosin; gDNA, genomic DNA; PCR, polymerase chain reaction; LOH, loss of heterozygosity.

2.2.12 Collecting tissue samples

For the preparation of the tissue samples, entire thoracic and abdominal organs including lungs, heart, thymus, trachea, esophagus, lymphatic tissues, large thoracic blood vessels, diaphragm, chest wall with ribs, thoracic vertebrae, liver, spleen, pancreas, bladder, and other evidently altered organs/tissues as well as tumors were removed separately using surgical disposable scalpels, straight scissors, and standard pattern forceps.

Tissue samples were preserved in 3.7% buffered formalin into the 100 ml sample beakers for at least 48 hours. The formalin solution consisted of 800 ml distilled water, 100 ml 10× phosphate-buffered saline (PBS; 80 g NaCl, 2 g KCl, 2.4 g $KH_2PO_4 \cdot 2H_2O$; set on pH 7.4), and 100 ml 37% formaldehyde solution (ROTIPURAN® 37% formaldehyde solution.

Small fragments of the tumors for DNA-extraction from *n* = 40 rats were shock-frozen in liquid nitrogen and stored at - 80 °C in a freezer (Panasonic MDF-DU700VH Freezer).

The representative workflow of removing and preparations the tissues for subsequent pathological and molecular examinations is expressed above in **Figure M7b**.

2.2.13 Histopathology

Organ samples from irradiated and unirradiated rats were prepared similarly.

These organs collected during the necropsy and saved in formalin were sectioned in about 0.5 cm thick slices under the cell bench (HERAsafe® KSP12) using scalpel (Surgical Disposable Scalpels), forceps (a standard pattern forceps, and a tissue forceps), and scissors (Fine scissor - sharp/blunt)

Chest organs such as the lungs (at least 4 samples), trachea (1), solid blood vessels (2 - 4), esophagus (1) with surrounding fat and mesothelium were cut axially at the PTV level.

Liver tissue samples (1-2) were taken from the apical parts of the medial lobe. Further tissue sections of diaphragm (at least 1), stomach (1 – 2), spleen (1) pancreas (1), colon (2 – 3), bladder (2 – 3), reproductive organs (2 – 3), brain (2 – 4), as well as left and right chest wall sections (2 – 4) with the nearest mamma fragments were cut always along the axial plane.

Soft tissue tumors were cut across the middle of the mass to visualize its center and periphery (at least 2 sections). Large tumors thereof were further sliced successively in approximately 0.5 cm thick sections (2 – 4). The neoplastic bone tissue structures were sectioned similarly to soft tissue tumors and soaked in a solution containing ethylenediaminetetraacetic acid (Decalcifier Soft), for at least 3 days.

The formalin-fixed tissue pieces were placed into the tissue cassettes (neoLab embedding cassettes) for dehydrogenizing by about 55 °C overnight in a drying cupboard (Heraeus®), before preparing formalin-fixed paraffin-embedded (FFPE) tissue blocks, which were poured on a paraffin-casting machine (Leica HistoCore Arcadia).

FFPE tissue blocks were cooled on a cooling plate unit (Leica EG 1150 C) before slicing in 4 – 6 µm sections with a microtome (Leica RM2245) using C35 carbon steel blades, common fine brushes and a Dumont #5 forceps.

To remove paraffin before the staining, FFPE tissue sections were placed on 76×26×1 mm microscope object-slides using 38 °C warm water bath (LEICA HI1210) and then incubated at about 55 °C overnight into the Heraeus® drying cupboard.
Histopathological staining of the tissue slides with hematoxylin and eosin (H&E) was carried out on an automatized tissue staining station (Leica Autostainer XL). The H&E-stained tissue samples on the object slides were embedded in a mounting medium (Roti®-Histokit), covered gently with covering glasses (Microscope Cover Glasses 15H 24×50 mm) using a forceps (Cover Glass Forceps 4×0.6×105 mm), and saved to dry overnight at room temperature in an air-flow safety bench (Prutscher S/TA/120/1297).
Morphological evaluation of samples was done using an upright microscope equipped with a digital microscope camera (LEICA DMBRE with Leica DFC 450). This final evaluation of H&E-stained tissue slides was performed in the Medical Research Center and the Institute of Pathology of the University Medical Center Mannheim by experienced pathologists.

2.2.14 Extraction of genomic DNA

For the extraction of genomic DNA (gDNA), the frozen tumor samples were fixed on a cryostat (Leica CM3050-S cryostat) using an adhesive compound (Tissue-Tek® O.C.T.™) to cut that in 6 µm thick layers using stainless steel R35 blades. The gDNAs were similarly extracted from ear punches and frozen tumor samples using an extraction kit (KAPA Express Extract Kit). The representative compilation of gDNA extraction mixtures is given in **Table M4**.

Table M4

Extraction of the gDNA. Components per 2 – 3 ear-punches or 3 – 5 tumor slices (6 µm).

Components	**Ear tissue samples**	**Frozen tumor samples**
10 × KAPA Express Extract Buffer	5 µl	10 µl
KAPA Express Extract Enzyme (1U/µl)	1 µl	2 µl
PCR grade H_2O	44 µl	88 µl

Abbreviations: gDNA, genomic DNA; PCR, polymerase chain reaction.

The extraction was performed by an initial lysis step (15 – 20 minutes at 75 °C) and followed by enzyme inactivation (5 minutes at 95 °C).

The extraction was carried out in standard 1.5 ml tubes (Eppendorf, Hamburg, Germany), and the thermo-chemical part of the procedure made using a thermo-mixer (Eppendorf® Thermomixer Compact). For long-term storage, gDNA extracts were saved at - 20 °C.

2.2.15 DNA amplification using PCR

Amplification of core fragments of endogenous *Tp53* gene from each 1 µl crude extracts, containing about 10 – 30 ng template gDNA per reaction, was performed using KAPA2G Fast PCR Kit. The PCR primer positions at the rat *Tp53*, flanking the thymine to adenine substitution site at the mutational hotspot site within C273 coding triplet, are represented in **Figure M8**.

Figure M8

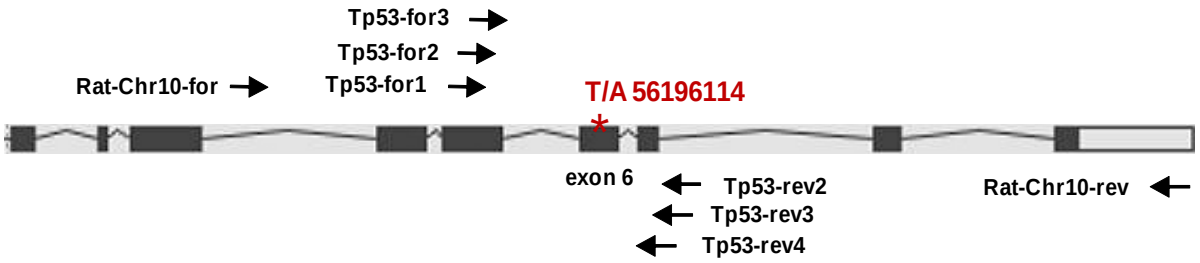

PCR primer-positions at the rat *Tp53* DNA. Schematic representation of Chr10 fragment of *Rattus norvegicus* containing the *Tp*53 gene with a T/A 56196114 alteration of the mutational hotspot codon C273 in 6th exon. Boxes and lines represent exons and introns, respectively. Arrows indicate the approximate positions of the PCR primers used in the experiment.

Abbreviations: *Tp53*, *Tumor protein 53*; for, forward; rev, reverse; T, thymine; A, adenine; Chr10, chromosome 10.

The illustration was published in Sci Rep. 2019 Oct 29;9(1):15489.

As a positive gDNA control, the 240 bp spanning fragments of the rat housekeeping gene *Glyceraldehyde-3-phosphate-dehydrogenase* (*Gapdh*) were amplified from the gDNA extracts of ear-punches and tumor samples using a self-designed specific primer-pair Gapdh-for and Gapdh-rev.

The purity of the reactions was tested by negative control PCRs containing H_2O instead of template DNA.

The expected sizes of the PCR products corresponding to used *Tp53* primer pairs were compiled in **Table M5**. See also Appendix (**Sequence information A1 and A2**)

Table M5

PCR primer pairs and expected sizes of corresponding amplicons.

Forward primer	Reverse primer	Product size
Rat-Tp53-for1	Rat-Tp53-rev3	879 bp
Rat-Tp53-for1	Rat-Tp53-rev4	729 bp
Rat-Tp53-for2	Rat-Tp53-rev3	834 bp
Rat-Tp53-for3	Rat-Tp53-rev2	772 bp
Rat-Chr10-for	Rat-Chr10-rev	4523 bp
Rat-Tp53-for1	Rat-Chr10-rev	2650 bp
Rat-Chr10-for	Rat-Tp53-rev3	2752 bp
Gapdh-for	Gapdh-rev	270 bp

Abbreviations: *Tp53, Tumor protein 53*; for, forward; rev, reverse; Chr, chromosome; bp, base pairs.

The forward primers Rat-Tp53-for1, Rat-Tp53-for2, or Rat-Tp53-for3 were combined with reverse primers Rat-Tp53-rev1, Rat-Tp53-rev3, or Rat-Tp53-rev4 to amplify 772 – 879 base pairs (bp) long fragments of the *Tp53* gene containing C273 coding site (**Table M5** and **Table M6a – a´**).

Table M6

PCR amplification of the rat *Tp53* gDNA: (**a**) rat and tumor genotyping *Tp53* PCR, (**b**) PCRs for tumor genotyping and *Tp53* LOH analyses, (**c**) nested *Tp53* PCR products. (**a´** – **c´**) The cycler programs for the reactions given in a – c.

a

PCR for 772 – 879 bp products	**50 µl/sample**
KAPA2G PCR mix	25 µl
Rat-Tp53-for1, Rat-Tp53-for2 or Rat-Tp53-for3	5 – 10 pmol/µl
Rat-Tp53-rev2, Rat-Tp53-rev3 or Rat-Tp53-rev4	5 – 10 pmol/µl
Template (gDNA)	0.5 – 1.5 µl
H_2O	up to 50 µl

b

PCR for 4523 bp products	**50 µl/sample**
GoTag®Long PCR Master Mix	25 µl
Rat-Chr-10for	5 – 10 pmol/µl
Rat-Chr10rev	5 – 10 pmol/µl
Template (gDNA)	1 – 1.5 µl
H_2O	up to 50 µl

c

Nested PCR for 2650 bp and 2752 bp products	**50 µl/sample**
GoTag® colorless PCR Master Mix	25 µl
Rat-Chr10-for or Rat-Tp53-for1	5 – 10 pmol/µl
Rat-Tp53-rev3 or Rat-Chr10-rev	5 – 10 pmol/µl
Template (4523 bp PCR product)	0,5 – 1 µl
H_2O	up to 50 µl

a´

Reaction steps	PCR for 772 – 879 bp products	
	Temperature	**Time**
Hot-start*	50 °C	3 – 5 minutes
Initial denaturing	95 °C	2 minutes
Denaturing**	95 °C	20 – 45 seconds
Annealing**	57 – 62 °C	20 – 45 seconds
Elongation**	72 °C	1 – 1.5 minutes
Final elongation	72 °C	3 – 5 minutes

* If required; ** steps were repeated in 34 – 36 cycles.

b´

Reaction steps	PCR for 4523 bp amplicons	
	Temperature	**Time**
Initial denaturing	94 °C	3 minutes
Denaturing*	95 °C	30 – 45 seconds
Annealing*	60 °C	15 – 20 seconds
Elongation*	60 – 72 °C	5 minutes
Final elongation	72 °C	12 minutes

* 32 or 34 cycles.

c´

Reaction steps	Nested PCR products	
	Temperature	**Time**
Initial denaturing	94 °C	3 minutes
Denaturing*	95 °C	15 seconds
Annealing*	60 °C	15 seconds
Elongation*	72 °C	3 minutes
Final elongation	72 °C	9 minutes

* 34 or 36 cycles.

Abbreviations: *Tp53, Tumor protein 53*; gDNA, genomic DNA; PCR, polymerase chain reaction; for, forward; rev, reverse; Chr, chromosome; bp, base pair.

The 4523 bp long PCR copies of *Tp53* were amplified with Rat-Ch10-for and Rat-Ch10-rev primer pair from approximately 0.5 – 1 µl tumor gDNA extracts using a long PCR kit (GoTag®Long PCR Master Mix), and an adapted protocol to optimize the yield of PCR products as given in **Table M6b – b´**.

The 4523 bp spanning PCR products were used as templates for the nested amplification of 2650 bp (Tp53-for1/Chr10-rev) or 2752 bp (Chr10-for/Tp53-rev3) DNA fragments (**Table M6c – c´**). These long sequence amplifications were performed to check the integrity of the C273 coding site within the *Tp53* gene locus.

For some PCRs producing DNA copies being not enough for purification and sequencing or could be poorly detected in agarose gels, a further nested PCR approach performed using primer pairs either Tp53-for1/Tp53-rev3 or Tp53-f2/Tp53-rev3 and GoTag® colorless PCR Master Mix.

2.2.16 Agarose gel electrophoresis

Agarose gels were prepared in 50 ml or 100 ml 1× TAE (121.14 g/mol TRIS [tromethamine ≥ 99.9%], 60.05 g/mol acetic acid [≥ 95.9%], and 292.25 g/mol EDTA [≥ 99%]) buffer with 1% – 1.2% agarose (Roti®garose Low Melt). Gels were stained with 6 µl DNA dye (Gel Red) per 100 ml gel volume.

For quality control of the PCR products, each 2 µl reaction was mixed with 2 µl loading buffer (Purple Loading Dye 6×) and filled with water, up to 12 µl total volume, to load on an agarose gel.

The electrophoretic separation of the PCR product DNA was done under electrical power, with a potential of 80 – 100 millivolt and a charge of 70 – 116 milliampere, for 0.5 – 1.5 hours using the standard gel-electrophoresis chamber. The chamber was filled with 1× TAE buffer and connected with a source (Owl™ EC-105 Compact Power Supply).

As molecular mass standard, a 0.1 – 10 kb (kilo-bases, 10^3 bases) DNA ladder (2-Log DNA Ladder, New England BioLabs, Frankfurt, Germany) was used.

The template-free negative controls for each PCR were also loaded on the gels to secure the purity of the PCR master mixes.

The PCR products stained in agarose gel during electrophoresis visualized using an ultra-violet transilluminator imager (INTAS Gel iX20). The data was documented with gel documentation device INTAS capture software. Representative gel images are shown below in results section 3.7.

2.2.17 DNA purification

PCR products purified either using column chromatography (mi-PCR50 Purification Kit) or enzymatically using a cleanup kit containing Exonuclease I and a shrimp alkaline phosphatase rSAP (Rapid PCR Cleanup Enzyme Set).
The column chromatography carried out according to the manufacturer's manual with variable elution volumes: 25 µl, 50 µl, and 100 µl.
For the enzymatic purification, each 1 µl Exonuclease I and 1 µl rSAP were added to 5 µl PCR product and incubated at 37 °C for 5 minutes prior to thermal inactivation of enzymes at 80 °C for 10 minutes in a thermal block (Eppendorf® Thermomixer Compact).
The concentration of purified PCR-products was ensured by photometry (Eppendorf Bio Photometer). For these measurements, 2 µl of each purified PCR products were mixed with 98 µl water and measured by specific extinction at λ = 260 nm in comparison to a blank sample (100 µl H_2O).

2.2.18 DNA sequence analysis

The PCR products were sequenced for genotyping of animals as well as analyzing of LOH in tumors.
For Sanger sequencing, about 10 – 100 ng/µl of purified PCR products were mixed with 5 µM either forward primers (Tp53-for1, Tp53-for2, Tp53-for3) or reverse primer Tp53-rev4 and filled with nuclease-free water up to 10 µl total volume in 1.5 ml Eppendorf tubes. Samples were incubated for 5 minutes at 95 °C to eliminate possible protein contaminations before labeling with Sample barcodes (LightRun Tube® Barcodes), and sent to Eurofins GATC Biotech to accomplish the sequencing reaction and data supply.
A plasmid Editor (ApE, v2.0.49) was used for the design of PCR-primers (which were synthesized by Metabion international AG, Germany) and for the analysis of the sequences based on *Rattus norvegicus* data version 6.0 (Rnor_6.0; INSDC Assembly GCA_000001895.4, July 2014).
The heterozygosity ($Tp53^{+/C273X}$) of experimental rats was ensured by recognizing the transition of C273 coding TGT to TGA (stop codon) in one of two *Tp53* alleles localized on chromosome 10 of the rat. Heterozygous $Tp53^{+/C273X}$ genotype, in which the C273-encoding triplet appears mutated in only one allele, was recognized by relatively similar levels of T/A nucleotide peaks

on the sequencing chromatograms. In contrast, LOH (*Tp53*$^{C273X/C273X}$) in tumors identified by an A/T ratio of ≥ 2.0.
Examples of sequencing chromatograms are shown below in results 3.7.

2.2.19 Inflammation analysis

Investigation of visible structural changes occurred evenly in cross-sections of irradiated and unirradiated chest organs, proposed to provide new information on the relationships between radiation-induced inflammation and SC development.
Inflammation in irradiated thoracic tissues from *n* = 19 rats developing tumors in the NIRV and *n* = 22 controls (AN/CBCT, combined) were analyzed microscopically (1 – 4 slides per rat) by a pathology professional at the institute for pathology at the university medical center Mannheim.
Agglomerations of lymphocytes, which were almost exclusively detected in the lungs during microscopy. These lymphocytes foci, assumed to be indicators of inflammation, were graded as 0 (none), 1 (rare), 2 (moderate), or 3 (frequent), according to their frequency.
The events detected by pathological inflammation analysis were compared between irradiated and non-irradiated animals and in animals treated with VMAT vs. AP/PA.

2.2.20 Storage and availability of data and samples

All experimental data are documented in laboratory books 1 and 2 which also refers to the data saved on WD Server (#WCC4E2NJO3Y6, WD®) comprising all the microscopy images, photos, as well as SOMATOM force CT data generated and saved on the server ('RADWIPACS') of the department of clinical radiology and nuclear medicine of the university medical center Mannheim.
All collected materials such as frozen tissue fragments, FFPE tissue blocks, and derived H&E-stained tissue slides, gDNA extracts, and PCR-Products are saved at the cellular and molecular radiation oncology laboratory of the department of radiation oncology of the university medical center Mannheim.

2.2.21 Statistical analyses

The frequency of tumor development in differently exposed volumes (HDV, BHDV, LDV) and non-exposed volume (NIRV), as well as the appearance of LOH in tumors and inflammation in tumor-free lungs, were compared using Fisher's exact test or Chi-square test (retrospective contingency analyses).

The lifespan between radiation treated and control groups was compared using Kaplan-Meier survival curves and the Gehan-Breslow-Wilcoxon test.

The latency TTT, from treatment time point to appearance of tumors, was tested using the Mann-Whitney test.

The comparisons were made with respect to treatment techniques (VMAT or AP/PA), radiation doses (3×5 Gy or 3×8 Gy), isodose levels (LDV, BHDV, and HDV), used treatment plan size (small or large), weight categories, sex, and the age at the treatment of animals.

The limit of significance for all statistical tests was defined as $\alpha < 0.05$.

GraphPad Prism 6.0 (GraphPad Software, San Diego, CA, USA) was used for data visualization and statistical comparisons.

3 RESULTS

3.1 Tumor incidence in different dose volumes

The occurrence of tumors was expected in both irradiated and non-irradiated body volumes of cancer-prone rats. The aim was to compare the rates of radiation-associated tumors between differently exposed volumes (LDV, BHDV, and HDV) with the rates of sporadic tumors in non-exposed volumes (NIRV).

At least one tumor (index tumor) was detected in $n = 84$ animals, while $n = 6$ animals were lost due to other causes and, therefore excluded from the analysis (**Table A1** and **Table A3**).

The data collected from $n = 84$ rats were used to analyze tumor development after VMAT vs. AP/PA and to specify tumorigenesis in the volumes receiving different radiation doses.

Table R1

Tumor incidence in unirradiated and irradiated body volumes. Numbers represent rats with index tumors. The total sums indicate the number of animals with index tumors within the same dose volume and the assignment of these animals to the treatment groups.

Incidence per group	NIRV	LDV	BHDV	HDV	Total
AN	13	0	0	0	13
CBCT	14	0	0	0	14
VMAT 3 × 5 Gy	5	2	1	7	15
AP/PA 3 × 5 Gy	7	1	1	5	14
VMAT 3 × 8 Gy	9	0	0	4	13
AP/PA 3 × 8 Gy	3	4	1	7	15
Total	51	7	3	23	84

Abbreviations: NIRV, non-irradiated volume; LDV, low-dose volume; BHDV, bordering high-dose volume; HDV, high-dose volume; AN, anesthesia only controls; CBCT, cone-beam computed tomography only controls; VMAT, volumetric-modulated arc therapy; AP/PA, anterior-posterior/posterior-anterior irradiation; Gy, Gray; 3×5 Gy or 3×8 Gy, three fractions of 5 or 8 Gy.

The analysis showed that, in both control groups (AN/CBCT), all $n = 27$ tumors were found in the sham NIRV of rats, similar to $n = 24$ of $n = 57$ animals from four irradiated groups with tumors in the corresponding NIRV. In contrast to this ($p < 0.0001$), tumors in $n = 33$ irradiated rats were found in the irradiated thoracic volume (LDV/BHDV/HDV, combined) (**Figure R1a**).

Figure R1

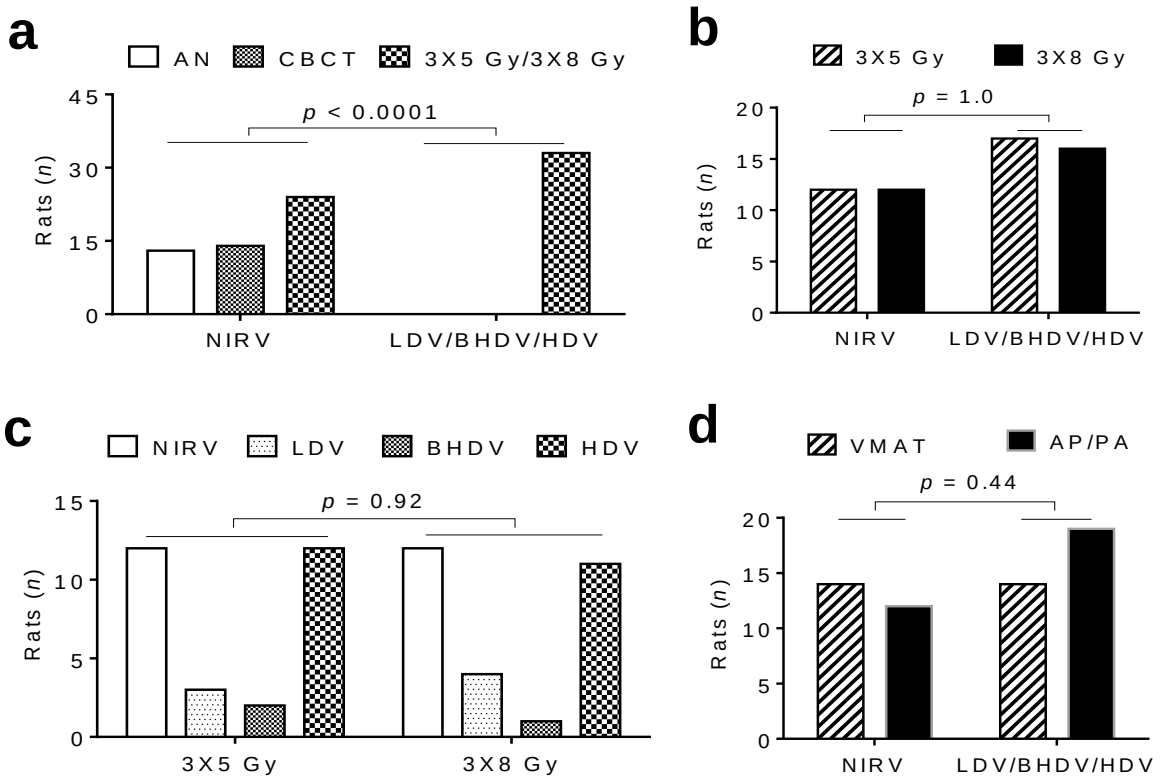

Development of sporadic and radiation-induced tumors. (**a**) All tumors in combined AN/CBCT controls were found within sham NIRV, similar to irradiated animals that developed tumors in NIRV and unlike rats with tumors found in the irradiated volume (LDV/BHDV/HDV) (Chi-square test). (**b**) Tumor rates between NIRV and LDV/BHDV/HDV were not significantly different after 3×5 Gy and 3×8 Gy (Fisher's exact test). (**c**) Proportions of tumors in either dose volumes were similar after 3×5 Gy vs. 3×8 Gy (Chi-square test). (**d**) Tumors in NIRV and LDV/BHDV/HDV similarly occurred in rats treated with VMAT and AP/PA (Fisher's exact test).

Abbreviations: AN, anesthesia only; CBCT, cone-beam computed tomography only; NIRV, non-irradiated volume; LDV, low-dose volume; BHDV, bordering high-dose volume; HDV, high-dose volume; VMAT, volumetric-modulated arc therapy; AP/PA, anterior-posterior/posterior-anterior irradiation; Gy, Gray; 3×5 Gy or 3×8 Gy, three fractions of 5 or 8 Gy. Connecting with a slash means combined volumes or groups.

The incidence of radiation-associated tumors in the LDV/BHDV/HDV and in NIRV did not differ significantly ($p = 0.1$) between rats treated with 3×5 Gy ($n = 17$ and $n = 12$) compared to 3×8 Gy ($n = 16$ and $n = 12$) (**Figure R1b**).

Importantly, the majority ($n = 23$) of $n = 33$ radiation-associated tumors were detected inside the volume receiving highest doses (HDV), only $n = 3$ in the BHDV, and $n = 7$ in the LDV (3×5 Gy/3×8 Gy combined). Thus, the total number of rats with a tumor within the HDV was more than doubled compared to the number of rats ($n = 10$) developing tumors in volumes exposed to relatively lower doses (BHDV/LDV, combined).

In rats treated with 3×5 Gy, compared to 3×8 Gy, no significant difference could be observed between the incidence frequencies within LDV, BHDV, HDV, and NIRV (**Figure R1c**).

Most notably, no increased tumor induction was observed in the volume irradiated with VMAT compared to AP/PA (14 of 28 vs. 19 of 29, $p = 0.44$) (**Figure R1d**). Thus, the RR of tumor development after VMAT (IMRT) was not increased compared to AP/PA (3D-CRT) treatment (RR = 0.79 with a 95% confidence interval of 0.46 – 1.34).

Taken together, no increased risk of radiation-induced tumors observed in the volumes exposed to lower doses compared to higher doses or in rats treated with VMAT compared to AP/PA.

3.2 Frequency distribution of tumors in different dose-volumes

To illustrate the frequency distribution of tumors developed in different dose-volumes (LDV, BHDV, or HDV) and NIRV, a ‘part of whole’ analysis performed. The test aimed to indicate the contingency or eventuality of tumor development in differently exposed and unexposed volumes. The sizes of unirradiated and uniformly irradiated volumes (**Table A3F**) summed, therefore, to determine the overall size (total volume in cm^3) of all tumor-affected NIRVs, LDVs, BHDVs, and HDVs (**Table A4**).

The frequency distribution of neoplastic events was calculated and displayed for each summed volume (NIRV, LDV, BHDV, and HDV), as the ratio of the events per unit volume (cm^3), in relation to the prescribed total doses (3×5 Gy and 3×8 Gy), treatment modalities (VMAT and AP/PA) (**Table A4** and **Figure R2**).

Figure R2

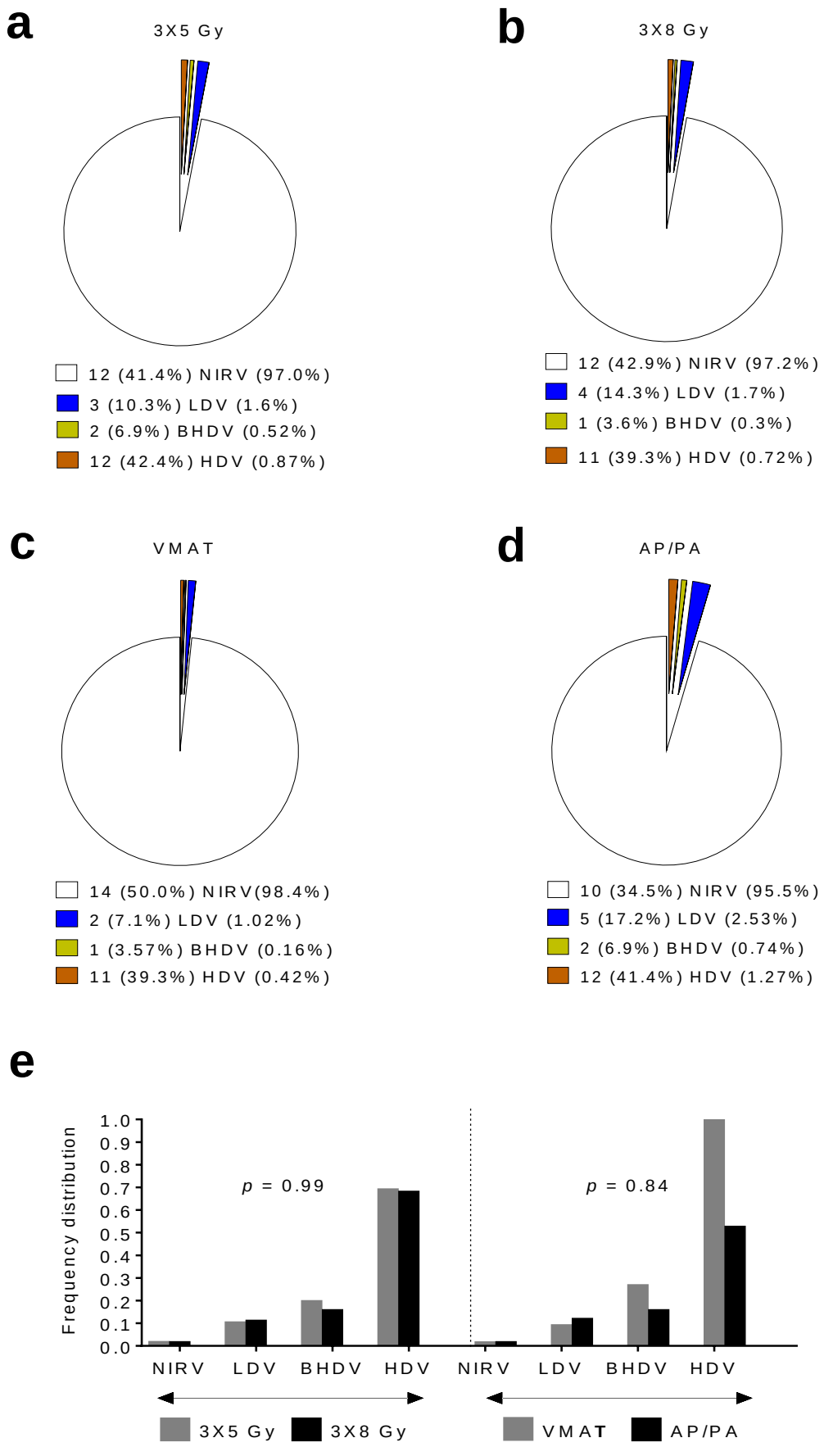
a
3X5 Gy
12 (41.4%) NIRV (97.0%)
3 (10.3%) LDV (1.6%)
2 (6.9%) BHDV (0.52%)
12 (42.4%) HDV (0.87%)
b
3X8 Gy
12 (42.9%) NIRV (97.2%)
4 (14.3%) LDV (1.7%)
1 (3.6%) BHDV (0.3%)
11 (39.3%) HDV (0.72%)
c
VMAT
14 (50.0%) NIRV(98.4%)
2 (7.1%) LDV (1.02%)
1 (3.57%) BHDV (0.16%)
11 (39.3%) HDV (0.42%)
d
AP/PA
10 (34.5%) NIRV (95.5%)
5 (17.2%) LDV (2.53%)
2 (6.9%) BHDV (0.74%)
12 (41.4%) HDV (1.27%)
e
Frequency distribution
1.0
0.9
0.8
0.7
0.6
0.5
0.4
0.3
0.2
0.1
0.0
p = 0.99
p = 0.84
NIRV LDV BHDV HDV NIRV LDV BHDV HDV
3X5 Gy 3X8 Gy
VMAT AP/PA

Frequency distribution of cancerous events in different dose-volumes. (**a** – **d**) Shown are the part of the whole diagrams of tumor-affected volumes receiving different doses. The numbers of index tumors reflect the numbers of the incident events within the NIRVs, LDVs, BHDVs, and HDVs receiving < 0.75 Gy, 0.75 – 7.5 Gy, 7.5 – 13.5 Gy, and 13.5 – 15 Gy during 3×5 Gy irradiation or < 1.12 Gy, 1.12 – 12 Gy, 12 – 21.6 Gy, and 21.6 – 24 Gy of the total of 3×8 Gy respectively. The percentages represent the portions of the total amounts of uniformly exposed volumes and portions of the total events grouped by (**a**) 3×5 Gy and (**b**) 3×8 Gy or (**c**) VMAT, and (**d**) AP/PA treatments. (**c**) The frequency distributions of tumors per NIRVs, LDVs, BHDVs, and HDVs was increased with increased estimated doses to normal tissue without significant differences between 3×5 Gy or 3×8 Gy and VMAT or AP/PA (Chi-square test).

Abbreviations: NIRV, non-irradiated volume; LDV, low-dose volume; BHDV, bordering high-dose volume; HDV, high-dose volume; VMAT, volumetric-modulated arc therapy; AP/PA, anterior-posterior/posterior-anterior irradiation; Gy, Gray; 3×5 Gy or 3×8 Gy, three fractions of 5 or 8 Gy.

Neither parameter was notably different between the NIRV and LDV while the frequency was somewhat increased for the BHDV, and was drastically raised to higher levels for the HDV. In particular, after 3×5 Gy (combined VMAT/AP/PA groups), the yield of tumors in the overall HDV was about 3.6 folds and 7.3 folds higher than in the BHDVs and LDVs respectively, whereas it was increased dramatically in comparison with NIRV (113.3 folds). A similar trend of tumor development was observed in the HDV vs. BHDV, LDV, and NIRV (4.6, 6.7, and 124.1 folds, respectively) after 3×8 Gy treatment. A comparison by treatment technique (3×5 Gy/3×8 Gy, combined) showed similar trends: VMAT and AP/PA (4.2, 22.5, 216 folds after VMAT, and 3.5, 4.8, 90 folds after AP/PA, for BHDV, LDV, and NIRV, respectively).

Thus, the frequency of cancerous events per unit volume was increased with increased doses to irradiated volume and not with enlarged volume receiving any lower doses in this experimental model.

Notably, no statistically significant difference between the effects of prescribed doses (3×5 Gy vs. 3×8 Gy; $p = 0.99$) nor irradiation technique (VMAT vs. AP/PA; $p = 0.84$) could be observed (**Figure R2e**).

Overall, an increased expectancy of tumors was directly associated with higher local doses to the normal tissue and not with an increased low dose volume after IMRT (VMAT).

3.3 Survival in unirradiated and irradiated rat groups

The observation phase from birth until tumor detection was median 348 [minimum to maximum: 175 – 504] days.

Notably, no animal developed any detectable tumor before attaining an incidence-free age border of at least 175 days from birth. Interestingly, this tumor-free time was equally valid for all groups (**Figure R3a**).

Figure R3

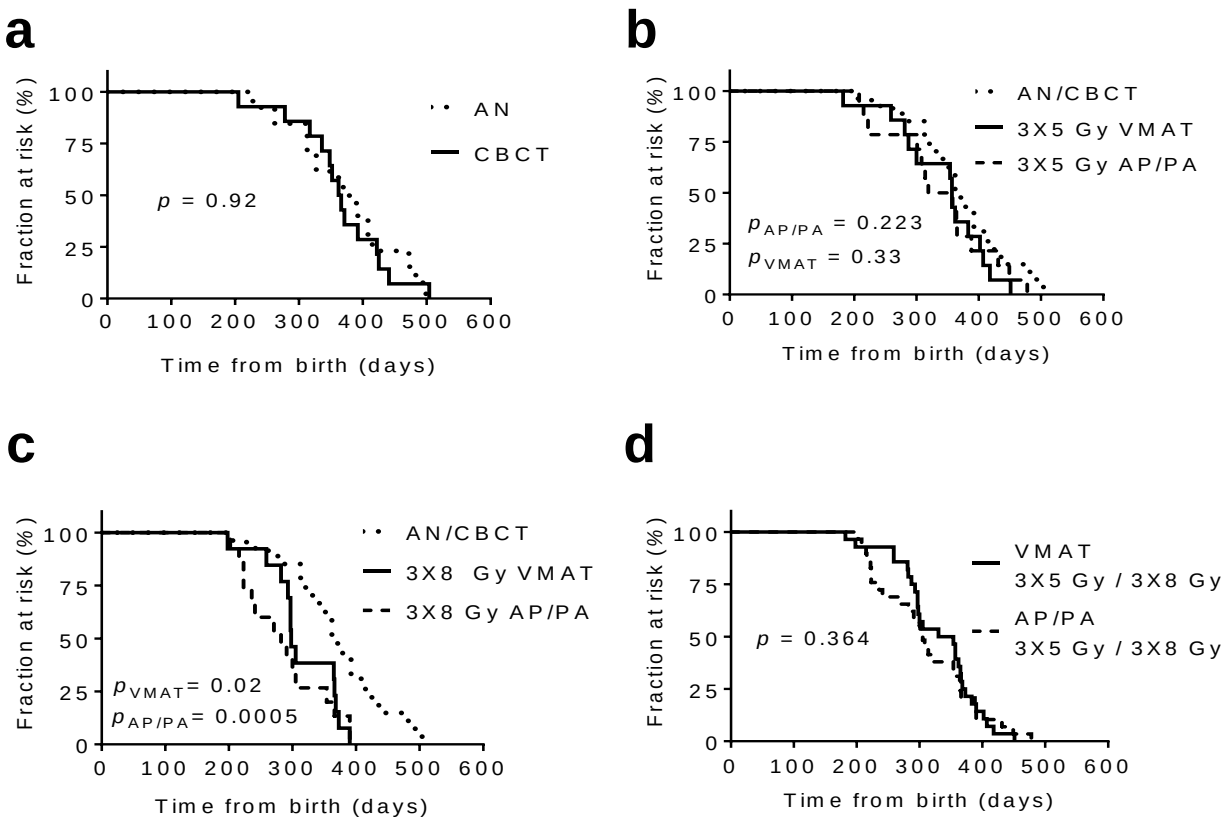

Survival of the rats. The Kaplan-Meier survival curves illustrate the declining fractions of living rats per time (attained age from birth). (**a**) No significant differences were observed between Kaplan-Meier survival curves of AN and CBCT groups, and (**b**) groups treated with 3×5 Gy VMAT or AP/PA. (**c**) The curves were significantly decreased for 3×8 Gy groups vs. combined AN/CBCT controls, however, not specifically for VMAT vs. AP/PA (**d**). Gehan-Breslow-Wilcoxon test.

Abbreviations: AN, anesthesia only controls; CBCT, cone-beam computed tomography only controls; VMAT, volumetric-modulated arc therapy; AP/PA, anterior-posterior/posterior-anterior irradiation; Gy, Gray; 3×5 Gy or 3×8 Gy, three fractions of 5 or 8 Gy. Connecting with a slash means combined groups.

Kaplan Meier survival curves, representing the attained age from birth, for control rat groups, were similar: median 379 [228 - 499] vs. 364 [205 - 504] days (p = 0.92). Thus, the effect of exposure to low doses of CBCT was not detectable in the presented experimental model. Therefore, the data belonging to each control group were combined (AN/CBCT) for comparison with irradiated groups.

No statistically significant differences were observed between survival curves for groups treated with 3×5 Gy VMAT (p = 0.33) and 3×5 Gy AP/PA (p = 0.223) compared to AN/CBCT: median 357 [182 – 451] days for VMAT and 338.5 [208 – 478] days for AP/PA vs. 366 [205 – 504] days for AN/CBCT (**Figure R3b**). By contrast, treatment with 3×8 Gy led to a significantly shortened lifespan due to earlier tumor appearance in both VMAT and AP/PA treated rats (**Figure R3c**). The difference compared to controls appeared marginally significant for VMAT (p = 0.02) and highly significant for AP/PA (p = 0.0005): median 298 [198 – 390] days for VMAT and 282 [202 – 390] days for AP/PA vs. AN/CBCT.

Most interestingly, comparison of the curves for radiation treatment groups, 3×5 Gy and 3×8 Gy combined, by RT techniques, did not reveal any significant evidence for a specifically decreased survival of the rats treated with VMAT compared to AP/PA (median 342 [182 – 451] days vs. 305 [202 – 478] days; p = 0.364; **Figure R3d**). Although not statistically significant, a 12% longer median 'survival' was observed in rats treated with VMAT vs. AP/PA.

Taken together, high radiation doses were able to shorten the tumor-prone lifespan in *Tp53*$^{+/C273X}$ rats, without regard to VMAT and AP/PA treatments. These observations demonstrated the first *in vivo* evidence for significantly decreased attained age (that corresponds to survival) in the rat groups irradiated with high local doses.

3.4 Dose to volume relationship for the latency time to tumors

Since the lifespan was shortened for rats from the high-dose groups (3×8 Gy), it was tested how far this shortening could be related to different radiation doses delivered to the defined irradiated volumes. Detailed analysis of the time span, from the first day of treatment to the tumor-related killing of the animals, showed that the TTT for n = 12 tumors found within the NIRV in rats treated with 3×5 Gy was quite similar to the TTT of sporadic events in AN/CBCT control groups (medians, with minimum to maximum, 295.5 [121 – 359] days vs. 296 [128 – 484] days, p = 0.74; **Figure R4a**).

Figure R4

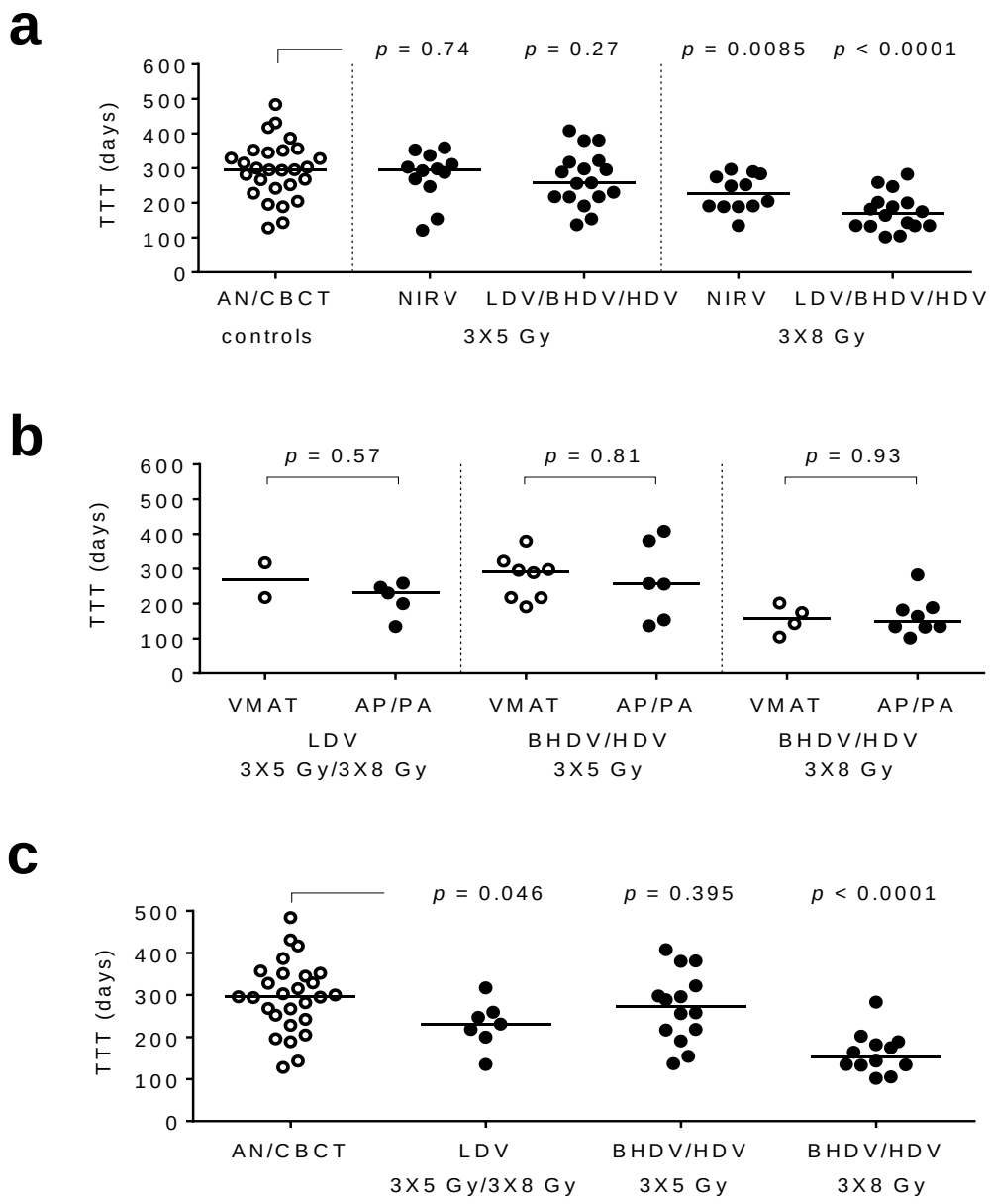

The latency of radiation-induced and spontaneous tumors. (**a**) Compared to combined controls (AN/CBCT), the TTT was significantly decreased for all tumors developing after 3×8 Gy but not 3×5 Gy. (**b**) No significant differences in TTT after VMAT vs. AP/PA treatments were observed at either dose level (3×5 Gy or 3×8 Gy) for tumors in the LDV/BHDV/HDV. (**c**) The median TTT was borderline significantly reduced for tumors in the LDV (all combined) while it was highly decreased for tumors developed within the volumes receiving the highest doses (combined BHDV/HDV). The Mann-Whitney test. Plots show individual values and medians.

Abbreviations: TTT, time to tumor; NIRV, non-irradiated volume; LDV, low-dose volume; BHDV, bordering high-dose volume; HDV, high-dose volume; Gy, Gray; AN, anesthesia only controls; CBCT, cone-beam computed tomography only controls; VMAT, volumetric-modulated arc therapy; AP/PA, anterior-posterior/posterior-anterior irradiation; 3×5 Gy or 3×8 Gy, three fractions of 5 or 8 Gy; Connecting with a slash means combined volumes or rat groups.

Similar to the NIRV, n = 17 tumors occurred in the irradiated volume (LDV/BHDV/HDV, combined) after 3×5 Gy treatment, did not show a statistically significant decrease in TTT compared to sporadic tumors (AN/CBCT): median 258 [137 – 408] days vs. 296 [128 – 484] (p = 0.27).

A significant decrease in TTT compared to AN/CBCT was measured for rats (n = 12) with tumors within the NIRV after 3×8 Gy irradiation: median 227 [135 – 297] vs. 296 [128 – 484] days, (p = 0.0085). A highly significant decrease in TTT in comparison to AN/CBCT was observed, however, in n = 16 rats with tumors in the LDV/BHDV/HDV receiving planned doses: median 169.5 [102 – 283] vs. 296 [128 - 484] days, (p < 0.0001).

Regarding the effects of dose, volume, and radiation modality, no significant difference in TTT was detected between tumors that arose within the LDV (3×5/3×8 Gy, combined), 3×5 Gy BHDV/HDV, and 3×8 Gy BHDV/HDV after VMAT vs. AP/PA treatment: median 267.5 [218 – 317] vs. 231 [135 – 259] days (p = 0.57); 292.5 [191 – 380] vs. 257 [137- 408] days (p = 0.81); and 159 [105 – 202] vs. 149.5 [102 – 283] days (p = 0.933), respectively (**Figure R4b**).

A maximum decrease in TTT compared to AN/CBCT revealed for tumors within the BHDV/HDV after 3×8 Gy treatment: median 153.5 [102 – 283] vs. 296 [128 – 484] days (p < 0.0001) (**Figure R4c**). Next to this, tumors detected in the LDV (3×5 Gy/3×8 Gy, combined) also showed a borderline significant reduction in TTT: median 231 [135 – 317] vs. 296 [128 – 484] days (p = 0.046).

Possible uncertainties in these comparisons regarding the somewhat older age of some rats in 3×8 Gy treated groups compared to other groups are discussed below in section 4.6.

Most importantly, no disadvantages of VMAT vs. AP/PA or enlarged low-dose volume (‘low-dose bath’) compared to smaller volumes exposed to highest doses were confirmed. Furthermore, the most of earliest tumors thereof rather arose in the volumes receiving higher doses, unlike lower doses.

3.5 Tumor detection using high-resolution low-dose CT

In some rats, tumors were recognized as palpable swellings that were not far from the body surface (e. g., tumors on the ribs and extremities). Deep-seated tumors (e. g., inside the thoracic or abdominal cavity or in the inner organs) were detected by high-resolution CT examination using SOMATOM Force CT.

A list of SOMATOM Force data for each scan is given in **Table A6**.

Bone tumors were easily determined on CT scans, based on skeletal alterations appearing as bulged regions, as it is shown in **Figure R5a**.

The majority of non-osseous solid tumors could be detected on native CTs as uncommon hyperplastic formations or deformed anatomical structures that were abundantly supplied with blood vessels and, therefore, more clearly visible in rats receiving an intravenous injection of the contrasting media Imeron®-300 before CT scans.

The representative CT images of rats developing tumors within the HDV are shown in **Figure R5b – c**.

Figure R5

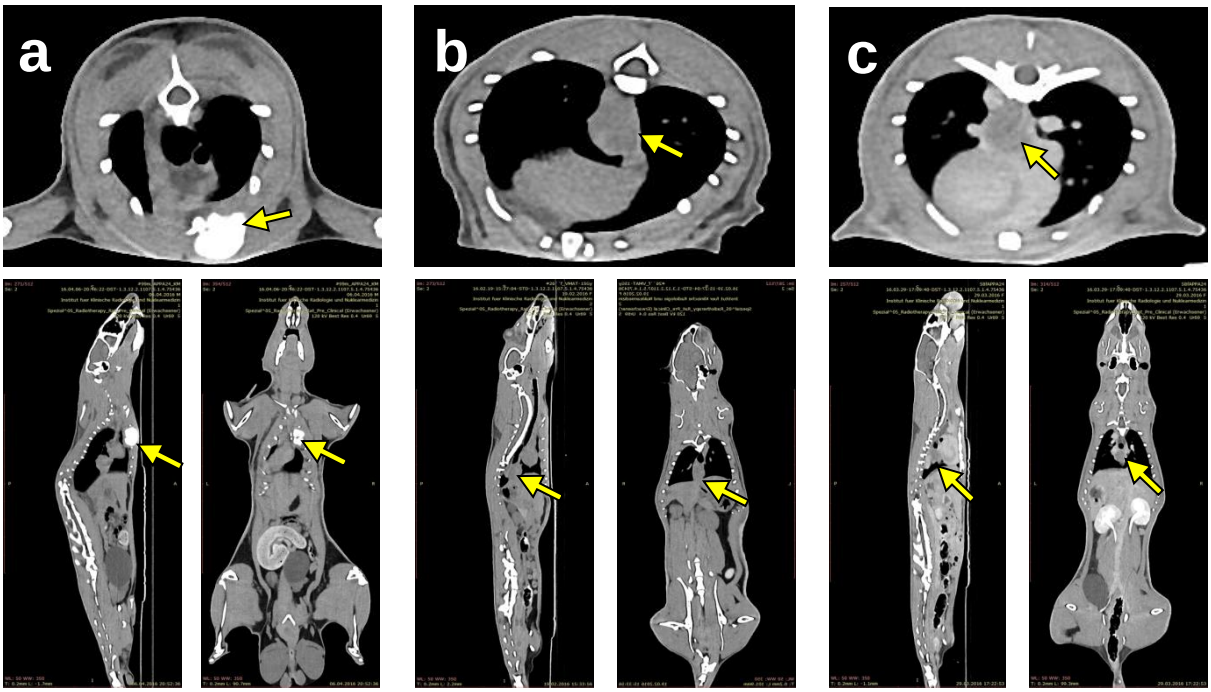

Detection of tumors using clinical CT. (**a**) A rib bone tumor within the LDV after 3×8 Gy AP/PA irradiation (native CT), (**b**) a native CT of rhabdomyosarcoma in the HDV after 3×8 Gy VMAT, and (**c**) contrast-enhanced (Imeron®-300, approx. 2 µl/g body mass) CT of mediastinal rhabdomyosarcoma in the HDV after 3×8 Gy AP/PA treatment. Axial, sagittal, and coronal (below) views are shown. Arrows indicate the position of tumors.

Abbreviations: CT, computed tomography; LDV, low-dose volume; AP/PA, anterior-posterior/posterior-anterior irradiation; HDV, high-dose volume; BHDV, bordering high-dose volume; VMAT, volumetric-modulated arc therapy; 3×8 Gy, three fractions of 8 Gray.

The illustration was published in Sci Rep. 2019 Oct 29;9(1):15489.

3.6 Entities and the latency of radiation-induced and sporadic tumors

Based on histopathology, *n* = 71 index tumors could be assigned to seven different primary origins (entities): bone sarcoma, soft tissue sarcoma (rhabdomyosarcoma and fibrosarcoma), lymphoma (unclear subtypes), carcinoma (adenocarcinoma or squamous cell carcinoma), breast cancer (obviously all carcinomas), malignant mesothelioma, and brain tumors. The entities of further *n* = 13 index tumors described below remained non-determined.

The estimated entities of tumors are compiled in **Table R2** and detailed in **Table A7C – J**. The representative microscopy images of these tumors are shown in **Figure R6**.

Table R2

Tumor entities in rats. Numbers represent index tumors of different entities belonging to control and irradiated groups (the volumes of tumor incidence are given in parentheses).

Tumor entities per volume and group	BSA	SSA	LY	MM	CA	BC	BT	ND
AN (sham NIRV)	4	0	0	0	3	2	1	3
CBCT (sham NIRV)	9	1	0	0	1	0	1	2
3×5 Gy VMAT/AP/PA comb. (NIRV)	4	1	0	0	2	0	0	5
3×8 Gy VMAT/AP/PA comb. (NIRV)	5	0	0	0	2	1	1	3
3×5 Gy VMAT (LDV/BHDV/HDV)	3	2	3	1	1	0	0	0
3×5 Gy AP/PA (LDV/BHDV/HDV)	0	2	4	0	1	0	0	0
3×8 Gy VMAT (LDV/BHDV/HDV)	0	1	2	1	0	0	0	0
3×8 Gy AP/PA (LDV/BHDV/HDV)	2	6	3	0	1	0	0	0
Total	27	13	12	2	11	3	3	13

Abbreviations: BSA, bone sarcoma; STSA, soft tissue sarcoma; LY, lymphoma; MM, malignant mesothelioma; CA, carcinoma; BC, breast cancer (all CA); BT, brain tumor; and ND, non-determined; AN, anesthesia only controls; CBCT, cone-beam computed tomography only controls; NIRV, non-irradiated volume; LDV, low-dose volume; BHDV, bordering high-dose volume; HDV, high-dose volume; Gy, Gray; VMAT, volumetric-modulated arc therapy; AP/PA, anterior-posterior/posterior-anterior irradiation; 3×5 Gy or 3×8 Gy, three fractions of 5 or 8 Gy. Connecting with a slash means combined volumes or rat groups.

Figure R6

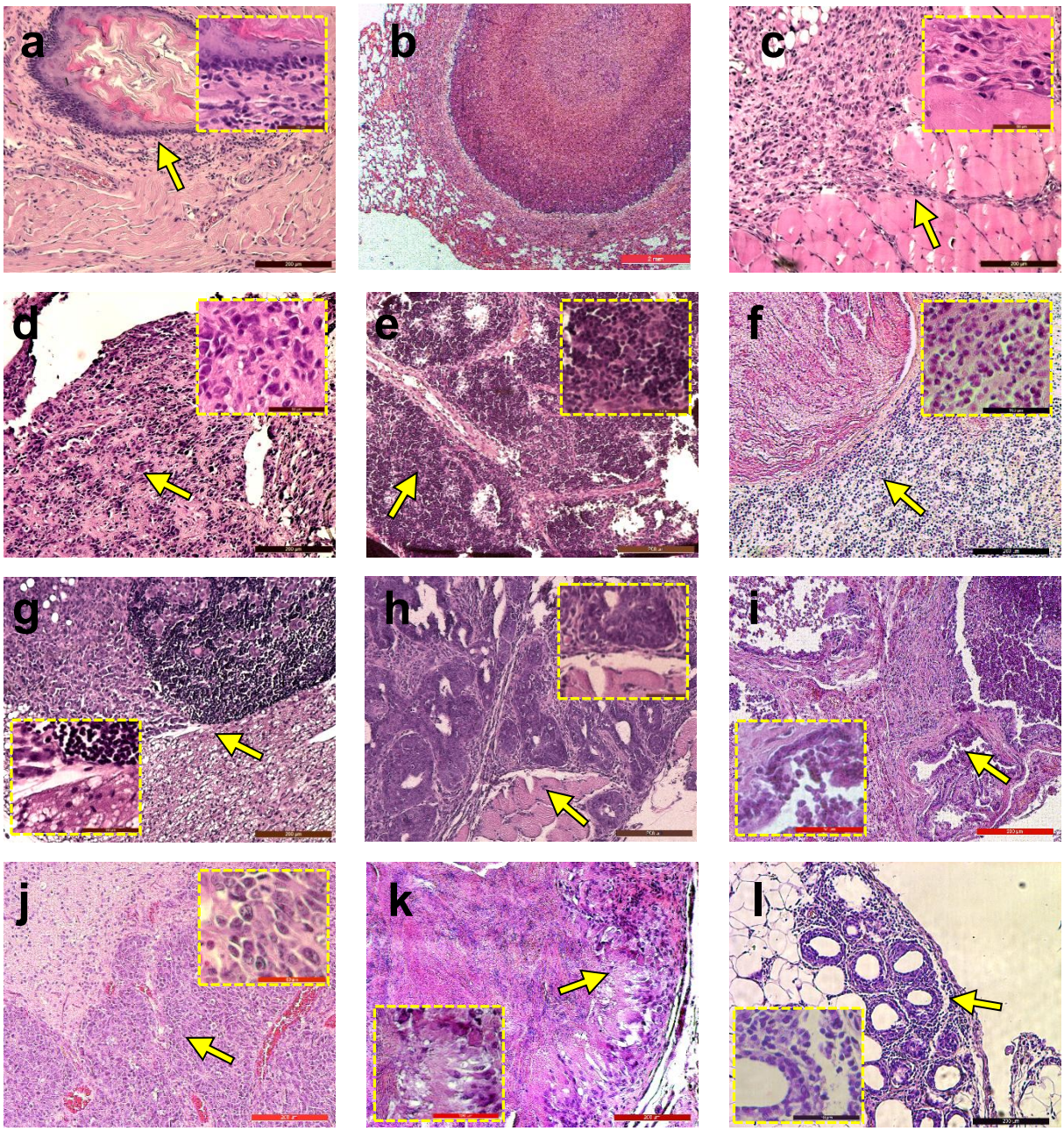

Representative microscopy images of different tumors. Tumor types (entities) detected in the experiment: (**a**) bone sarcoma, (**b**) bone sarcoma lung metastasis (osteoid), (**c**) soft tissue sarcoma (rhabdomyosarcoma), (**d**) soft tissue sarcoma (fibrosarcoma), (**e**) lymphoma, (**f**) lymphoma (lymphosarcoma), (**g**) malignant mesothelioma, (**h**) carcinoma (adenocarcinoma), (**i**) carcinoma (squamous cell carcinoma), (**j**) brain tumor, (**k**) non-determined testicular tumor, and (**l**) non-determined pelvic tumor. Shown are microscopy images of 4 – 6 µm thick tissue slices (stained with H&E). Blue-enriched (oxidized) hematoxylin is due to acidic DNA while proteins are dyed red by eosin. Scale bars: 200 µm and 50 µm.

The illustration was published in Sci Rep. 2019 Oct 29;9(1):15489.

Bone sarcoma appeared as cartilaginous and ossified masses of tissue that aggressively invaded neighboring structures such as muscles, skin, thoracic or pelvic organs and, in some cases, metastasized to distant organs (e.g., lungs). Upon microscopic evaluation of the H&E-stained tissue slides, bone sarcoma was recognized by an increased occurrence of calcified cell masses (inside), and rapidly dividing osteoblasts (many mitotic figures) outwards of the center of the tumor mass (**Figure R6a**). Most bone sarcomas appeared as highly aggressive tumors attacking also distant organs. Thus, multiple lung metastases, mostly in form of multiple macroscopic osteoids (**Figure R6b**), found in 5 out of 23 rats with bone sarcomas of the scapula, tailbone, femur, tibia, or sacral vertebra.

The majority (12 of 13) of soft tissue sarcomas were solid tumor masses that originated from the muscles and revealed rhabdomyosarcoma morphology. Under the microscope, rhabdomyosarcoma cells displayed anaplastic nuclei, scattered mitotic figures, and a few apoptotic bodies. Also, one fibrosarcoma was detected as a large, aggressively grown solid tumor invading the surrounded thoracic organs and in the liver. Fibrosarcoma cells, commonly derived from differentiated fibroblasts, show large nuclei and variable protein rates. Representative images of these mesenchymal soft tissue malignancies are shown in **Figure R6c – d**.

The group of lymphomas (n = 12), a disease that usually can take many forms in animals and can spread into almost any tissue in the body, contained tumors aggressively incorporating into the neighboring normal tissues. Lymphomas mostly looked like white to slightly yellowish, relatively uniform cell masses (clumps), sometimes with necrotic tissues in the center of the mass. Under the microscope, these tumors were distinguishable due to lymphocyte-derived rounded cell cohorts disseminating into the neighboring normal tissues (**Figure R6e – f**).

Two thoracic malignant mesotheliomas were found as relatively large tumors that widely occupied the thoracic space and were ingrown in adjacent tissues. Out of further two abdominal mesotheliomas, one was invaded in the pancreas and another in the pelvic organs (both NIRV). Malignant mesotheliomas were occurred as uniformly formed cell masses attacking normal tissues as shown in **Figure R6g**.

Carcinomas were represented by lung adenocarcinomas or squamous cell carcinomas with intensive proliferated, variably-sized and shaped clusters of arranged epithelial tumor cells derived from different organs (**Figure R6h – i**).

All three animals with brain tumors showed coordination disorders and problems with movement. One tumor was found between the frontal lobes, another one at the cerebellum, and a further one was scattered within the cortex and cerebellum. Entities of these brain tumors

could not be determined exactly. However, the morphological appearance of these tumors argues for sarcoma or gliosarcoma rather than for classical glioma (**Figure R6j**).

As mentioned above, the tumor entities could not be exactly specified in some rats developing pelvic and abdominal none-osseous tumors: n = 8 (NIRV), n = 3 (AN), and n = 2 (CBCT). These tumors were assumed as tumors with non-determined entities. Exemplary images of such non-determined, testicular and pelvic tumors are shown in **Figure R6k – l**.

In n = 11 rats one or more tumors of a different type (entity) were found in addition to the index tumor. These malignancies were not included in the analysis of index tumors. The entities and the locations of additional tumors are given in **Table A8**.

Tumors of the same entities were grouped by their appearance in the different dose volumes and compared to indicate whether a particular tumor entity might be typical of unirradiated or irradiated body parts. In addition, it was tested, whether any type of found tumors could be specific for low dose volumes or high dose volumes. Upon evaluation of sporadic tumors in control rats and tumors from the NIRV, no lymphoma was detected, whereas the most frequent tumors were bone sarcoma (n = 22) or carcinoma (n = 8). Other tumors entities like soft tissue sarcoma (n = 2), malignant mesothelioma (n = 2), breast cancer (n = 3), and brain tumors (n = 3) were rare (**Table R2** and **Figure R7a**). In contrast to NIRV, lymphoma (n = 12) and soft tissue sarcoma (n = 11) were the most frequently detected tumors in the irradiated volume while bone sarcoma (n = 5), malignant mesothelioma (n = 2), and carcinoma (n = 3) were also found. Thus, lymphoma ($p < 0.0001$) and soft tissue sarcoma ($p = 0.0001$) were strongly associated with irradiated volume in contrast to bone sarcoma detected predominantly in NIRV.

Interestingly, the shortening of the TTT for malignancies after 3×8 Gy vs. 3×5 Gy treatment was not associated with either tumor entity (**Figure R7b**). An exception was lymphoma, with a decreased median TTT after 3×8 Gy compared to 3×5 Gy: 143 [102 – 202] vs. 258 [154 – 408] days ($p = 0.0101$).

Figure R7

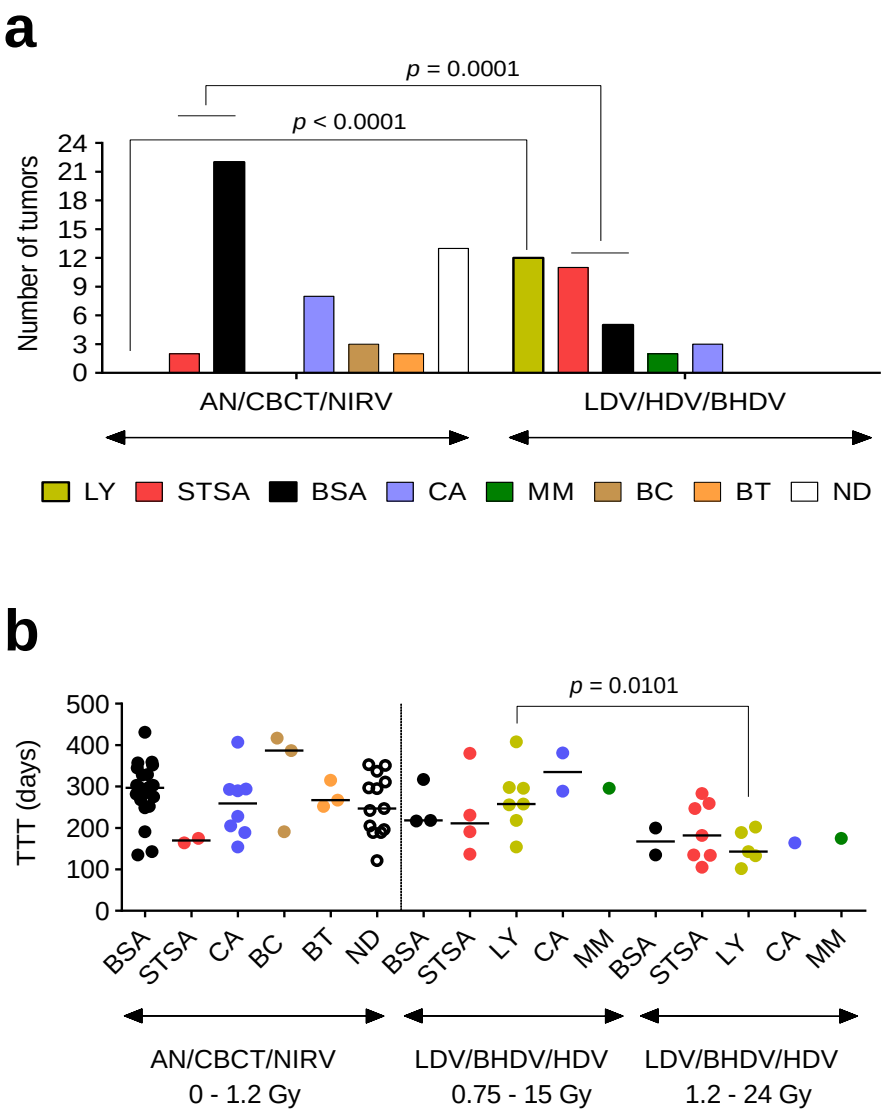

Tumors grouped by their entities and occurrence in different volumes. (**a**) BSA predominantly, but no LY, and only two STSA were detected in AN/CBCT controls and the NIRV of irradiated rats. In contrast, LY was exclusively, and STSA was specifically developed in the irradiated volume (LDV/BHDV/HDV) and bone sarcoma in the NIRV (Fisher's exact tests). (**b**) Median TTTs were not significantly different between tumor types after either dose treatment, while it was reduced only for LY developed in the volume irradiated with 3×8 Gy vs. 3×5 Gy (Fisher's exact test). Received dose levels for each groupe are shown. See also **Table R2**.

Abbreviations: BSA, bone sarcoma; CA, carcinoma, STSA, soft tissue sarcoma; BT, brain tumor; BC, breast cancer; LY, lymphoma; MM, malignant mesothelioma; ND, not determined; TTT, time to tumor; AN, anesthesia only controls; CBCT, cone-beam computed tomography only controls; NIRV, non-irradiated volume; LDV, low-dose volume; BHDV, bordering high-dose volume; HDV, high-dose volume; Gy, Gray; 3×5 Gy or 3×8 Gy, three fractions of 5 or 8 Gy. Connecting with a slash means combined volumes or groups.

3.7 Loss of *Tp53*$^{+/C273X}$ heterozygosity in radiation-associated and sporadic tumors

From the idea that radiation-associated tumor development might be driven by the loss of intact *Tp53* allele (LOH), $n = 40$ index tumors from irradiated and non-irradiated rats were genotyped for the presence of mutations in *Tp53* gene core fragment (**Table A7K – L**).

To test whether the missed second intact *Tp53* allele (LOH) could be associated with radiation, tumors were grouped either by the volume of their origin (irradiated or unirradiated), initially prescribed doses (3×5 Gy or 3×8 Gy), or used dose delivery technique (VMAT or AP/PA). The analysis revealed no notable difference between the fractions of tumors with and without LOH developed in controls (8 of all tested 11), in the NIRV (4 of 12), or in LDV/BHDV/HDV (10 of 17) (**Table R3**).

Interestingly, in all tumors, LOH showed the same T/A mutation, and no other gained sequence changes in tested *Tp53* fragments were found. Representative PCR products and sequencing chromatograms for different rat *Tp53* genotypes are shown in **Figure R8**.

A further comparison of the tumor genotypes (*Tp53*$^{+/C273X}$ or LOH) indicated that LOH was not specifically appeared in tumors developed within the irradiated volume (10 of 17 in irradiated LDV/BHDV/HDV vs. 12 of 23 unirradiated AN/CBCT/NIRV, $p = 0.76$; **Figure R9a**).

Table R3

LOH of *Tp53*$^{+/C273X}$ in tumors. LOH in sporadic and radiation-related tumors in different volumes.

Events per volume	Sham-NIRV	NIRV		LDV/BHDV/HDV	
	< 0.04 Gy	3×5 Gy	3×8 Gy	3×5 Gy	3×8 Gy
LOH	8	3	1	3	7
Tp53$^{+/C273X}$	3	2	6	5	2

Abbreviations: LOH, loss of heterozygosity; *Tp53*$^{+/C273X}$, heterozygous for *Tp53*; AN/CBCT, combined controls receiving anesthesia/cone-beam computed tomography only; NIRV, non-irradiated volume; LDV/BHDV/HDV, entire low-dose, bordering high-dose, and high dose volumes; Gy, Gray; 3×5 Gy or 3×8 Gy, three fractions of 5 or 8 Gy. Connecting with a slash means combined volumes.

Figure R8

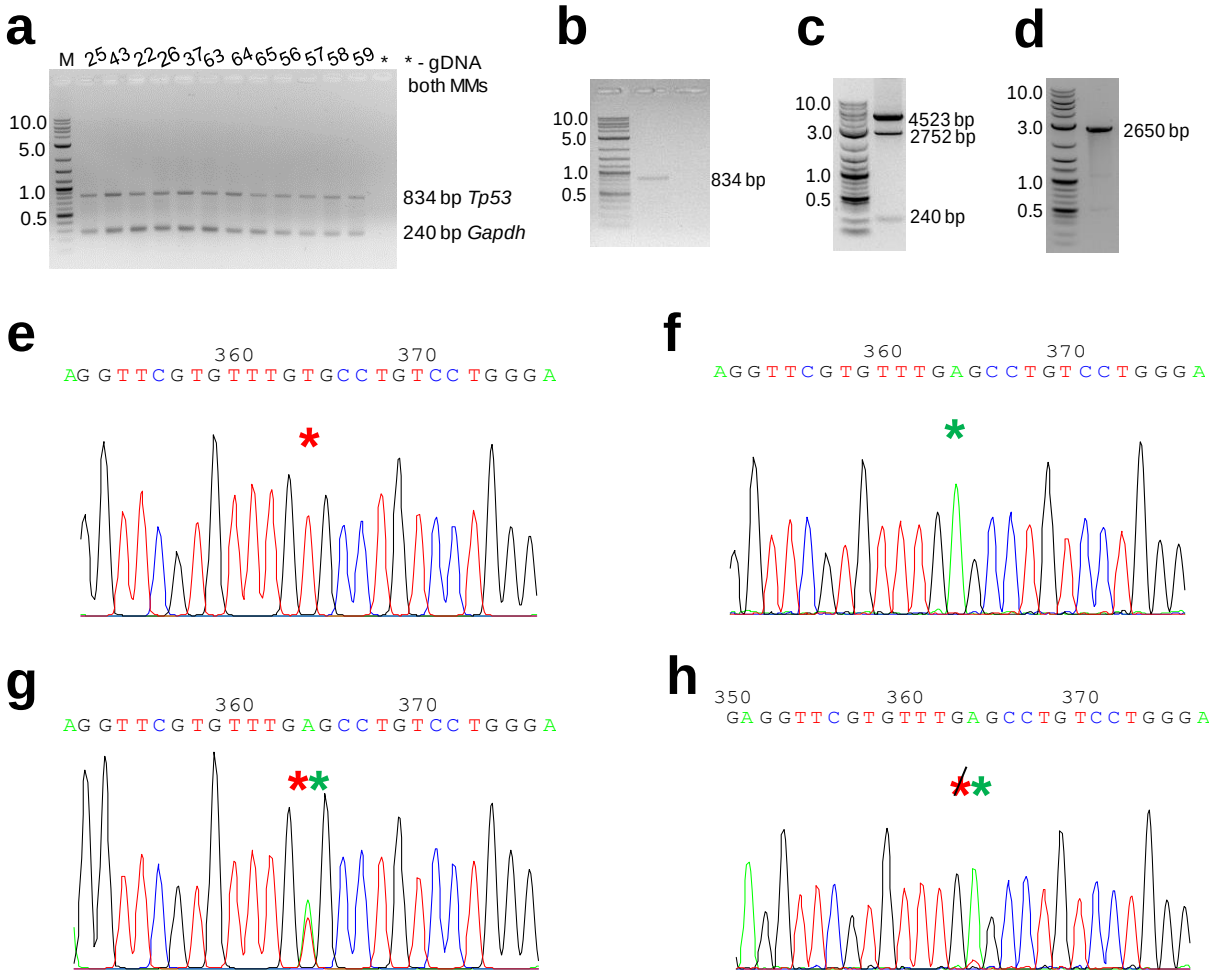

Fig. R8. Genotyping of normal and tumor *Tp53*. (**a**) PCR copies of 834 bp spanning *Tp53* and 240 bp *Gapdh* DNAs alongside negative controls (MMs)*. (**b**) A purified 834 bp PCR product before sequencing. (**c**) A 4523 bp spanning Chr10 amplicon from tumor gDNA with derived 2752 bp nested PCR product, and a 240 bp tumor *Gapdh*. (**d**) Nested PCR product with 2650 bp length amplified from 4523 bp PCR product. Typical sequencing chromatogram fragments for (**e**) $Tp53^{C273/C273}$, (**f**) $Tp53^{C273X/C273X}$, and (**g**) $Tp53^{+/C273X}$. (**h**) LOH ($Tp53^{C273X/C273X}$) in a tumor expressed as a strongly declined T-peak compared to A (the small T level may refer to tumor-adjacent residual normal tissue). Numbers above the nucleotide sequences represent readable base positions.

Abbreviations: gDNA, genomic DNA; M, marker; bp, base pair; *Tp53*, *Tumor protein 53*; *Gapdh*, *Glycerinaldehide-3-phosphate-dehydrogenase*; MMs, master mixes; PCR, polymerase chain reaction.

Figure R9

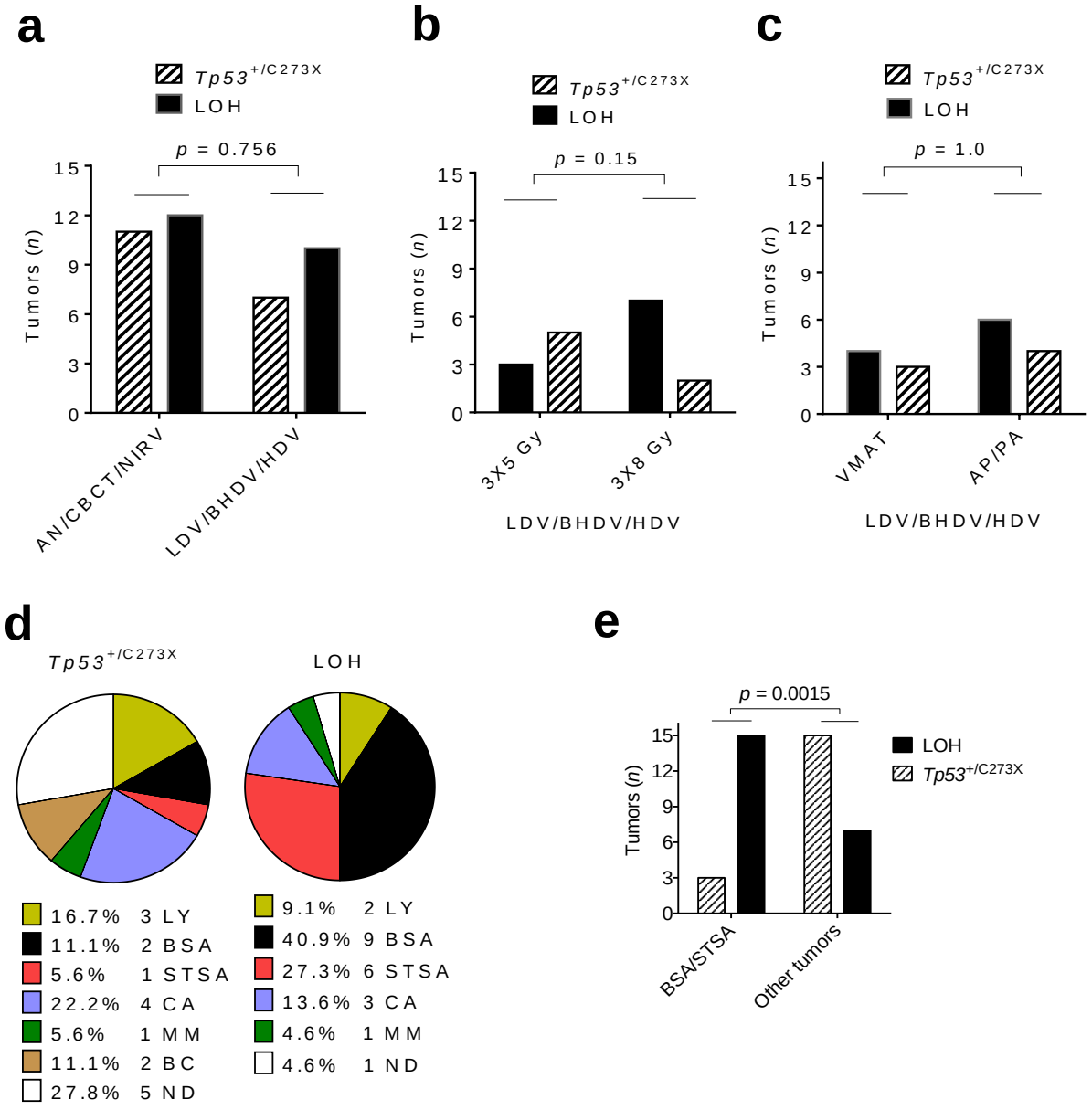

LOH analysis in tumors. (**a**) LOH was similarly occurred in tumors detected in irradiated (LDV/BHDV/HDV) and unirradiated (AN/CBCT/NIRV) body regions and no statistically significant differences in proportions of radiation-induced tumors with and without LOH in the LDV/BHDV/HDV between (**b**) 3×5 Gy and 3×8 Gy or (**c**) VMAT and AP/PA treated rats. (**d**) Analysis of different index tumors with and without LOH. **e**) LOH was more specific for sarcoma (BSA/STSA) compared to all other tumor types combined (Fisher's exact test).

Abbreviations: LOH, loss of heterozygosity; *Tp53*$^{+/C273X}$, heterozygous for *Tumor protein 53*; BSA, bone sarcoma; CA, carcinoma, STSA, soft tissue sarcoma; BT, brain tumor; BC, breast cancer; LY, lymphoma; MM, malignant mesothelioma; ND, non-determined; AN, anesthesia only controls; CBCT, cone-beam computed tomography only controls; NIRV, non-irradiated volume; LDV/BHDV/HDV, low-dose, bordering high-dose, and high dose volumes combined; Gy, Gray; 3×5 Gy or 3×8 Gy, three fractions of 5 or 8 Gy. Connecting with a slash means combined volumes, rat groups, or tumor entities.

LOH in tumors developed in the LDV/BHDV/HDV could not be specifically associated with prescribed total doses (3 of 8 tumors after 3×5 Gy vs. 7 of 9 tumors after 3×8 Gy, $p = 0.15$; **Figure R9b**) or with VMAT or AP/PA treatments (4 of 7 tumors after VMAT vs. 6 of 10 tumors after AP/PA, $p = 1.0$; **Figure R9c**).

Interestingly, most soft tissue sarcomas (6 out of 7) and bone sarcomas (9 of 11) revealed LOH in contrast to other tumors (7 of 22, $p = 0.0015$; **Figure R9d – e**).

A comparison of the median latency TTT and lifespan of $n = 18$ rats with *Tp53*$^{+/C273X}$ tumors with corresponding median values of $n = 22$ rats with tumors with LOH resulted in slightly reduced values for animals with tumors containing LOH led to slightly reduced values for animals with tumors with LOH, compared to those with heterozygous *Tp53*$^{+/C273X}$ tumors (**Figure R10**).

Figure R10

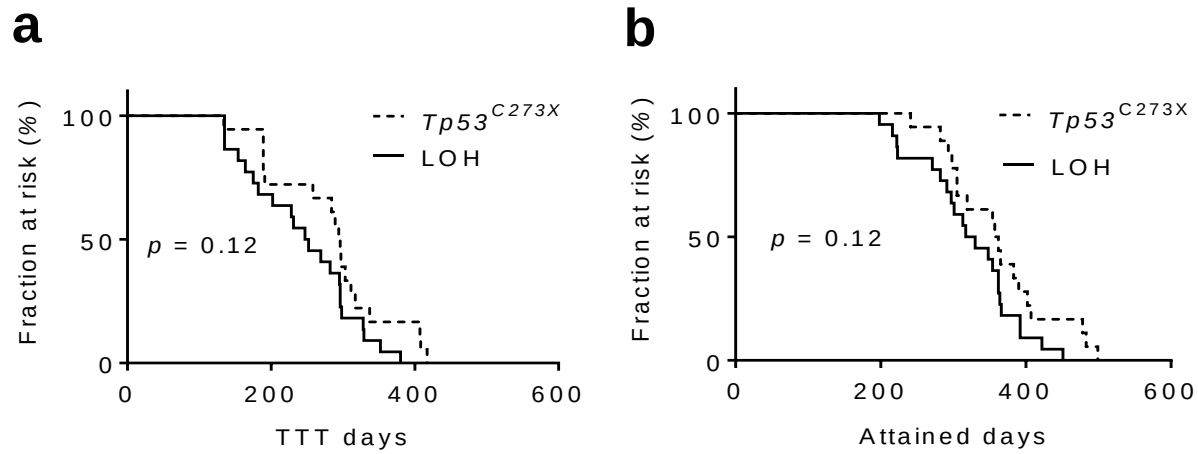

LOH and the latency of tumors. The Kaplan-Meier survival curves represent the proportions of living rats that decrease over time. (**a**) The median latency TTT from treatment of tested $n = 22$ rats developing tumors with LOH was somewhat but insignificantly shortened vs. rats developing tumors with *Tp53*$^{+/C273X}$ genotype ($n = 18$). (**b**) A similar trend shown in (a) was detected for attained days (full lifespan).

Abbreviations: LOH, loss of heterozygosity; TTT, time to tumor; *Tp53*$^{+/C273X}$, heterozygous for *Tumor protein 53*.

An analogous illustration was published in Sci Rep. 2019 Oct 29;9(1):15489.

Thus, the median TTT for tumors with LOH was 45.5 days shorter in comparison to tumors with *Tp53*$^{+/C273X}$: 249.5 [135 – 380] days vs. 295 [134 – 417] days, (p = 0.12). Accordingly, also the median lifespan was shortened by 36 days for tumors with LOH vs. *Tp53*$^{+/C273X}$: 395 [222 – 499] days vs. 323.5 [216 – 451] days (p = 0.12). Therefore, no significant difference between the latency of tumors with and without LOH could be observed.

3.8 Inflammatory alterations in irradiated and unirradiated rat lungs

Testing whether the malignant effects of radiation in rats could be influenced by radiation-specific inflammatory late alterations in irradiated thoracic volumes, several H&E-stained histology slides from thoracic organs were examined (**Table A7M**).

The numbers of rats with and without inflammatory events in the lungs are given in **Table R4**. Pathological examination of the thoracic tissue samples derived from the rats with tumors outside the thoracic region indicated predominant pulmonary inflammatory changes – multiple microscopic inflammatory foci appeared as agglomerated lymphocytes scattered into the normal cell community (**Figure R11a**).

Table R4

Inflammation in the lungs: scored as none (0), rare (1), moderate (2) and frequent (3) grade events.

Events per group	Grade 0	Grade 1	Grade 2	Grade 3	Total
AN	2	4	2	3	11
CBCT	3	2	6	0	11
VMAT 3×5 Gy	1	1	1	0	3
AP/PA 3×5 Gy	3	1	0	0	4
VMAT 3×8 Gy	1	5	3	0	9
AP/PA 3×8 Gy	1	1	1	0	3

Abbreviations: AN, anesthesia only controls; CBCT, cone-beam computed tomography only controls; NIRV, non-irradiated volume; VMAT, volumetric-modulated arc therapy; AP/PA, anterior-posterior/posterior-anterior irradiation; Gy, Gray; 3×5 Gy or 3×8 Gy, three fractions of 5 or 8 Gy.

Figure R11

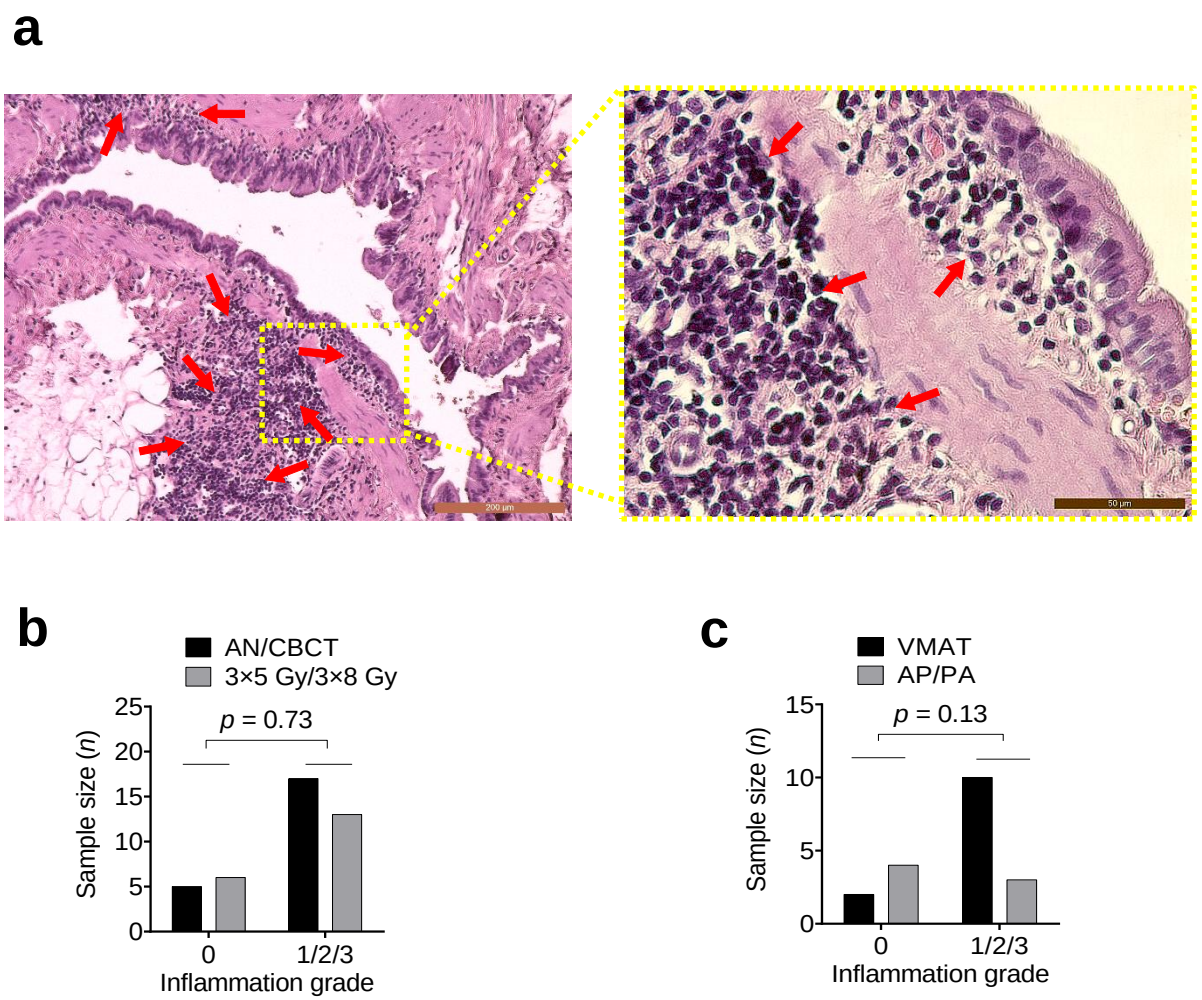

Inflammation in irradiated and unirradiated lungs. (**a)** Microscopically small inflammatory clusters in a tumor-free lung at a segmental bronchus. Arrows indicate the lymphocyte foci. H&E stain. Scale-bars: 500 µm and 50 µm. (**b**) Inflammation (any grades 1 – 3) was similarly detected in irradiated (3×5 Gy/3×8 Gy) and unirradiated (AN/CBCT) rat lungs (Fisher's exact test). (**d**) No significant connection of VMAT to inflammation, compared to AP/PA, was detected (Fisher's exact test). Connecting with a slash means combined groups or combined inflammation grades.

Abbreviations: AN, anesthesia only controls; CBCT, cone-beam computed tomography only controls; VMAT, volumetric-modulated arc therapy; AP/PA, anterior-posterior/posterior-anterior beams; Gy, Gray; 3×5 Gy or 3×8 Gy, three fractions of 5 or 8 Gy.

The images (a) and (b) were published in Sci Rep. 2019 Oct 29;9(1):15489.

No notable relationships between inflammation and irradiated volume or VMAT and AP/PA treatment could be detected in this experiment (**R11b – c**). Thus, both presence and absence of recognizable inflammation of any grade (1 – 3) were not significantly different between unirradiated and irradiated rats (n = 17 and n = 5, AN/CBCT vs. n = 13 and n = 6, 3×5 Gy/3×8 Gy respectively; p = 0.73). These events were also not significantly different for the rats treated with VMAT compared to AP/PA (n = 10 and n = 2 vs. n = 3 and n = 4, presence and absence respectively; p = 0.13).

3.9 Sex-associated features of tumors

The next question that was derived from the results obtained was, whether the malignant effects of radiation could be influenced by individual parameters such as sex. It was mentioned above that sex is related to the size of the rats and therefore to the size of the irradiated and non-irradiated volumes (see **Table M3** and **Table M4**).

There was no difference between the numbers of female and male rats in terms of the yield of tumors in NIRV or combined LDV/BHDV/HDV (**Figure R12a**).

The median TTTs in female and male rats developing tumors within the irradiated LDV/BHDV/HDV after irradiation with small or large radiation plans respectively were insignificantly (p = 0.17) different: 231 [134 – 408] days vs. 201 [102 – 322] days for n = 15 females and n = 18 males (**Figure R12b**). However, soft tissue sarcoma was frequent and lymphoma - rare in female rats, while inversely, fewer soft tissue sarcomas and more lymphomas were found in male rats: n = 18 sarcomas and n = 3 lymphomas compared to n = 2 sarcomas and n = 9 lymphomas (p = 0.0048) (**Figure R12c**).

An additional comparison of the median latency TTT for female sarcoma with corresponding TTT for male lymphoma resulted in an insignificant difference: 239 [134 – 380] days vs. 210 [102 – 298] days (p = 0.52), respectively (**Figure R12d**).

Taken together, the incidence of sarcoma and lymphoma within the volume exposed to highest doses in this experiment were coupled with female and male sex respectively while no notable difference in the TTT between these tumor types observed. See also discussion section 4.6.

Figure R12

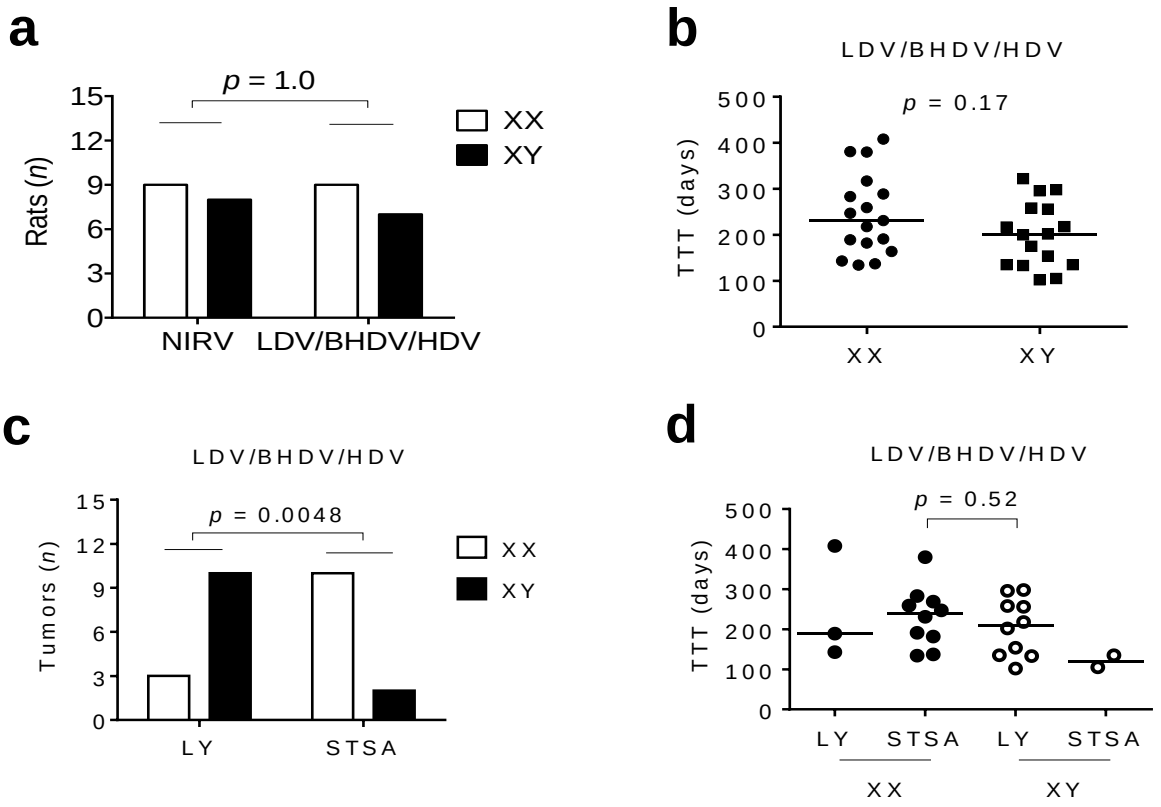

Some sex-linked traits of tumors. (**a**) Tumor development in irradiated and unirradiated volumes in female and male rats was not notably different. (**b**) No significant difference between median TTTs of radiation-associated tumors in female vs. male rats detected. (**c**) Significantly more LY than STSA were found in male rats in comparison to female rats that predominantly developed STSA. (**d**) No significant difference between TTTs for female STSA and male LY were detected.

Abbreviations: XX, females; XY, males; NIRV, non-irradiated volume; LDV/BHDV/HDV, low dose-, bordering high dose-, and high dose volumes combined; TTT, time to tumor; LY, lymphoma; STSA, soft tissue sarcoma. Connecting with a slash means combined dose volumes.

4 DISCUSSION

4.1 State of the art and aim of the study

There are prognostic studies predicting a worldwide increase in cancer incidence in the future [116,117]. Consequently, an increasing number of cancer patients will receive RT, also because of the increasing availability of RT centers worldwide. Due to improvements in oncology, and especially in RT, the rate of patients surviving cancer will be much higher in the future than ever before. Accordingly, the overall incidence of radiation-associated SC could rise with the increasing number of cancer survivors who underwent RT. Hence, it is becoming increasingly important to reduce the risk of radiation-associated SC.

There is an experimentally unproven dogma that IMRT can increase the risk of SC compared to 3D-CRT. Modern IMRT techniques are consequently avoided in many cases because of supposed disadvantages of low doses that conflict recommended reduction of unwanted high doses to normal tissue for prevention of radiation-related side effects.

The assumption of an additional increase in SCR after multi-beam IMRT, compared to 3D-CRT, have been estimated due to the longer irradiation time that IMRT requires to deliver the same radiation dose to the target volume than conventional 3D-CRT. Longer exposure times correlate with increased exposure to secondary low radiation doses (integral doses), and extended integral doses may increase the dose-response, especially in young RT patients [54-58]. However, the modern high-speed VMAT technique can reduce integral doses, due to advanced planning drafts, compared to older multi-beam IMRT.

In contrast to low doses, conventional 3D-CRT delivers more unwanted high doses to normal tissue than modern IMRT, and therefore, can even increase the dose-response (toward adverse effects including SC) as recognized by retrospective epidemiological studies [80,82,84,118].

It is consistent with clinical findings indicating that the risk of SC and other normal tissue complications decreases in childhood cancer survivors over the last decades with increased RT conformality [31,40,45]. Therefore, a reduction in the volume of normal tissue receiving high doses by high-conformal IMRT techniques, could even decrease the risk of SC. So, withholding modern IMRT techniques from patients because of the suspected disadvantages of a low-dose may increase the risk of side effects associated with high doses.

At the time of this study, no *in vivo* results were available that investigated to what extent different RT modalities can positively or negatively influence the risk of radiation-associated SC. The present study provides the first experimental evidence that SCR may increase with increased radiation dose to normal tissue and not specifically after IMRT vs. 3D-CRT (VMAT

vs. AP/PA), at least in a cancer-prone rat model. Since the presented experiment was a single study, more translational studies have to be done that may lead to a reevaluation of the common practice of withdrawal modern IMRT techniques from juvenile patients especially.

4.2 Relationships of radiation dose and RT technique to tumor development

At the beginning of the experiment, it was expected that radiation-induced tumors would occur within the irradiated body volume of rats and sporadic tumors within the NIRV. Since all sporadic tumors in controls were detected within the sham-NIRV and n = 33 treated rats developed tumors in the irradiated thoracic volume, tumors that developed in the sham-NIRV and NIRV were assumed to be spontaneous, and the tumors found in the irradiated volume assumed as radiation-induced or, at least, associated with radiation.

The AN control group was not exposed to any radiation other than follow-up CT scans and aimed to be a unirradiated reference group. The CBCT control group was used in the experiment to assess any possible effect of very low doses applied to rats during positioning on LINAC. In the absence of an accurate dosimetry method for calculating the radiation doses to which the rats were exposed during the CBCT scan, the CBCT fraction dose was roughly estimated at approximately 0.04 Gy per cm^3 exposed volume, according to the manufacturer's information. Therefore, rats belonging to this control group were exposed to cumulatively estimated doses of about 0.12 Gy during 3×CBCT-positioning, similar to those from radiation treatment groups. As illustrated in **Figure M5b**, the cone-beam covers almost the entire body of the rat from the head to the pelvic area. Thus, these CBCT doses are approximately comparable to the whole-body doses to which Japanese ABS were exposed. Since no notable differences in tumor incidence sites and TTTs were recognized between AN and CBCT controls, the rat model with applied experimental settings was unable to show any response to very low doses.

Modeling of radiation-induced carcinogenesis generally assumes a linear DRR in the low-dose region reaching saturation at higher doses [74,77,119-121]. The main uncertainty in SCR prediction bases on the dogma that 3D-CRT will lead to lower risk compared to IMRT. It rests on the assumption that the DRR increases linearly approximately between 4 – 8 Gy received doses with no further increase at higher doses [66,120]. This is explained by the proposed theory that exposed cells could survive low doses and cause SC while being sterilized by higher doses. The results obtained from the presented experiment, in contrast, do not confirm the increase in tumor induction in the tissues receiving lower doses compared to higher doses and are rather consistent with the results of epidemiological studies on cancer survivors assuming a linearly increase in

dose-response to RT for second sarcomas, basal cell carcinoma, meningioma, salivary gland cancer, glioma, breast cancer [80,122,123]. The predominant development of irradiated volume-associated tumors (23/33) in the HDV (receiving 13.5 – 15 Gy or 21.6 – 24 Gy) in the experiment further mirrors the evidence of clinical studies showing that most SCs after RT develop near the edge or inside the PTV and only approximately 20% in tissues receiving lower doses [15,84].

As indicated in **Table A4** and illustrated in **Figure R3**, the frequency distribution of tumors (the ratio of events per unit volume) was much higher in smaller-sized HDVs than in larger BHDVs and LDVs, without the specific influence of VMAT vs. AP/PA.

Most notably, no increased response to VMAT compared to AP/PA was observed with regard to radiation-induced tumor development, and therefore, no disadvantages of IMRT compared to 3D-CRT could be recognized.

4.3 Latency time of tumors related to local high-dose irradiation

In the experiment, an incidence-free follow-up period of at least 175 days was observed in which no detectable tumors occurred in any of 84 rats (both control and irradiated). A most simple, but indeed plausible explanation could be that aging determines the incidence time of tumors in these heterozygous rats. After translating the lifespan of rats into the lifespan of humans, the incidence-free follow-up period of 175 days in rats is comparable to around 12.7 years in humans because 13.8 days of life in rats correspond to one year of life in humans [124,125]. Thus, the tumor-free period in rats actually appears as translatable to a long-term SC-free period in humans, indicating that the animal model used in this study was suitable for studying the long-term response to high-dose radiation.

As expected previously, radiation-associated tumors may have some specific features that differ from sporadic tumors. At the end of the experiment, there was evidence found that the lifespan of some rats was shortened due to the decreased TTT latency for malignancies within the HDV exposed to the highest target dose (**Figure R3** and **Figure R4**).

Most importantly, the observed decrease in lifespan in 3×8 Gy treated rats was not stronger associated with VMAT than AP/PA since a median 16 days longer lifespan (282 days) after treatment with VMAT than AP/PA detected, compared to controls. According to the translation of the lifespan from rats to humans, every rat day equals approximately 34.8 human days, as described in Sengupta et al [125]. This could mean that the median lifetime after VMAT was by about 1.52 human years (557 human days) longer in contrast to AP/PA. Albeit such a

hypothetical translation may not seem plausible for RT professionals, the trend remains still conceivable. Thus, reducing undesirably high doses to normal tissue using IMRT could at least hypothetically postpone the development of SCs at later time points.

Since shortened lifespan and TTT in 3×8 Gy treated groups were caused by a specific decrease in TTT values for soft tissue sarcomas and lymphomas occurring within the HDV after 3×8 Gy treatment, the early development of these tumors could be directly associated with high doses and, correspondingly, with the increased response of tissues exposed to high doses. However, this does not imply that tissues that receive low doses had been protected against the development of radiation-related tumors. Even cumulative doses between 7.5 Gy and 12 Gy are more likely to cause cancer in this animal model, but such LDV tumors cannot be detectable due to the killing of the animals developing earlier sporadic or HDV tumors. Indeed, some irradiated animals euthanized also because of spontaneous tumor development. Otherwise, these animals might someday develop radiation-induced tumors in the LDV, HDV, and HDV.

It should be noted that the initial *Tp53*$^{+/C273X}$ heterozygosity in the original rat line was associated with shortened telomeres and decreased telomerase activities, but also prolonged tumor latency, in contrast to *Tp53*$^{C273X/C273X}$ homozygosity leading to early malignancies having longer telomeres [124]. This implies the hypothesis that the telomere context could have an impact on radiation carcinogenesis. In particular, studies of telomeres in radiation-induced and spontaneous tumors can provide interesting information about the telomere context in the case of radiation-induced shortening of the latency of *Tp53*-mutated tumors.

Interactions between radiation doses and genetic conditions in radiation carcinogenesis are interesting research subjects for which further experiments could address this problem.

4.4 Characteristics of radiation-associated and sporadic tumors

Radiation-related and sporadic tumor entities

Because both cumulatively applied doses (15 Gy and 24 Gy) in the experiment were responsible for the induction of radiation-associated tumors within the irradiated volume and a shortening of the TTT after 3×8 Gy irradiation was observed, it was questioned whether these effects could be specifically related to the recognized tumor entities. The hypothesis was that the entities might differ between tumors in differently irradiated and unirradiated volumes. Pathological examination of tumors detected in the experiment demonstrated that bone sarcoma and carcinoma were developed predominantly in the NIRV and sham NIRV, while all lymphoma and most soft tissue sarcoma were associated with the irradiated volume.

In the studies by van Boxtel *et al* [108] and Hermsen *et al* [124], most of the sporadic tumors in *Tp53*$^{+/C273X}$ rats were either bone sarcoma or soft tissue sarcoma whereas no carcinoma was detected. Unlike this, half of all sporadic tumors in another heterozygous *Tp53*$^{tm1[EGFP-pac]}$ rat line were lymphomas, while about a quarter of detected tumors were hemangiosarcomas and breast cancers, while sarcomas rarely occurred [110]. The homozygous rats of mentioned both lines mostly developed hemangiosarcomas but rarely also fibrosarcomas, rhabdomyosarcomas, B-type lymphomas, carcinomas, and some very rare non-determined tumors. These facts indicate that the spectra of sporadic tumors could vary between rats carrying different *Tp53* mutations.

The data obtained by the presented experiment show, however, no evidence of a sporadic specificity of lymphomas and soft tissue sarcomas (mostly rhabdomyosarcoma). Indeed, the specific appearance of lymphoma and sarcoma in irradiated body volumes (receiving doses of at least 13.5 Gy – 24 Gy) indicates the specific association of these tumor entities with high radiation doses. These translational findings are rather consistent with retrospective clinical data, showing the association of the second lymphoma and soft tissue sarcoma with volumes irradiated with high RT doses [80,82-85].

Out of all n = 31 bone sarcomas in the study, two were developed at the vertebra, two at the ribs, and one at the sternum in irradiated rats, while nine were found in the NIRV, nine in CBCT controls, and four in AN control group (**Table A7B – C**). Apparently, bone sarcoma was a highly metastatic tumor in p53 insufficient rats since the development of pulmonary metastases was observed in the presented experiment (**Figure R6a – b**). Sporadic bone sarcoma was also found in other *Tp53*$^{+/C273X}$ and *Tp53*$^{tm1[EGFP-pac]}$ rats mentioned above. Although five index and four additional bone sarcomas detected in the irradiated volume, this tumor type could not be truly associated with radiation. Since bone sarcoma predominantly occurred in NIRVs and controls in the presented experiment, and also in the studies by van Boxtel and Hermsen et al, that could be mostly assumed as sporadic tumors in this rat line. However, in patients, also second bone sarcomas have been evidently associated with high radiation doses [80].

Malignant mesothelioma is a relatively uncommon tumor in labor rats, but it was also found in the experiment. In particular, index mesotheliomas were detected in the mediastinum of two rats, one irradiated with 3×5 Gy VMAT (BHDV) and another with 3×8 Gy VMAT (HDV), but also in the NIRV, additionally to carcinomas, in the abdomen of two rats receiving anesthesia only (**Table A7B, F**). Therefore, it is not clear whether these mesotheliomas were surely related to radiation. However, it is to note that the second mesotheliomas were rarely detected within the large cohort of patients cured with RT against HL or non-HL [125].

There is no plausible reason to associate found carcinomas with radiation, as eight of these epithelial malignancies have occurred in parts of the body distant from the chest volume and only three cases were found in irradiated lungs. This either indicates that carcinomas can be only marginally associated with radiation, or the animal model and the methods used in this experiment were limited to study radiation-induced epithelial tumors. Moreover, the development of second carcinomas could be a species-specific sign of humans but not of rats used in the presented study.

The tumor developing sites in the animals of this study are given in **Table A7B**. Most of the tumors in control animals and in the NIRV of irradiated animals were developed at specific body parts such as limb bones or pelvic organs. These body parts may have an elevated cancer risk than other sites.

The primary origin of evidently non-osseous tumors, developed outside the thoracic volume in control and irradiated rats ($n = 5$ and $n = 8$, respectively), could not be determined exactly with H&E histology only. Additional tests on tumors using antibody-based immunohistochemistry can provide more information about the exact subtypes of these malignancies.

Taken together, there was a clear difference between the entities of tumors from irradiated and non-irradiated volumes. Thus, the development of lymphoma and soft tissue sarcoma was more likely related to irradiation, while bone sarcoma, malignant mesothelioma, carcinoma, breast cancer, brain tumors, and other non-determined tumors appeared to be sporadic tumors.

The next interesting topic was to review the possible relationship between a particular tumor type and corresponding TTT.

It must be mentioned again here that most of the rats remained tumor-free over a long period, without any detectable behavioral or conditional abnormalities during this time. Sick animals, by contrast, showed more than 10% weight loss of attained body masses and displayed several abnormalities of the general condition, coordination, activity, food and water uptake, or social behavior. These symptoms (not always all of them) appeared in rats a few days before tumors were discovered.

The TTTs could be possibly influenced by the entities of occurred tumors because some tumor types probably could tend to develop or grow more rapidly than the others. Therefore, the observed shortening of the TTT after a cumulative dose of about 24 Gy for tumors developed in HDV could be influenced by certain tumor entities. In addition, it should not be underestimated that the individual predisposition of rats to earlier cancer development somehow influenced the entity and latency of sporadic and radiogenic tumors in the present experiment.

In order to closely study the developmental properties of tumors at the cellular and molecular level, further investigations of the tumor samples are required. For example, a comparison of the activity of the marker of proliferation Ki-67 in tumor samples may provide evidence about the velocity of the tumor development in rats because Ki67 is an established marker of tumor growth, in particular for breast cancers in women [126-128].

An interesting trait of radiation-associated lymphomas in the experiment was the significantly earlier (by median 115 days) appearance in the HDV after 3×8 Gy compared to 3×5 Gy, as described in section 3.6 and shown in **Figure R7b**. This observation indicates that high radiation doses promote the early development of radiation-associated lymphoma in p53 insufficient rats. Anyway, a significant shortening of the TTT after 3×8 Gy irradiation was an effect of cumulatively received the highest doses that were responsible not only for the induction of radiation-associated tumors in the HDV but also suitable to shorten the latency of these tumors.

The findings concerning tumor entities are limited to some extent by restricted sample sizes. Further studies have to be conducted to verify the obtained research results. Expanding the groups of experimental subjects could possibly achieve greater statistical significance and thus clearer results. Indeed, a detailed characterization of radiation-related tumors in preclinical models could have important translational relevance for radiation-induced SC research.

LOH in radiation-related and sporadic tumors

The likelihood of spontaneous tumor development in mammals increases with *Tp53* insufficiency because the *Tp53* gene protects mammals from cancer, primarily through its role in cell cycle control, DNA repair, and apoptosis-mediated cell death [100,106,129,130]. Consequently, *TP53* mutations are found in approximately half of all and, mainly, in highly aggressive metastatic human tumors [94,131]. Loss of *Tp53* leads to dissemination and migration and, therefore, to tumor cell aggressiveness triggered by downregulation of cell adhesion signaling pathways [132,133]. Under these circumstances, LOH of $Tp53^{+/C273X}$ heterozygosity in rats may also result in an aggressive growth of tumors in rats. As detected in the experiment, at least 57% of all tested $n = 40$ tumors had LOH (**Table R3** and **Figure R9**). This data appears to be at least partially consistent with results reported by van Boxtel *et al* [108] and Hermsen *et al* [124] as LOH was detected in almost all (22 of 23) sporadic tumors (in both reports combined). In line with this, almost all tested bone and soft tissue sarcomas (83%, 15 of 17 combined) displayed LOH of the *Tp53* gene, in contrast to about a third (31.8%, 7 of 22) of all other tumors in our study.

It indicates that both bone and soft tissue sarcomas were highly prone to *Tp53*$^{+/C273X}$ LOH relative to other tumors.

A study comparing the hyper-reactivity of CpG dinucleotides between sporadic und radiation-related human tumors reveals evidence for specificity of *TP53* mutational 'hot spot codons' 134, 135, and 237 for radiation tumorigenesis in contrast to codons 175, 248, 273, 282, and 245, that are frequently found in human sporadic tumors [97]. In the present study, however, none of the homologous of these mutations recognized in tested tumors besides *Tp53*$^{+/C273X}$ shown in **Figure R8h**. Despite this, it is unknown whether other radiation-induced mutations than *Tp53*$^{C273X/C273X}$ LOH were involved in the tumorigenesis in this experiment.

In summary, LOH was not associated with radiation generally, with any lower or higher target doses (3×5 Gy or 3×8 Gy) as well as with irradiation modality (VMAT or AP/PA). More likely, LOH was of the same origin (C273X) in spontaneous and radiation-associated tumors. This may indicate that the *Tp53*$^{C273/X}$ LOH was rather spontaneous than radiation-induced.

4.5 Inflammatory alterations in irradiated and unirradiated tumor-free lungs

The development of SC in RT patients seems certainly not only due to the residual DNA damage that has occurred in a single cell. A study dealing with cancer evolution across the tree of life reports that cancer is generally characterized by a breakdown of the central features of the multicellularity, including proliferation, cell death, division of labor, resource allocation, and, extracellular environmental maintenance [134]. Presumably, there are various intrinsic and extrinsic causative factors acting over many years to establish a pre-cancerous environment, promoting SC in cancer survivors. Other findings have demonstrated that the quality of the changes in micro- and systemic- environments may promote radiation carcinogenesis[135-137]. Thus, the microenvironment appears to play an important role in promoting radiation dose-dependent effects that can emerge due to the anti-inflammatory effect of low doses [138] or pro-inflammatory effects caused by high doses [139]. Therefore, radiation used in the experiment could have caused some radiation-induced abnormalities, such as inflammation or fibrosis, paving the way for radiation-induced tumor development in irradiated normal tissues. So, it has been hypothesized that radiation can trigger SC development via determining the late effects within the irradiated normal tissue.

To recognize detectable non-neoplastic alterations in tumor-free lungs and mediastinal tissues, non-irradiated and irradiated tumor-free thoracic organ samples were examined by microscopy. However, this test revealed no significant differences in the number of inflammatory foci

between irradiated and unirradiated rat lungs or lungs exposed to different target doses (3×5 Gy or 3×8 Gy) or dose delivering techniques (VMAT or AP/PA) (**Figure R11b – c**). The lower incidence after AP/PA, in contrast to VMAT, relates there to a lower number of rats with tumor-free thorax after AP/PA treatment. Moreover, no other alterations, such as typical radiation-associated pneumonitis and/or fibrosis detected among these samples.
In general, inflammation in the tumor-free lungs of tested rats could not be specifically linked to radiation and, thus, also not with radiation-induced tumor development.

4.6 Study design

Animal model

As introduced above, only a small fraction of second primary cancers being considered radiation-induced in RT-treated cancer survivors. In line with this, wild-type rats are not well compatible for radiation-induced carcinogenesis experiments since the rate of expected radiogenic tumors would be very low and scarcely detectable in these animals. Since *Tp53* mutant rats develop spontaneous tumors, they should also be prone to radiation-induced cancer. Indeed, the detection of radiation-associated tumors in this experimental setup was only possible due to the susceptibility to tumors caused by the *Tp53* mutation. It was also taken into account that, due to earlier tumor development, homozygous rats have a very short life expectancy compared to wild-type and heterozygous animals [108,124]. For these reasons, functionally p53-haploinsufficient heterozygous rats, with expected longer survival than homozygous ones, were preferred for the experiment. Indeed, the $Tp53^{+/C273X}$ rat model was quite well suited to study the dose-response relationships of local irradiation and radiation-induced tumor development.
As mentioned above, cancer-prone $Tp53^{+/C273X}$ rats are haploinsufficient for p53 owing to a nonsense mutation in one of the *Tp53* sister alleles. This genetic condition mimics the genetic background of LFS in humans, as both rats and humans develop spontaneous tumors of various entities. In addition, specific point mutations have been found in LFS families that, due to their position within the *TP53* gene appear to be functionally similar to C273X of *Tp53* gene in rats. Due to evolutionary conservation, there are actually not large differences between DNA sequences of the core DNA-binding domain of the rat *Tp53* and human *TP53* genes. An example of a *Tp53* core fragment conserved evolutionary between humans and rats is shown in Appendix (**Sequence Information A1** – **A2**).

In *Tp53*$^{+/C273X}$ rats, codon C273 of the *Tp53* gene corresponds to codon 275 in human *TP53*. The neighboring mutational 'hotspot codons' H273 and R282 are similar to C273X in rats and frequently found in human tumors, including tumors in persons with LFS [102]. All these mutations are located within the same central fragment of the gene (rat exon 6 and human exon 8, respectively), encoding the core DNA-binding protein domain. Accordingly, the *Tp53*$^{+/C273X}$ haploinsufficiency in the experimental animal model increases the likelihood of radiation-associated cancer development similarly to LFS families. However, even small differences could influence the functions of genes. About 30% of mutations in human tumors, recorded in the somatic mutation database of the international agency for research on cancer – IARC, are missense mutations [97,104]. In contrast, C273X is a nonsense mutation, which does not result in a detectable truncated p53 protein in rats because of nonsense-mediated mRNA decay [108], while the missense mutations may result in new proteins with aberrant activities [93,94,140]. Thus, the *Tp53*^{C273X} mutation causes a real p53 insufficiency in the presented rat model, without possible residual effects of a truncated p53 variant.

Animal experiments are indispensable in biomedical research to examine very complex processes in a living system. At the same time, limiting the number of test animals to a necessary minimum is a prerequisite for the approval of an animal experiment by the competent authorities. As a guideline, the ethical principle of 3R [replace, reduce, refine] coined by William Russell and Rex Burch in 1959 should be implemented [141]. Since the aim of the experiment was to compare the number of rats developing radiation-induced malignancies between non-irradiated control groups, a sufficient number of control animals were required. In particular, for the Kaplan-Meier survival analysis, at least 12 – 14 animals per group is required, as described in Yan et al. [110]. Taking into account a possible dropout of about 10% of the animals, 15 rats per group considered as sufficient for such a study. The expected loss of experimental rats believed because of developing undetectable tumors or other non-tumor-related reasons. In the study, six rats were lost during the entire follow-up period, about 6.7% of all experimental animals (n = 90).

In addition to the main tumor-suppressive function, *Tp53* is involved in distinct essential cell-signaling pathways that regulate the development, metabolism, and self-renewal capacity of the cells [142,143]. Apparently, *Tp53* is not a key gene of laboratory rat development since homozygous mutants are born. Moreover, the reproduction of rats of this line in the presented study was possible as at least six male zero mutants were able to produce F2 generation through mating with wild-type females (also see **Table A1** and **Table A2**). Based on PCR amplification and sequence analysis of *Tp53* DNAs, n = 35 experimental rats with heterozygous *Tp53*$^{+/C273X}$

genotype were selected from F1 rat generation. Other experimental rats (n = 55) were not genotyped because these were the progeny of F1 wild-type female and homozygous male rats producing heterozygous progeny only. Thus, all rats used in the experiment had the same *Tp53*$^{+/C273X}$ background. Using homozygous males and wild-type females for breeding significantly reduces the total number of animals required for generating the *Tp53*$^{+/C273X}$ rats compared with heterozygous parents. The low number of ancestor rats limits the individual genetic heterogeneity in this experimental model and provides the possibility to compare radiation effects in genetically closely related animals. The balanced allocation of rats from each litter to different treatment groups done to balance possible false positive or negative influences of the ancestral background (**Table M1** and **Table A2**). At the same time, a possibly balanced distribution by sex, as well as the age and weight of rats at the treatment, aspired (**Table M2**, **Figure A1 – A2**).

Other p53-insufficient animal species would also have an interesting translational meaning for local dose-response research in order to determine the typical dose-response patterns that were conserved through the evolution between different species. Unlike *Tp53*^{C273X} rats, in *Transformation-related protein 53* (*Trp53*) knockout mice used in other studies, exon 2 – 6 has been replaced by the *neo* gene insert [144-146]. Also in *Tp53*$^{tm1[EGFP-pac]}$ rats, exon 2 – 5 fragment of *Tp53* gene is replaced by a reporter gene cassette [147]. Although some differences in Tp53 mutational signatures, there are general similarities, in terms of the type and the latency of sporadic tumors, between the other animal models mentioned above and rats used in this study. It is not clear, however, if the minor mutational differences between these models may influence the risk of radiation-induced carcinogenesis. Anyway, the comparison of the DRRs between these models could help to distinguish between radiation-specific and genetic-specific responses. However, it will be a long-lasting, very time-consuming, and expensive purpose.

Taken together, all experimental rats, whether recruited to controls or radiation treatment groups, had a similar genetic background and living conditions. Therefore, a similar background risk was expected. Ultimately, it was well possible to study the relationships between simulated SCs and different irradiation techniques with the chosen, standardized tumor-prone animal model.

Radiation planning and delivery

No published data were available on irradiation of rats of the strain used in this experiment. Therefore, it was assumed that the planned total doses are theoretically similar to the total doses of 19 Gy and 36 Gy recommended by the German Hodgkin study group for the treatment of

mediastinal HL. This consonance between rats and humans remains limited translatable, because exact dose-response models for rats do not exist.

A body size of a rat allows the radiation treatment carried out with a modern clinical LINAC equipped by a multi-leaf collimator system able to form the beam with a very small width at isocenter. It is less limited for rats than for smaller mice. However, there could be some limitations by means of precision in dose delivery to rats.

An accuracy of irradiation was ensured by an advanced beam-forming collimator system. Given the width of the x-ray beam, the collimator system of the LINAC used in this experiment enabled to cover a 300 mm^3 PTV with target doses while protecting the adjacent tissues, only a few millimeters distant from the PTV, from high doses.

The precision in irradiation could be negatively impaired in rats due to the high-frequency heart- and lung activities. On the other hand, after CBCT-positioning using the MOSAIQ® platform, the differences between the particularly used radiation plan and the actual position of the PTV were usually decreased as maximally as possible.

Both, the early and late effects of irradiation, can be influenced by the fractionation schedule [148]. The hypofractionated radiation regimen for every other day in the conducted experiment possibly helped to minimize expected negative physiological consequences of extensive anesthesia on successive days and to extend the total treatment time-window to five days.

Regarding radiation protection of radiosensitive organs such as, for example, spine and lungs, which are commonly also protected in patients during RT. The irradiation plans, therefore, were made with an avoiding the delivery of high doses to these organs as maximally as possible.

Taken together, all technical requirements were meet for creating radiation plans that are generally translatable in clinical VMAT and AP/PA plans.

Sex-associated differences in tumor development

In addition to organ-specific sensitivities to radiation in humans or even in rats, the induction of radiation-induced cancer can be influenced by the sex of an irradiated subject. An update of atomic bombing survivor's data in 2007 showed that the rates of solid tumors per Gy was higher for women than man (58% vs. 35%) [78]. In another study, cumulative SC incidence at 25 years after HL cure, was about 19% for females and 14% for males, whereas, excluding female breast cancer and prostate cancers, females have lower absolute risk for SC than males [22].

The sex-specific difference in dose-response after thoracic irradiation of women and men, especially in HL treatment, is represented by increased female second breast cancer incidence, as described in the literature [28,88,149]. Interestingly, although all four post-axillary mammary

glands in female rats were exposed to initial low doses during VMAT, no thoracic breast cancer could be observed in the low-dose volumes in female rats. Apparently, this rat model is also not notably prone to spontaneous breast cancer especially, since only three sporadic inguinal breast cancers were found in unirradiated volumes (**Table R3**).

The weight at treatment and the growth increment were lower in female than in male rats, but the treatment weight was balanced between the groups and there was no notable difference observed in the growth pattern of unirradiated and irradiated rats (**Figure A1**). Somewhat more variability in the body sizes at treatment and during the growth was observed between male rats, while the weight of female rats was more invariant. Since female rats were irradiated with small radiation plans and males with large plans, the overall number of irradiated cells should be lower in females than males. This could have consequences for dose-response toward tumor incidence and latency. However, a comparison showed that neither the incidence nor the TTT was significantly different for radiation-associated tumors between female and male rats (**Figure R12**).

By taking into the focus the entities of radiation-related tumors and to test a possible sex-specificity of tumors, radiation-associated lymphoma and soft tissue sarcoma appeared to be coupled with sex, without any notable variability between the median TTTs. Therefore, the strong TTT shortening after 3×8 Gy treatment could not be influenced by sex-coupled incidence of lymphoma and soft tissue sarcoma.

The increase in lymphoma incidence could also be related to increased received doses by larger thymus of male rats compared to females. This organ was exposed to high doses since located within the volume receiving more than 50% of each prescribed dose (3×5 Gy or 3×8 Gy).

Age at treatment and attained age

Childhood RT patients with mediastinal HL have an elevated risk of SC compared to adults [18,19,28,88]. An increase in risk of radiation-induced SC in children compared to adults has been supposed to be based on these three main reasons: first, the higher sensitivity of children to RT due to accelerated stem and progenitor cell proliferation rates, second, more critical response of the small body size of children to secondary scattered radiation, and third, genetic susceptibilities based on the frequent somatic mutations among pediatric cancer patients which are very rare [30,31,56,150]. Therefore, younger rats could have a bit higher risk for radiation-induced tumor development than older congeners. However, this was not confirmed in the presented experiment, since the age in 3×8 Gy irradiated groups (gender-mixed) was median 37.5 days higher compared to other groups (106 [81 – 124] vs. 68.5 [58 – 108] days), with insignificant

small variability between rats recruited to VMAT compared to AP/PA treatment groups (**Figure A2a**). According to the literature [151,152], laboratory rats are approximately 60 to 120 postnatal days in the young adult phase of their life. Therefore, all rats in the six experimental groups were young adults at the time of treatment and should have relatively similar background risks for tumor development. The main aim of the study, however, was to compare the response between two RT modalities and not between two different doses.

For the compensation of the older age in 3×8 Gy treated rats a rough simulation of the data by addition of the median 37.5 days to the TTTs was performed. Although the extension of the TTTs by 37.5 days, the simulated TTT compared to AN/CBCT remained significantly decreased for the malignancies developed in the HDV after 3×8 Gy irradiation only (191 [139.5 – 320.5] days, $p = 0.0005$), but no more for other tumors: median 264.5 [172.5 – 334.5] days for tumors in the NIRV, $p = 0.23$ and 261 [172.5 – 296.5] days for tumors within the LDV/BHDV combined, $p = 0.22$; **Figure A2b**). This indicates that a slightly older age should not be assumed to have a significant influence on the shortened latency of tumors after 3×8 Gy treatment of rats. Thus, there is clear evidence that high total doses could shorten the latency period for radiation-induced tumors, at least in cancer-prone rats.

Potential risk modifiers

The scenario of radiation-induced tumor development comprises several very complex successive events that are generated over time and interact with each other. In line with this, the risk of radiation-induced malignant late effects could be partly based on distinct early effects of the exposed normal tissues that display specific DRRs [118]. Indeed, it is currently believed that radiation carcinogenesis is the result of radiation-induced earlier and later effects on normal tissues, which can include multiple systemic reactions, such as premature aging, inflammation, genetic instability, vascular and immunity disorders, etc [153-157].

In this context, an increased risk for the development of radiation-associated breast cancer in a translational mice model has been associated with locally established tumor micro-environment [135-137,158,159].

Anyway, the micro-environment of tumors and the immune response of exposed tissues to different radiation doses will be a substantial topic for future studies as it is also described in different studies compiled in a paper by Deloch *et al* [160].

Overall, translational RT research is faced with the challenge of further expanding interdisciplinary and cross-thematic areas in order to determine in-depth knowledge of possible risk modifiers and to take this into account for clinical oncology and especially for RT.

5 CONCLUSION

The development of SC related to radiation treatment of cancers has been over a long time associated with received low doses based on the dose-response data derived from ABSs. Recent technological advances in RT allow treatment beams to be precisely tailored to different tumor geometries, achieving high conformality and avoiding high doses to normal tissue. A consequence of such highly conformal IMRT technology (such as VMAT) is that larger volumes of healthy tissue are exposed to low and moderate radiation doses. However, a widely accepted dogma in radiation oncology postulates that IMRT increases the risk of SC compared to conventional simple 3D-CRT techniques, such as AP/PA irradiation. For this reason, IMRT is avoided in patients, especially young patients, expected to survive long-term, and the withholding of the benefits of dose-sparing IMRT from patients, accepting thereby high dose-related risks for heart, breast, and other critical organs.

Challenging the assumption of increased late toxicity of IMRT by performing the first-of-its-kind experiment with cancer-susceptible rats irradiated with either VMAT or AP/PA, resulted in a predominant appearance of radiation-induced tumors in the regions receiving high doses unlike to low doses. The results obtained do not support the hypothesis that a larger low-dose volume during IMRT can increase the risk of SC, but rather suggest a greatly increased risk of SC per unit volume at higher doses. Most importantly, no increased tumor rates or decreased latency after VMAT vs. AP/PA were observed. Furthermore, the results for the first time demonstrated a significantly decreased latency time to tumors developing in the volume exposed to very high doses (24 Gy). Obtained results corroborate recent evidence from localized RT assuming a linear increase in a DRR up to 4 – 8 Gy received doses and does not support classical radiation carcinogenesis models assuming a saturation or even a decrease above this dose range, with no further increase at higher doses.

Because a reduction of doses and irradiated volumes in the treatment of childhood cancer has led to fewer SC and serious complications within the healthy tissue after RT, the reduced high-dose volume in modern conformal IMRT might decrease the risk of SC and possibly balance the hypothetical increase in risk associated with larger low-dose volumes.

Future translation studies looking at a more detailed characterization of dose-response relationships and the underlying mechanisms of radiation carcinogenesis after RT in living animals should be conducted to support the clinical use of modern IMRT techniques as safer modalities for cancer treatment as older RT techniques.

6 BIBLIOGRAPHY

1 Tobias, J. S. The role of radiotherapy in the management of cancer--an overview. *Ann Acad Med Singapore* **25**, 371-379 (1996).

2 Delaney, G., Jacob, S., Featherstone, C. & Barton, M. The role of radiotherapy in cancer treatment: estimating optimal utilization from a review of evidence-based clinical guidelines. *Cancer* **104**, 1129-1137, doi:10.1002/cncr.21324 (2005).

3 Atun, R. *et al.* Expanding global access to radiotherapy. *The Lancet Oncology* **16**, 1153-1186, doi:10.1016/S1470-2045(15)00222-3 (2015).

4 Oeffinger, K. C., Baxi, S. S., Friedman, D. N. & Moskowitz, C. S. Solid Tumor Second Primary Neoplasms: Who is at Risk, What Can We Do? *Semin Oncol* **40**, 676-689, doi:10.1053/j.seminoncol.2013.09.012 (2013).

5 Bernstein, J. L. *et al.* Radiation Exposure, the ATM Gene, and Contralateral Breast Cancer in the Women's Environmental Cancer and Radiation Epidemiology Study. *J Natl Cancer Inst* **102**, 475-483, doi:10.1093/jnci/djq055 (2010).

6 Bernstein, J. L. *et al.* Contralateral breast cancer after radiotherapy among BRCA1 and BRCA2 mutation carriers: a WECARE study report. *Eur J Cancer* **49**, 2979-2985, doi:10.1016/j.ejca.2013.04.028 (2013).

7 Best, T. *et al.* Variants at 6q21 implicate PRDM1 in the etiology of therapy-induced second malignancies after Hodgkin's lymphoma. *Nat Med* **17**, 941-943, doi:10.1038/nm.2407 (2011).

8 Pierce, L. J. & Haffty, B. G. Radiotherapy in the treatment of hereditary breast cancer. *Semin Radiat Oncol* **21**, 43-50, doi:10.1016/j.semradonc.2010.08.008 (2011).

9 Calle, E. E., Rodriguez, C., Walker-Thurmond, K. & Thun, M. J. Overweight, obesity, and mortality from cancer in a prospectively studied cohort of U.S. adults. *N Engl J Med* **348**, 1625-1638, doi:10.1056/NEJMoa021423 (2003).

10 Boffetta, P., Hashibe, M., La Vecchia, C., Zatonski, W. & Rehm, J. The burden of cancer attributable to alcohol drinking. *Int J Cancer* **119**, 884-887, doi:10.1002/ijc.21903 (2006).

11 Praud, D. *et al.* Cancer incidence and mortality attributable to alcohol consumption. *Int J Cancer* **138**, 1380-1387, doi:10.1002/ijc.29890 (2016).

12 Lorigan, P., Radford, J., Howell, A. & Thatcher, N. Lung cancer after treatment for Hodgkin's lymphoma: a systematic review. *Lancet Oncol* **6**, 773-779, doi:10.1016/s1470-2045(05)70387-9 (2005).

13 Do, K. A. *et al.* Longitudinal study of smoking patterns in relation to the development of smoking-related secondary primary tumors in patients with upper aerodigestive tract malignancies. *Cancer* **101**, 2837-2842, doi:10.1002/cncr.20714 (2004).

14 Henderson, T. O. *et al.* Breast Cancer Risk in Childhood Cancer Survivors Without a History of Chest Radiotherapy: A Report From the Childhood Cancer Survivor Study. *J Clin Oncol* **34**, 910-918, doi:10.1200/jco.2015.62.3314 (2016).

15 Travis, L. B. *et al.* Lung cancer following chemotherapy and radiotherapy for Hodgkin's disease. *J Natl Cancer Inst* **94**, 182-192 (2002).

16 Dores, G. M. *et al.* Second malignant neoplasms among long-term survivors of Hodgkin's disease: a population-based evaluation over 25 years. *J Clin Oncol* **20**, 3484-3494, doi:10.1200/jco.2002.09.038 (2002).

17 Sigurdson, A. J. *et al.* Primary thyroid cancer after a first tumour in childhood (the Childhood Cancer Survivor Study): a nested case-control study. *Lancet* **365**, 2014-2023, doi:10.1016/s0140-6736(05)66695-0 (2005).

18 Bhatia, S. *et al.* Breast Cancer and Other Second Neoplasms after Childhood Hodgkin's Disease. *New England Journal of Medicine* **334**, 745-751, doi:10.1056/nejm199603213341201 (1996).

19 Travis, L. B. *et al.* Breast cancer following radiotherapy and chemotherapy among young women with Hodgkin disease. *Jama* **290**, 465-475, doi:10.1001/jama.290.4.465 (2003).
20 Barbaro, P. M. *et al.* Reduced incidence of second solid tumors in survivors of childhood Hodgkin's lymphoma treated without radiation therapy. *Ann Oncol* **22**, 2569-2574, doi:10.1093/annonc/mdr013 (2011).
21 Ng, J. & Shuryak, I. Minimizing second cancer risk following radiotherapy: current perspectives. *Cancer Management and Research* **7**, 1-11, doi:10.2147/CMAR.S47220 (2015).
22 Curtis RE, F. D., Ron E, Ries LAG, Hacker DG, Edwards BK, Tucker MA, Fraumeni JF Jr. (eds). New Malignancies Among Cancer Survivors: SEER Cancer Registries, 1973-2000. *National Cancer Institute. NIH Publ. No. 05-5302. Bethesda, MD* (2006).
23 Howlader, N. N., AM.; Krapcho, M.; Garshell, J.; Neyman, N.; Altekruse, SF.; Kosary, CL.;, Yu, M. R., J.; Tatalovich, Z.; Cho, H.; Mariotto, A.; Lewis, DR.; Chen, HS.; Feuer, EJ.; Cronin, & KA., e. in *Bethesda, MD: National Cancer Institute; 1975–2010* Vol. http://seer.cancer.gov/csr/1975_2010/, based on November 2012 SEER data submission,
posted to the SEER web site, April 2013 (2013).
24 Zaorsky, N. G. *et al.* Causes of death among cancer patients. *Annals of oncology : official journal of the European Society for Medical Oncology* **28**, 400-407, doi:10.1093/annonc/mdw604 (2017).
25 Berrington de Gonzalez, A. *et al.* Proportion of second cancers attributable to radiotherapy treatment in adults: a cohort study in the US SEER cancer registries. *Lancet Oncol* **12**, 353-360, doi:10.1016/s1470-2045(11)70061-4 (2011).
26 Epstein, R., Hanham, I. & Dale, R. Radiotherapy-induced second cancers: are we doing enough to protect young patients? *Eur J Cancer* **33**, 526-530, doi:10.1016/s0959-8049(97)00056-7 (1997).
27 Boivin, J. F. *et al.* Incidence of second cancers in patients treated for Hodgkin's disease. *J Natl Cancer Inst* **87**, 732-741 (1995).
28 Travis, L. B. *et al.* Cumulative absolute breast cancer risk for young women treated for Hodgkin lymphoma. *J Natl Cancer Inst* **97**, 1428-1437, doi:10.1093/jnci/dji290 (2005).
29 Ng, A. K. *et al.* Second malignancy after Hodgkin disease treated with radiation therapy with or without chemotherapy: long-term risks and risk factors. *Blood* **100**, 1989-1996, doi:10.1182/blood-2002-02-0634 (2002).
30 Omer, B. *et al.* Patterns of subsequent malignancies after Hodgkin lymphoma in children and adults. *Br J Haematol* **158**, 615-625, doi:10.1111/j.1365-2141.2012.09211.x (2012).
31 Turcotte, L. M. *et al.* Temporal Trends in Treatment and Subsequent Neoplasm Risk Among 5-Year Survivors of Childhood Cancer, 1970-2015. *Jama* **317**, 814-824, doi:10.1001/jama.2017.0693 (2017).
32 Dörffel, W., Riepenhausen, M., Lüders, H., Brämswig, J. & Schellong, G. Secondary Malignancies Following Treatment for Hodgkin's Lymphoma in Childhood and Adolescence: A Cohort Study With More Than 30 Years' Follow-up. *Dtsch Arztebl Int* **112**, 320-327, doi:10.3238/arztebl.2015.0320 (2015).
33 Maule, M. *et al.* Risk of second malignant neoplasms after childhood leukemia and lymphoma: an international study. *J Natl Cancer Inst* **99**, 790-800, doi:10.1093/jnci/djk180 (2007).
34 O'Brien, M. M., Donaldson, S. S., Balise, R. R., Whittemore, A. S. & Link, M. P. Second Malignant Neoplasms in Survivors of Pediatric Hodgkin's Lymphoma Treated

With Low-Dose Radiation and Chemotherapy. *J Clin Oncol* **28**, 1232-1239, doi:10.1200/jco.2009.24.8062 (2010).

35 Metayer, C. *et al.* Second cancers among long-term survivors of Hodgkin's disease diagnosed in childhood and adolescence. *J Clin Oncol* **18**, 2435-2443, doi:10.1200/jco.2000.18.12.2435 (2000).

36 Fuchs, M., Diehl, V. & Re, D. Current Strategies and New Approaches in the Treatment of Hodgkin's Lymphoma. *Pathobiology* **73**, 126-140 (2006).

37 Wenz, F., Abo-Madyan, Y., Welzel, G. & Giordano, F. A. ABVD vs. radiotherapy in early stage Hodgkin's lymphoma. *Strahlentherapie und Onkologie* **188**, 649-652, doi:10.1007/s00066-012-0151-y (2012).

38 Castellino, S. M. *et al.* Morbidity and mortality in long-term survivors of Hodgkin lymphoma: a report from the Childhood Cancer Survivor Study. *Blood*, doi:10.1182/blood-2010-04-278796 (2010).

39 Constine, L. S. *et al.* The Role of Radiation Therapy in Patients With Relapsed or Refractory Hodgkin Lymphoma: Guidelines From the International Lymphoma Radiation Oncology Group. *International Journal of Radiation Oncology*Biology*Physics* **100**, 1100-1118, doi:https://doi.org/10.1016/j.ijrobp.2018.01.011 (2018).

40 LeMieux, M. H., Solanki, A. A., Mahmood, U., Chmura, S. J. & Koshy, M. Risk of second malignancies in patients with early-stage classical Hodgkin's lymphoma treated in a modern era. *Cancer Med* **4**, 513-518, doi:10.1002/cam4.405 (2015).

41 De, A. *et al.* Correlation of pulmonary function abnormalities with dose volume histograms in children treated with lung irradiation. *Pediatr Pulmonol* **50**, 596-603, doi:10.1002/ppul.23034 (2015).

42 Yahalom, J. & Mauch, P. The involved field is back: issues in delineating the radiation field in Hodgkin's disease. *Ann Oncol* **13 Suppl 1**, 79-83, doi:10.1093/annonc/13.s1.79 (2002).

43 Specht, L. *et al.* Modern radiation therapy for Hodgkin lymphoma: field and dose guidelines from the international lymphoma radiation oncology group (ILROG). *Int J Radiat Oncol Biol Phys* **89**, 854-862, doi:10.1016/j.ijrobp.2013.05.005 (2014).

44 Maraldo, M. V. *et al.* Estimated risk of cardiovascular disease and secondary cancers with modern highly conformal radiotherapy for early-stage mediastinal Hodgkin lymphoma. *Ann Oncol* **24**, 2113-2118, doi:10.1093/annonc/mdt156 (2013).

45 Koeck, J. *et al.* Radiotherapy for early mediastinal Hodgkin lymphoma according to the German Hodgkin Study Group (GHSG): the roles of intensity-modulated radiotherapy and involved-node radiotherapy. *Int J Radiat Oncol Biol Phys* **83**, 268-276, doi:10.1016/j.ijrobp.2011.05.054 (2012).

46 Willner, J., Jost, A., Baier, K. & Flentje, M. A little to a lot or a lot to a little? An analysis of pneumonitis risk from dose-volume histogram parameters of the lung in patients with lung cancer treated with 3-D conformal radiotherapy. *Strahlenther Onkol* **179**, 548-556 (2003).

47 Ng, A. K. Current survivorship recommendations for patients with Hodgkin lymphoma: focus on late effects. *Blood* **124**, 3373-3379, doi:10.1182/blood-2014-05-579193 (2014).

48 Vijayakumar, S. & Chen, G. T. Implementation of three dimensional conformal radiation therapy: prospects, opportunities, and challenges. *Int J Radiat Oncol Biol Phys* **33**, 979-983, doi:10.1016/0360-3016(95)02060-8 (1995).

49 Ezzell, G. A. *et al.* Guidance document on delivery, treatment planning, and clinical implementation of IMRT: Report of the IMRT subcommittee of the AAPM radiation therapy committee. *Medical Physics* **30**, 2089-2115, doi:10.1118/1.1591194 (2003).

50 Otto, K. Volumetric modulated arc therapy: IMRT in a single gantry arc. *Medical Physics* **35**, 310-317, doi:10.1118/1.2818738 (2008).

51 Teoh, M., Clark, C. H., Wood, K., Whitaker, S. & Nisbet, A. Volumetric modulated arc therapy: a review of current literature and clinical use in practice. *Br J Radiol* **84**, 967-996, doi:10.1259/bjr/22373346 (2011).

52 Wolff, D. *et al.* Volumetric modulated arc therapy (VMAT) vs. serial tomotherapy, step-and-shoot IMRT and 3D-conformal RT for treatment of prostate cancer. *Radiother Oncol* **93**, 226-233, doi:10.1016/j.radonc.2009.08.011 (2009).

53 Wolff, D. *et al.* Clinical implementation of volumetric intensity-modulated arc therapy (VMAT) with ERGO++. *Strahlenther Onkol* **186**, 280-288, doi:10.1007/s00066-010-2071-z (2010).

54 Followill, D., Geis, P. & Boyer, A. Estimates of whole-body dose equivalent produced by beam intensity modulated conformal therapy. *International Journal of Radiation Oncology*Biology*Physics* **38**, 667-672, doi:https://doi.org/10.1016/S0360-3016(97)00012-6 (1997).

55 Hall, E. J. Henry S. Kaplan Distinguished Scientist Award 2003. The crooked shall be made straight; dose-response relationships for carcinogenesis. *Int J Radiat Biol* **80**, 327-337, doi:10.1080/09553000410001695895 (2004).

56 Hall, E. J. Intensity-modulated radiation therapy, protons, and the risk of second cancers. *Int J Radiat Oncol Biol Phys* **65**, 1-7, doi:10.1016/j.ijrobp.2006.01.027 (2006).

57 Kry, S. F. *et al.* The calculated risk of fatal secondary malignancies from intensity-modulated radiation therapy. *Int J Radiat Oncol Biol Phys* **62**, 1195-1203, doi:10.1016/j.ijrobp.2005.03.053 (2005).

58 Paganetti, H. ASSESSMENT OF THE RISK FOR DEVELOPING A SECOND MALIGNANCY FROM SCATTERED AND SECONDARY RADIATION IN RADIATION THERAPY. *Health physics* **103**, 652-661, doi:10.1097/HP.0b013e318261113d (2012).

59 Sterzing, F., Engenhart-Cabillic, R., Flentje, M. & Debus, J. Image-guided radiotherapy: a new dimension in radiation oncology. *Deutsches Arzteblatt international* **108**, 274-280, doi:10.3238/arztebl.2011.0274 (2011).

60 Boda-Heggemann, J. *et al.* Fiducial-based quantification of prostate tilt using cone beam computer tomography (CBCT). *Radiother Oncol* **85**, 247-250, doi:10.1016/j.radonc.2007.09.008 (2007).

61 Boda-Heggemann, J., Lohr, F., Wenz, F., Flentje, M. & Guckenberger, M. kV cone-beam CT-based IGRT: a clinical review. *Strahlenther Onkol* **187**, 284-291, doi:10.1007/s00066-011-2236-4 (2011).

62 Wertz, H. *et al.* Image-guided in vivo dosimetry for quality assurance of IMRT treatment for prostate cancer. *Int J Radiat Oncol Biol Phys* **67**, 288-295, doi:10.1016/j.ijrobp.2006.09.008 (2007).

63 Wertz, H. *et al.* Dosimetric consequences of a translational isocenter correction based on image guidance for intensity modulated radiotherapy (IMRT) of the prostate. *Phys Med Biol* **52**, 5655-5665, doi:10.1088/0031-9155/52/18/012 (2007).

64 Kan, M. W., Leung, L. H., Wong, W. & Lam, N. Radiation dose from cone beam computed tomography for image-guided radiation therapy. *Int J Radiat Oncol Biol Phys* **70**, 272-279, doi:10.1016/j.ijrobp.2007.08.062 (2008).

65 Hess, C. B. *et al.* Exposure Risks Among Children Undergoing Radiation Therapy: Considerations in the Era of Image Guided Radiation Therapy. *International Journal of Radiation Oncology • Biology • Physics* **94**, 978-992, doi:10.1016/j.ijrobp.2015.12.372 (2016).

66 Hall, E. J. & Wuu, C.-S. Radiation-induced second cancers: the impact of 3D-CRT and IMRT. *International Journal of Radiation Oncology • Biology • Physics* **56**, 83-88, doi:10.1016/S0360-3016(03)00073-7.

67 Schneider, U. & Walsh, L. Cancer risk estimates from the combined Japanese A-bomb and Hodgkin cohorts for doses relevant to radiotherapy. *Radiat Environ Biophys* **47**, 253-263, doi:10.1007/s00411-007-0151-y (2008).

68 Schneider, U. Modeling the Risk of Secondary Malignancies after Radiotherapy. *Genes* **2**, 1033-1049, doi:10.3390/genes2041033 (2011).

69 Schneider, U., Zwahlen, D., Ross, D. & Kaser-Hotz, B. Estimation of radiation-induced cancer from three-dimensional dose distributions: Concept of organ equivalent dose. *International Journal of Radiation Oncology • Biology • Physics* **61**, 1510-1515, doi:10.1016/j.ijrobp.2004.12.040.

70 Schneider, U., Sumila, M. & Robotka, J. Site-specific dose-response relationships for cancer induction from the combined Japanese A-bomb and Hodgkin cohorts for doses relevant to radiotherapy. *Theor Biol Med Model* **8**, 27, doi:10.1186/1742-4682-8-27 (2011).

71 Hall, E. J. G., Amato J. . *Radiobiology for the radiologist*. (Wolters Kluwer Health/Lippincott Williams & Wilkins, c2012., 2011).

72 Hall, E. J. & Wuu, C. S. Radiation-induced second cancers: the impact of 3D-CRT and IMRT. *Int J Radiat Oncol Biol Phys* **56**, 83-88 (2003).

73 Hall, E. J. Is there a place for quantitative risk assessment? *J Radiol Prot* **29**, A171-184, doi:10.1088/0952-4746/29/2a/s12 (2009).

74 Wheldon, E. G., Lindsay, K. A. & Wheldon, T. E. The dose-response relationship for cancer incidence in a two-stage radiation carcinogenesis model incorporating cellular repopulation. *Int J Radiat Biol* **76**, 699-710 (2000).

75 Fowler, J. F. The linear-quadratic formula and progress in fractionated radiotherapy. *Br J Radiol* **62**, 679-694 (1989).

76 Joiner, M. C. & van der Kogel, A. in *123Library* (CRC Press, 2009).

77 Schneider, U. Mechanistic model of radiation-induced cancer after fractionated radiotherapy using the linear-quadratic formula. *Med Phys* **36**, 1138-1143, doi:10.1118/1.3089792 (2009).

78 Preston, D. L. *et al.* Solid Cancer Incidence in Atomic Bomb Survivors: 1958–1998. *Radiation Research* **168**, 1-64, doi:10.1667/RR0763.1 (2007).

79 Ozasa, K. *et al.* Studies of the mortality of atomic bomb survivors, Report 14, 1950-2003: an overview of cancer and noncancer diseases. *Radiat Res* **177**, 229-243 (2012).

80 Berrington de Gonzalez, A. *et al.* Second solid cancers after radiation therapy: a systematic review of the epidemiologic studies of the radiation dose-response relationship. *Int J Radiat Oncol Biol Phys* **86**, 224-233, doi:10.1016/j.ijrobp.2012.09.001 (2013).

81 Ng, J. *et al.* Predicting the risk of secondary lung malignancies associated with whole-breast radiation therapy. *Int J Radiat Oncol Biol Phys* **83**, 1101-1106, doi:10.1016/j.ijrobp.2011.09.052 (2012).

82 Gilbert, E. S. *et al.* Stomach Cancer Following Hodgkin Lymphoma, Testicular Cancer and Cervical Cancer: A Pooled Analysis of Three International Studies with a Focus on Radiation Effects. *Radiat Res* **187**, 186-195, doi:10.1667/rr14453.1 (2017).

83 Tukenova, M. *et al.* Radiation therapy and late mortality from second sarcoma, carcinoma, and hematological malignancies after a solid cancer in childhood. *Int J Radiat Oncol Biol Phys* **80**, 339-346, doi:10.1016/j.ijrobp.2010.02.004 (2011).

84 Diallo, I. *et al.* Frequency distribution of second solid cancer locations in relation to the irradiated volume among 115 patients treated for childhood cancer. *Int J Radiat Oncol Biol Phys* **74**, 876-883, doi:10.1016/j.ijrobp.2009.01.040 (2009).

85 Dorr, W. & Herrmann, T. Second primary tumors after radiotherapy for malignancies. Treatment-related parameters. *Strahlenther Onkol* **178**, 357-362 (2002).
86 Preston, D. L., Shimizu, Y., Pierce, D. A., Suyama, A. & Mabuchi, K. Studies of mortality of atomic bomb survivors. Report 13: Solid cancer and noncancer disease mortality: 1950-1997. *Radiat Res* **160**, 381-407 (2003).
87 Wolden, S. L., Lamborn, K. R., Cleary, S. F., Tate, D. J. & Donaldson, S. S. Second cancers following pediatric Hodgkin's disease. *Journal of Clinical Oncology* **16**, 536-544, doi:10.1200/jco.1998.16.2.536 (1998).
88 Schellong, G. *et al.* Breast Cancer in Young Women After Treatment for Hodgkin's Disease During Childhood or Adolescence: An Observational Study With up to 33-Year Follow-up. *Dtsch Arztebl Int* **111**, 3-9, doi:10.3238/arztebl.2014.0003 (2014).
89 ICRP. The 2007 Recommendations of the International Commission on Radiological Protection. ICRP publication 103. *Ann ICRP* **37**, 1-332, doi:10.1016/j.icrp.2007.10.003 (2007).
90 Huszno, J., Budryk, M., Kolosza, Z. & Nowara, E. The influence of BRCA1/BRCA2 mutations on toxicity related to chemotherapy and radiotherapy in early breast cancer patients. *Oncology* **85**, 278-282, doi:10.1159/000354834 (2013).
91 Thompson, D. & Easton, D. The genetic epidemiology of breast cancer genes. *J Mammary Gland Biol Neoplasia* **9**, 221-236, doi:10.1023/B:JOMG.0000048770.90334.3b (2004).
92 Álvarez-Quilón, A. *et al.* ATM specifically mediates repair of double-strand breaks with blocked DNA ends. *Nature communications* **5**, 3347-3347, doi:10.1038/ncomms4347 (2014).
93 Guimaraes, D. P. & Hainaut, P. TP53: a key gene in human cancer. *Biochimie* **84**, 83-93 (2002).
94 Rivlin, N., Brosh, R., Oren, M. & Rotter, V. Mutations in the p53 Tumor Suppressor Gene: Important Milestones at the Various Steps of Tumorigenesis. *Genes Cancer* **2**, 466-474, doi:10.1177/1947601911408889 (2011).
95 Hisada, M., Garber, J. E., Fung, C. Y., Fraumeni, J. F., Jr. & Li, F. P. Multiple primary cancers in families with Li-Fraumeni syndrome. *J Natl Cancer Inst* **90**, 606-611 (1998).
96 Malkin, D. *et al.* Germ line p53 mutations in a familial syndrome of breast cancer, sarcomas, and other neoplasms. *Science* **250**, 1233-1238 (1990).
97 Gonin-Laurent, N. *et al.* Specific TP53 mutation pattern in radiation-induced sarcomas. *Carcinogenesis* **27**, 1266-1272, doi:10.1093/carcin/bgi356 (2006).
98 Nakanishi, H. *et al.* Mutation of the p53 gene in postradiation sarcoma. *Lab Invest* **78**, 727-733 (1998).
99 Rümenapp, C. *et al.* Secondary Radiation-Induced Bone Tumours Demonstrate a High Degree of Genomic Instability Predictive of a Poor Prognosis. *Curr Genomics* **13**, 433-437, doi:10.2174/138920212802510420 (2012).
100 Levine, A. J., Momand, J. & Finlay, C. A. The p53 tumour suppressor gene. *Nature* **351**, 453, doi:10.1038/351453a0 (1991).
101 Tada, M., Sawamura, Y., Abe, H. & Iggo, R. Homozygous p53 gene mutation in a radiation-induced glioblastoma 10 years after treatment for an intracranial germ cell tumor: case report. *Neurosurgery* **40**, 393-396 (1997).
102 Pfeifer, G. P. p53 mutational spectra and the role of methylated CpG sequences. *Mutat Res* **450**, 155-166 (2000).
103 Petitjean, A. *et al.* Impact of mutant p53 functional properties on TP53 mutation patterns and tumor phenotype: lessons from recent developments in the IARC TP53 database. *Hum Mutat* **28**, 622-629, doi:10.1002/humu.20495 (2007).

104 Olivier, M., Hollstein, M. & Hainaut, P. TP53 mutations in human cancers: origins, consequences, and clinical use. *Cold Spring Harb Perspect Biol* **2**, a001008, doi:10.1101/cshperspect.a001008 (2010).
105 Rashi-Elkeles, S. *et al.* Transcriptional modulation induced by ionizing radiation: p53 remains a central player. *Mol Oncol* **5**, doi:10.1016/j.molonc.2011.06.004 (2011).
106 Marcel, V. *et al.* Biological functions of p53 isoforms through evolution: lessons from animal and cellular models. *Cell Death Differ* **18**, 1815-1824, doi:10.1038/cdd.2011.120 (2011).
107 Ootsuyama, A. *et al.* Frequent p53 mutation in mouse tumors induced by repeated beta-irradiation. *Mol Carcinog* **11**, 236-242 (1994).
108 van Boxtel, R. *et al.* Homozygous and heterozygous p53 knockout rats develop metastasizing sarcomas with high frequency. *Am J Pathol* **179**, 1616-1622, doi:10.1016/j.ajpath.2011.06.036 (2011).
109 Wang, D., Weghorst, C. M., Calvert, R. J. & Stoner, G. D. Mutation in the p53 tumor suppressor gene in rat esophageal papillomas induced by N-nitrosomethylbenzylamine. *Carcinogenesis* **17**, 625-630 (1996).
110 Yan, H. X., Wu, H. P., Ashton, C., Tong, C. & Ying, Q. L. Rats deficient for p53 are susceptible to spontaneous and carcinogen-induced tumorigenesis. *Carcinogenesis* **33**, 2001-2005, doi:10.1093/carcin/bgs238 (2012).
111 Smits, B. M. *et al.* Generation of gene knockouts and mutant models in the laboratory rat by ENU-driven target-selected mutagenesis. *Pharmacogenet Genomics* **16**, 159-169, doi:10.1097/01.fpc.0000184960.82903.8f (2006).
112 van Boxtel, R. & Cuppen, E. Rat traps: filling the toolbox for manipulating the rat genome. *Genome Biol* **11**, 217, doi:10.1186/gb-2010-11-9-217 (2010).
113 Ackert-Bicknell, C. *et al.* in *The Laboratory Mouse (Second Edition)* (ed Hans J. Hedrich) xv-xviii (Academic Press, 2012).
114 Felix, M. C. *et al.* Image-Guided Radiotherapy Using a Modified Industrial Micro-CT for Preclinical Applications. *PLoS One* **10**, e0126246, doi:10.1371/journal.pone.0126246 (2015).
115 Kirschner, S. *et al.* Imaging of Orthotopic Glioblastoma Xenografts in Mice Using a Clinical CT Scanner: Comparison with Micro-CT and Histology. *PLoS One* **11**, e0165994, doi:10.1371/journal.pone.0165994 (2016).
116 Miller, K. D. *et al.* Cancer treatment and survivorship statistics, 2019. *CA Cancer J Clin*, doi:10.3322/caac.21565 (2019).
117 Bray, F. *et al.* Global cancer statistics 2018: GLOBOCAN estimates of incidence and mortality worldwide for 36 cancers in 185 countries. *CA Cancer J Clin* **68**, 394-424, doi:10.3322/caac.21492 (2018).
118 Dörr, W. Radiobiology of tissue reactions. *Annals of the ICRP* **44**, 58-68, doi:10.1177/0146645314560686 (2015).
119 Sachs, R. K. & Brenner, D. J. Solid tumor risks after high doses of ionizing radiation. *Proc Natl Acad Sci U S A* **102**, 13040-13045, doi:10.1073/pnas.0506648102 (2005).
120 Dasu, A., Toma-Dasu, I., Olofsson, J. & Karlsson, M. The use of risk estimation models for the induction of secondary cancers following radiotherapy. *Acta Oncol* **44**, 339-347, doi:10.1080/02841860510029833 (2005).
121 Shuryak, I., Hahnfeldt, P., Hlatky, L., Sachs, R. K. & Brenner, D. J. A new view of radiation-induced cancer: integrating short- and long-term processes. Part I: approach. *Radiat Environ Biophys* **48**, 263-274, doi:10.1007/s00411-009-0230-3 (2009).
122 Berrington de Gonzalez, A., Kutsenko, A. & Rajaraman, P. Sarcoma risk after radiation exposure. *Clin Sarcoma Res* **2**, 18, doi:10.1186/2045-3329-2-18 (2012).
123 Inskip, P. D. *et al.* Radiation-related New Primary Solid Cancers in the Childhood Cancer Survivor Study: Comparative Radiation Dose-response and Modification of

Treatment Effects. *Int J Radiat Oncol Biol Phys* **94**, 800-807, doi:10.1016/j.ijrobp.2015.11.046 (2016).
124 Hermsen, R. *et al.* Lack of Major Genome Instability in Tumors of p53 Null Rats. *PLoS One* **10**, doi:10.1371/journal.pone.0122066 (2015).
125 Chang, E. T., Lau, E. C., Mowat, F. S. & Teta, M. J. Therapeutic radiation for lymphoma and risk of second primary malignant mesothelioma. *Cancer Causes Control*, doi:10.1007/s10552-017-0929-4 (2017).
126 Jonat, W. & Arnold, N. Is the Ki-67 labelling index ready for clinical use? *Ann Oncol* **22**, 500-502, doi:10.1093/annonc/mdq732 (2011).
127 Viale, G. *et al.* Prognostic and predictive value of centrally reviewed Ki-67 labeling index in postmenopausal women with endocrine-responsive breast cancer: results from Breast International Group Trial 1-98 comparing adjuvant tamoxifen with letrozole. *J Clin Oncol* **26**, 5569-5575, doi:10.1200/jco.2008.17.0829 (2008).
128 Inwald, E. C. *et al.* Ki-67 is a prognostic parameter in breast cancer patients: results of a large population-based cohort of a cancer registry. *Breast Cancer Res Treat* **139**, 539-552, doi:10.1007/s10549-013-2560-8 (2013).
129 Kastenhuber, E. R. & Lowe, S. W. Putting p53 in Context. *Cell* **170**, 1062-1078, doi:https://doi.org/10.1016/j.cell.2017.08.028 (2017).
130 Abegglen, L. M. *et al.* Potential Mechanisms for Cancer Resistance in Elephants and Comparative Cellular Response to DNA Damage in Humans. *Jama* **314**, 1850-1860, doi:10.1001/jama.2015.13134 (2015).
131 Hollstein, M., Sidransky, D., Vogelstein, B. & Harris, C. C. p53 mutations in human cancers. *Science* **253**, 49-53, doi:10.1126/science.1905840 (1991).
132 Ponta, H., Sherman, L. & Herrlich, P. A. CD44: from adhesion molecules to signalling regulators. *Nat Rev Mol Cell Biol* **4**, 33-45, doi:10.1038/nrm1004 (2003).
133 Xu, H. *et al.* The role of CD44 in epithelial–mesenchymal transition and cancer development. *Onco Targets Ther* **8**, 3783-3792, doi:10.2147/ott.S95470 (2015).
134 Aktipis, C. A. *et al.* Cancer across the tree of life: cooperation and cheating in multicellularity. *Philos Trans R Soc Lond B Biol Sci* **370**, doi:10.1098/rstb.2014.0219 (2015).
135 Barcellos-Hoff, M. H., Park, C. & Wright, E. G. Radiation and the microenvironment - tumorigenesis and therapy. *Nat Rev Cancer* **5**, 867-875, doi:10.1038/nrc1735 (2005).
136 Barcellos-Hoff, M. H. & Nguyen, D. H. Radiation carcinogenesis in context: how do irradiated tissues become tumors? *Health Phys* **97**, 446-457, doi:10.1097/HP.0b013e3181b08a10 (2009).
137 Nguyen, D. H. *et al.* Radiation acts on the microenvironment to affect breast carcinogenesis by distinct mechanisms that decrease cancer latency and affect tumor type. *Cancer Cell* **19**, 640-651, doi:10.1016/j.ccr.2011.03.011 (2011).
138 Rodel, F., Keilholz, L., Herrmann, M., Sauer, R. & Hildebrandt, G. Radiobiological mechanisms in inflammatory diseases of low-dose radiation therapy. *Int J Radiat Biol* **83**, 357-366, doi:10.1080/09553000701317358 (2007).
139 Herskind, C., Wenz, F. & Giordano, F. A. Immunotherapy Combined with Large Fractions of Radiotherapy: Stereotactic Radiosurgery for Brain Metastases-Implications for Intraoperative Radiotherapy after Resection. *Front Oncol* **7**, 147, doi:10.3389/fonc.2017.00147 (2017).
140 Senturk, S. *et al.* p53Ψ is a transcriptionally inactive p53 isoform able to reprogram cells toward a metastatic-like state. *Proceedings of the National Academy of Sciences* **111**, E3287-E3296, doi:10.1073/pnas.1321640111 (2014).
141 Russell, W. M. S. & Burch, R. L. *The principles of humane experimental technique*. (Methuen, 1959).

142 Van Nostrand, J. L., Bowen, M. E., Vogel, H., Barna, M. & Attardi, L. D. The p53 family members have distinct roles during mammalian embryonic development. *Cell Death And Differentiation* **24**, 575, doi:10.1038/cdd.2016.128 (2017).
143 Jain, A. K. & Barton, M. C. p53: emerging roles in stem cells, development and beyond. *Development* **145**, doi:10.1242/dev.158360 (2018).
144 Lemon, J. A., Phan, N. & Boreham, D. R. Single CT Scan Prolongs Survival by Extending Cancer Latency in Trp53 Heterozygous Mice. *Radiat Res* **188**, 505-511, doi:10.1667/rr14576.1 (2017).
145 Lemon, J. A., Phan, N. & Boreham, D. R. Multiple CT Scans Extend Lifespan by Delaying Cancer Progression in Cancer-Prone Mice. *Radiat Res* **188**, 495-504, doi:10.1667/rr14575.1 (2017).
146 Carlisle, S. M., Burchart, P. A. & Mitchel, R. E. Cancer and non-cancer risks in normal and cancer-prone Trp53 heterozygous mice exposed to high-dose radiation. *Radiat Res* **173**, 40-48, doi:10.1667/rr1875.1 (2010).
147 Tong, C., Li, P., Wu, N. L., Yan, Y. & Ying, Q. L. Production of p53 gene knockout rats by homologous recombination in embryonic stem cells. *Nature* **467**, 211-213, doi:10.1038/nature09368 (2010).
148 Sachs, R. K. *et al.* Second cancers after fractionated radiotherapy: stochastic population dynamics effects. *J Theor Biol* **249**, 518-531, doi:10.1016/j.jtbi.2007.07.034 (2007).
149 Schellong, G. *et al.* Brustkrebs bei jungen Frauen nach Therapie eines Hodgkin-Lymphoms im Kindes- und Jugendalter. *Dtsch Arztebl International* **111**, 3-9, doi:10.3238/arztebl.2014.0003 (2014).
150 Berrington de Gonzalez, A. *et al.* Second solid cancers after radiotherapy: a systematic review of the epidemiological studies of the radiation dose-response relationship. *Int J Radiat Oncol Biol Phys* **86**, doi:10.1016/j.ijrobp.2012.09.001 (2013).
151 Sengupta, P. The Laboratory Rat: Relating Its Age With Human's. *Int J Prev Med* **4**, 624-630 (2013).
152 Quinn, R. Comparing rat's to human's age: how old is my rat in people years? *Nutrition* **21**, 775-777, doi:10.1016/j.nut.2005.04.002 (2005).
153 Sharma, G. G. *et al.* Telomere stability correlates with longevity of human beings exposed to ionizing radiations. *Oncol Rep* **10**, 1733-1736 (2003).
154 Calado, R. T. & Dumitriu, B. Telomere dynamics in mice and humans. *Semin Hematol* **50**, 165-174, doi:10.1053/j.seminhematol.2013.03.030 (2013).
155 Sabatino, L., Picano, E. & Andreassi, M. G. Telomere shortening and ionizing radiation: A possible role in vascular dysfunction? *International Journal of Radiation Biology* **88**, 830-839, doi:10.3109/09553002.2012.709307 (2012).
156 Mirjolet, C. *et al.* The role of telomeres in predicting individual radiosensitivity of patients with cancer in the era of personalized radiotherapy. *Cancer Treatment Reviews* **41**, 354-360, doi:10.1016/j.ctrv.2015.02.005 (2015).
157 Formenti, S. C. & Demaria, S. Systemic effects of local radiotherapy. *Lancet Oncol* **10**, 718-726, doi:10.1016/s1470-2045(09)70082-8 (2009).
158 Barcellos-Hoff, M. H. & Ravani, S. A. Irradiated mammary gland stroma promotes the expression of tumorigenic potential by unirradiated epithelial cells. *Cancer Res* **60**, 1254-1260 (2000).
159 Bissell, M. J. & Radisky, D. Putting tumours in context. *Nat Rev Cancer* **1**, 46-54, doi:10.1038/35094059 (2001).
160 Deloch, L. *et al.* Modern Radiotherapy Concepts and the Impact of Radiation on Immune Activation. *Front Oncol* **6**, doi:10.3389/fonc.2016.00141 (2016).

7 DISCLOSURES

Ethical approval

The present study was carried out in accordance with legal EU Directive 2010/63/EU for animal welfare and experimental conduct after approval by the regional animal care committee (Regierungspräsidium Karlsruhe; approval number: 35-9185 81/G184/14).

Funding

This work was supported by the 'Deutsche Forschungsgemeinschaft' (grants FL 880/1-1, GI 771/1-1, GL 236/9-1, and WE 2063/9-1).

The funding body had no influence on study design, data analysis or publication of the study.

Data availability

All the datasets generated during the current study are available from the Department of Radiation Oncology and Laboratory of Cellular and Molecular Radiation Oncology of University Medical Center Mannheim of Heidelberg University.

Research article

Gomarteli, K., J. Fleckenstein, S. Kirschner, V. Bobu, M. A. Brockmann, T. Henzler, M. Meyer, et al. "Radiation-Induced Malignancies after Intensity-Modulated Versus Conventional Mediastinal Radiotherapy in a Small Animal Model." [In eng]. Sci Rep 9, no. 1 (Oct 29, 2019): 15489. https://doi.org/10.1038/s41598-019-51735-3.

Presentations

'Deutsche Gesellschaft für Radioonkologie e.V.' (DEGRO), annual meeting 2016, Mannheim, Germany (poster presentation).

'Deutsche Gesellschaft für Biologische Strahlenforschung e.V.' (DeGBS), annual meeting 2016, Erlangen, Germany (oral presentation).

American Society for Radiation Oncology (ASTRO), annual meeting 2017, San Diego, USA (oral presentation).

8 APPENDIX

Sequence information A1

Rat and human DNA-binding *Tp53* fragments. (a) An exemplary sequence of endogenous rat *Tp53* DNA containing exon 6 with a C273X nonsense mutation TGT/TGA (asterisk, stop codon) at position 817. **(b)** Representative human *TP53* exon 8 containing sequence, showing deep similarity to the orthologous DNA and amino acid sequences of the rat. Evolutionary conserved (identical) amino acid sequences are colored green and red are the alterations. The triplets coding the rat C273 (817 – 819), and its orthologous human C275 (TGT 824 – 826), are underscored. The two major mutational sites in exon 8 of the human *Tp53*, CpG hotspot codons H273 and R282, are italicized.

a

```
257  D   S   S   G   N   L   L   G   R   D   S   F   E   V   R   V   272
769 GAC TCC AGT GGG AAT CTT CTG GGA CGG GAC AGC TTT GAG GTT CGT GTT  816

273  *   A   C   P   G   R   D   R   R   T   E   E   E   N   F   R   288
817 TGA GCC TGT CCT GGG AGA GAC CGT CGG ACA GAG GAA GAA AAT TTC CGC  864

289  K   K   E   E   H   C   P   E   L   P   P   G   S   A   K   R   304
865 AAA AAA GAA GAG CAT TGC CCG GAG CTG CCC CCA GGG AGT GCA AAG AGA  912
```

b

```
257  L   E   D   S   S   G   N   L   L   G   R   N   S   F   E   V   272
769 CTG GAA GAC TCC AGT GGT AAT CTA CTG GGA CGG AAC AGC TTT GAG GTG  816

273  H   V   C   A   C   P   G   R   D   R   R   T   E   E   E   N   288
817 CAT GTT TGT GCC TGT CCT GGG AGA GAC CGG CGC ACA GAG GAA GAG AAT  864

289  L   R   K   K   G   E   P   H   H   E   L   P   P   G   S   T   304
865 CTC CGC AAG AAA GGG GAG CCT CAC CAC GAG CTG CCC CCA GGG AGC ACT  912
```

Sequence information A2

Representative 4523 bases long *Tp53* PCR product (5´- 3´). The capitals represent exons and bolded are the hotspot (C273) and primer (Ch10-for and Chr10-rev) positions.

cttcggtctcttctctgacttgctcatttcatctccctgccagatagtccaccttctttctaacctaccctttcctataggccatagtttttaattgacaaactatgcatccat
acagtacacagatgttctctctgcagataactgtcATGGAGGATTCACAGTCGGATATGAGCATCGAGCTCCCTCTGAGT
CAGGAGACATTTTCATGCTTATGGAAACTgtgagtggatcttacagggcccctgaggtgctatcccccagctgaggcctgtgagaaac
aaaactaatagtgttaaagcacggtgtgctattgggtgcctctgatccctgcacttgggaggtggagggaagggtatcacacagaagtctaagatcatccttgactat
atagcaagtttgtggctagcctggggtaagtgagattctgtctccaaagaacggaaggaaatcagcggaactaattctctgctcttgttctccagtcttcctccagatga
tattctggtaaggagccgggcaagaggggacttaggccttggtgagctggtgggttggtagcccgagagcacaatactgaggttcttctttggcccatccacaGC
CCACCACAGCGACAGGGTCACCTAATTCCATGGAAGATCTGTTCCTGCCCCAGGATGTTGCAGAGT
TGTTAGAAGGCCCAGAGGAAGCCCTCCAAGTGTCAGCTCCTGCAGCACAGGAACCTGGAACTGAG
GCCCCTGCACCCGTGGCCCCTGCTTCAGCTACACCGTGGCCTCTGTCATCTTCCGTCCCTTCTCAAA
AAACTTACCAAGGCAACTATGGCTTCCACCTGGGCTTCCTGCAGTCAGGGACAGCCAAGTCTGTTA
TGTGCACGgtcagtgggcctgaagagttgcttttcgtctgactttaaatgcctctgtctagattttggggttcctctttagcctgtggactttgactatgcctcagag
tttaatttctccctgaaccttttcttagccttttatccttcctctcatattctccgcatctctccaggggacatggaactttcttccctcacattccttttcttggcttttgaaaataatc
ttctgaagccaggcacagaggcatgtgctgtagtcccagctgctagagacattgaggcaggattgcttaaggccagcctgagcattaaagcaagacccctcctcac
cagaaccaaagcagagcccagtggggtgacccacccatatctccagcactgggcaggctagggcaggagaaacaagagttcaaggccatccttgactacacag
taagatggcctctctgaaaaagagaaggcaggtgtggtggccatctctggggttgaggacagtcagggctatatagagaaactgtctcaaaaaaccagagggagg
aaaacaaactggtgtgtagactccagtcctgtcactgctggctgccgtctgccacagcactgttggacactgtctttcattagagccccactttgacccttgatccttagt
tggcttgtccgctgacctttgattctttctcctctcctacagTACTCAATTTCCCTCAATAAGCTGTTCTGCCAGCTGGCGAAGA
CATGCCCTGTGCAGTTGTGGGTCACCTCCACACCTCCACCTGGTACCCGTGTCCGTGCCATGGCCAT
CTACAAGAAGTCACAACACATGACTGAGGTCGTGAGACGCTGCCCCCACCATGAGCGTTGCTCTGA
TGGTGACGGtgagcactgggcactgcctgtggggttagaactggttgtccagggtctcccggcctctgacttattcttgctcttaggCCTGGCTCCT
CCCCAACATCTTATCCGGGTGGAAGGAAATCCGTATGCTGAGTATCTGGACGACAGGCAGACTTTT
CGGCACAGCGTGGTGGTACCGTATGAGCCACCTGAGGTCGGCTCCGACTATACCACTATCCACTAC
AAGTACATGTGCAACAGCTCCTGCATGGGGGGCATGAACCGCCGGCCCATCCTTACCATCATCACG
CTGGAAGACTCCAGgtaggaagctgtgtgccaggttgggctggcaccggtcctccccagcctcggcctgtttttgttccatgagccccgcccctacca
caggcccagccctctttaccctaccctatctacataaatgaagtctcctctgttccctggtggtcttagggacatctcttatctgtggcatcttgggttccctataaccaga
gcttcagctccagataggacaagaggagttgggaacaggtagggcctggtttacagtcaggatggagcccagctttcttactgccttgtgctgtgcctcctcttgtcc
cgggtagTGGGAATCTTCTGGGACGGGACAGCtttgaggttcgtgtt**tgt**gcctgtcctgggAGAGACCGTCGGACAGAG
GAAGAAAATTTCCGCAAAAAAGAAGAGCATTGCCCGGAGCTGCCCCCAGGGAGTGCAAAGAGAGg
tgagcaggcaggacaaagaaggtggaggcgcccttcagcttcaccccaaagtcacccctgctctctccttccatagCACTGCCCACCAGCACAA
GCTCCTCTCCCCAGCAAAAGAAAAAACCACTCGATGGAGAATATTTCACCCTTAAGgtaccaaggttattattg
gattaatattctaagtctaggacacaaaacgctgtatcttttgcagctgcttcttctctagCTATGACATTATCGTCAGAGCGCAtgctctgaggct
gtggtttctcacttataactaacttgagaacaccaacttataatacatacgtaatacaggtgctccgctacttaggaggggaacgtgtcttaggaaactcatcatcggttg
aaaataccatatgtcaaaatgtagttagaggcaggcctggctgacgtatgcctgtaattacagaactgaggaatgtggtacaaagctggcagggaaatgtaacccaa
gaaaggacatttgggtttaaggatgtaactcagttcagaatacgtgccaagtgtataccaagccctggactcgatccccagcggcacacagtgcatttaatccaccta
tcccactggattccacagctcagcagcaggattgccctgttaagtgtgtccccatcagtaacagcatcctactctgttcccccaactgaaaaaacccaagtttgttatac
actttctactgaatacctgttactttcacaccatcataaagacctccccaaaaaaccgataagtctagccagctcgggttggggatttagctcagtggtagagcgcttgc
ctaggaagtgtgaggccctgggtttggttcccagctccggaaaaaaaaaaaaaaagaaccaaaaaaaaaagtctagccagctcaagttggggatcaactttcagaa
agaaagttgttaaaaggatgaaagtggctctgtgactttgtccagcacttctgtcctacttcatccttgctacagATCCGTGGGCGTGAGCGCTTCG
AGATGTTCCGAGAGCTGAATGAGGCCTTGGAATTAAAGGATGCCCGTGCTGCCGAGGAGTCAGGA
GACAGCAGGGCTCACTCCAggtgagtgacctggggcagcgcctggctgtggtgcttgcccctgacctccctgagcacggcctttgtggtaaaag
acaataactaactccaccagatgtccatcgtccgccagacgatgtggttatggttactcagccctggcaaatgcaagggtcctatgaagtcttactactcaaccatttca
ggctctggaaaatgggatgagggacaaggtatggtatcatgctcctataatctcagcagtagggaagcagtaagtcaggagggtttggggaagtttgaagccttcat
aaactatataaaactttaggctagccaggactagctacatagcaagatcctgtctctcggtggtggtggtggtggtggtggtggtggtggtggtggtggtggtgg
tggtggtggtggtcaaagggaagatgaactgattctagaagtactccggcatattctgtgaatacacctactacccatggtagaagtcatcttaaattccctttttttcagc
ctccagcctagaaccttccaagccttgatcaagaaggaaagcccaaactgctagctcccatcacttcatccctccctttttctgtcttcctatagCTACCCGAA
GACCAAGAAGGGCCAGTCTACGTCCCGCCATAAAAAACCAATGATCAAGAAAGTGGGGCCTGACT
CAGACTGAcagcctctgcatcctgtccccatcaccagcctccccgtcccctccttttcttgccattttatgactttagggcttgttatgagagctgacaagacaatg
ctagtcccttcactgccttttttaccttgtagatagtactcggccccctctatgcaaactggttcctggcccagattggggaatgggttggtagttgctgggtctctgctg
gtccagcg**aaatcctatccggtcagttg**

APPENDIX TABLES

Table A1

Rat data 1. (**A**) Rat identity and sex (female/male), (**B**) parental *Tp53*-background of $Tp53^{X/C273}$ individuals of the L1 - L11 litters of F1 and F2 generations derived from three female *Aa*, *Bb*, *Cc* and two male *Dd* and *Ee* allele pairs (the capital letters represent intact *Tp53* alleles and the regular letters mean the $Tp53^{+/C273X}$ knock out variants); (**C**) weight at treatment(± 5 g); (**D**) attained weight (± 5 g); (**E**) weight increment (± 5 g); (**F**) growth rate (gram per follow up day); (**G**) the age at first follow-up CT (days); (**H**) the attained age (days); and (**I**) the age at treatment (days).

A	B	C	D	E	F	G	H	I
91m	F1, L1; f [*A* or *a*] × m [*D* or *d*]	250	420	170	0,78	−	287	69
65m	F1, L1; f [*A* or *a*] × m [*D* or *d*]	230	425	195	0,66	257	362	66
5m	F1, L2; f [*C* or *c*] × m [*B* or *b*]	240	435	195	0,9	−	−	64
51"m	F2, L9; f [*B* or E] × m [*a* or *d*]	235	465	230	0,78	216	380	58
46"m	F2, L7; f [*A* or *D*] × m [*b* or *e*]	275	515	240	0,81	219	−	59
15'f	F1, L1; f [*A* or *a*] × m [*D* or *d*]	185	330	145	0,38	312	451	71
28"f	F2, L7; f [*A* or *D*] × m [*b* or *e*]	170	330	160	0,55	282	357	68
26"f	F2, L7; f [*A* or *D*] × m [*b* or *e*]	180	245	65	0,34	−	259	68
85f	F1, L3; f [*B* or *b*] × m [*E* or *e*]	180	245	65	0,3	268	300	82
88f	F1, L3; f [*B* or *b*] × m [*E* or *e*]	185	260	75	0,24	271	402	85
14'f	F1, L1; f [*A* or *a*] × m [*D* or *d*]	185	200	15	0,11	−	−	71
50"m	F2, L9; f [*B* or *E*] × m [*a* or *d*]	245	400	155	0,61	216	291	58
41"m	F2, L4; f [*C* or *B*] × m [*a* or *d*]	225	400	175	0,68	216	310	61
43"m	F2, L4; f [*C* or *B*] × m [*a* or *d*]	285	485	200	1,3	−	575	61
95f	F1, L1; f [*A* or *a*] × m [*D* or *d*]	190	300	110	0,27	347	478	70
33"f	F2, L4; f [*C* or *B*] × m [*a* or *d*]	155	250	95	0,25	282	449	68
10f	F1, L3; f [*B* or *b*] × m [*E* or *e*]	175	276	101	0,44	−	301	70
43´´´m	F2, L10; f [*A* or *D*] × m [*b* or *e*]	220	310	90	0,45	243	297	95
29´´m	F2, L8; f [*A* or *D*] × m [*b* or *e*]	290	405	115	1,1	−	−	93
64"f	F2, L6; f [*B* or *C*] × m [*a* or *d*]	220	250	30	0,17	263	282	107
86"f	F2, L10; f [*A* or *D*] × m [*b* or *e*]	200	225	25	0,17	−	246	116
22´´m	F2, L6; f [*B* or *C*] × m [*a* or *d*]	280	345	65	0,64	−	202	100
27´´´m	F2, L5; f [*C* or *B*] × m [*a* or *d*]	260	335	75	0,56	215	−	103
93"m	F2, L11; f [*A* or *D*] × m [*b* or *e*]	265	345	80	0,59	−	223	88
99"m	F2, L11; f [*A* or *D*] × m [*b* or *e*]	250	330	80	0,59	−	223	88
24´´m	F2, L6; f [*B* or *C*] × m [*a* or *d*]	330	440	110	0,55	235	300	100
82"f	F2, L10; f [*A* or *D*] × m [*b* or *e*]	205	240	35	0,19	246	305	116
58"f	F2, L6; f [*B* or *C*] × m [*a* or *d*]	190	220	30	0,22	−	241	107
52´´f	F2, L6; f [*B* or *C*] × m [*a* or *d*]	205	285	80	0,28	263	390	107
60"f	F2, L6; f [*B* or *C*] × m [*a* or *d*]	205	245	40	0,24	−	263	107

81´´f	F2, L11; f [*A* or *D*] × m [*b* or *e*]	180	215	35	0,19	239	291	109
44´´f	F2, L11; f [*A* or *D*] × m [*b* or *e*]	215	265	50	0,20	256	354	107
79f	F2, L11; f [*A* or *D*] × m [*b* or *e*]	215	300	85	0,33	–	–	107
38"m	F2, L4; f [*C* or *B*] × m [*a* or *d*]	225	395	170	0,63	219	330	61
48"m	F2, L7; f [*A* or *D*] × m [*b* or *e*]	280	440	160	1,32	–	176	61
20'm	F1, L1; f [*A* or *a*] × m [*D* or *d*]	245	415	170	0,48	317	–	65
71f	F1, L1; f [*A* or *a*] × m [*D* or *d*]	165	270	105	0,34	256	383	72
9f	F1, L3; f [*B* or *b*] × m [*E* or *e*]	180	325	145	0,43	304	407	70
39"f	F2, L4; f [*C* or *B*] × m [*a* or *d*]	225	380	155	0,63	216	–	61
16'm	F1, L1; f [*A* or *a*] × m [*D* or *d*]	250	435	185	0,63	317	358	65
63m	F1, L1; f [*A* or *a*] × m [*D* or *d*]	280	490	210	0,70	257	364	66
69f	F1, L1; f [*A* or *a*] × m [*D* or *d*]	160	265	105	0,29	256	431	72
23"f	F2, L7; f [*A* or *D*] × m [*b* or *e*]	175	245	70	0,45	–	–	68
18f	F1, L3; f [*B* or *b*] × m [*E* or *e*]	160	235	75	0,26	–	365	77
89f	F1, L3; f [*B* or *b*] × m [*E* or *e*]	210	290	80	0,26	271	388	85
47´´f	F2, L11; f [*A* or *D*] × m [*b* or *e*]	225	280	55	0,29	255	297	106
37´´m	F2, L8; f [*A* or *D*] × m [*b* or *e*]	330	470	140	0,48	262	390	100
98"m	F2, L11; f [*A* or *D*] × m [*b* or *e*]	240	385	145	0,71	236	293	88
31´´m	F2, L8; f [*A* or *D*] × m [*b* or *e*]	335	480	145	0,53	262	368	93
42´´´m	F2, L10; f [*A* or *D*] × m [*b* or *e*]	285	450	165	0,58	–	365	81
6´´f	F2, L5; f [*C* or *B*] × m [*a* or *d*]	220	270	50	0,20	252	373	124
54"f	F2, L6; f [*B* or *C*] × m [*a* or *d*]	200	265	65	0,26	263	–	114
90"f	F2, L10; f [*A* or *D*] × m [*b* or *e*]	185	220	35	0,19	246	305	116
56"f	F2, L6; f [*B* or *C*] × m [*a* or *d*]	215	275	60	0,31	263	298	107
33´´´m	F2, L8; f [*A* or *D*] × m [*b* or *e*]	280	435	155	0,52	–	390	93
32´´m	F2, L8; f [*A* or *D*] × m [*b* or *e*]	290	390	100	0,53	–	282	93
36´´m	F2, L10; f [*A* or *D*] × m [*b* or *e*]	330	425	95	0,70	–	216	81
49"m	F2, L7; f [*A* or *D*] × m [*b* or *e*]	295	480	185	0,69	–	–	68
75m	F1, L3; f [*B* or *b*] × m [*E* or *e*]	275	490	215	0,5	249	504	73
42"m	F2, L4; f [*C* or *B*] × m [*a* or *d*]	285	500	215	0,73	–	359	68
21'm	F1, L1; f [*A* or *a*] × m [*D* or *d*]	275	485	210	0,83	397	317	65
3´ m	F1, L2; f [*C* or *c*] × m [*B* or *b*]	240	425	185	0,56	–	392	64
59m	F1, L1; f [*A* or *a*] × m [*D* or *d*]	265	455	190	0,67	257	–	66
19f	F1, L3; f [*B* or *b*] × m [*E* or *e*]	185	235	50	0,39	–	–	77
34"f	F2, L4; f [*C* or *B*] × m [*a* or *d*]	165	235	70	0,23	282	–	68
87f	F1, L3; f [*B* or *b*] × m [*E* or *e*]	190	275	85	0,32	271	352	85
96f	F1, L1; f [*A* or *a*] × m [*D* or *d*]	200	280	80	0,23	310	441	96
92f	F1, L1; f [*A* or *a*] × m [*D* or *d*]	195	285	90	0,46	–	268	82
12'f	F1, L1; f [*A* or *a*] × m [*D* or *d*]	180	270	90	0,31	312	366	71
7f	F1, L3; f [*B* or *b*] × m [*E* or *e*]	165	245	80	0,23	304	304	70
30"f	F2, L4; f [*C* or *B*] × m [*a* or *d*]	155	255	100	0,28	282	–	68
11m	F1, L3; f [*B* or *b*] × m [*E* or *e*]	175	335	160	0,49	326	392	63
35"m	F2, L4; f [*C* or *B*] × m [*a* or *d*]	265	450	185	0,62	219	408	108

57m	F1, L1; f [*A* or *a*] × m [*D* or *d*]	250	410	160	0,54	257	362	66
13m	F1, L3; f [*B* or *b*] × m [*E* or *e*]	280	490	210	0,6	316	415	64
62m	F1, L1; f [*A* or *a*] × m [*D* or *d*]	270	410	140	0,74	–	262	73
27"m	F2, L9; f [*B* or *E*] × m [*a* or *d*]	220	450	230	0,95	262	283	85
40"m	F2, L4; f [*C* or *B*] × m [*a* or *d*]	300	450	150	0,73	285	294	108
8f	F1, L3; f [*B* or *b*] × m [*E* or *e*]	185	260	75	0,24	304	379	64
2"f	F2, L9; f [*B* or *E*] × m [*a* or *d*]	150	235	85	0,59	–	–	85
4"f	F2, L9; f [*B* or *E*] × m [*a* or *d*]	145	285	140	0,36	262	472	85
94f	F1, L1; f [*A* or *a*] × m [*D* or *d*]	165	300	135	0,32	313	499	82
1"f	F2, L9; f [*B* or *E*] × m [*a* or *d*]	155	290	135	0,59	262	–	85
20f	F1, L3; f [*B* or *b*] × m [*E* or *e*]	190	320	130	0,32	–	483	76
Rats killed due to non-tumor-related causes:								
53"f	F2, L6; f [*B* or *C*] × m [*a* or *d*]	210	245	35	0,2	263	–	107
45´´f	F2, L11; f [*A* or *D*] × m [*b* or *e*]	210	255	45	0,27	256	–	107
97f	F1, L1; f [*A* or *a*] × m [*D* or *d*]	180	215	35	0,38	–	–	82
21"f	F2, L7; f [*A* or *D*] × m [*b* or *e*]	185	290	105	0,45	–	–	68
19'm	F1, L1; f [*A* or *a*] × m [*D* or *d*]	263	435	172	0,56	–	–	65
83f	F1, L3; f [*B* or *b*] × m [*E* or *e*]	190	290	100	0,64	240	–	85

Abbreviations: rat identity and sex (e. g. #1´´f, number 1´´ female), m, male; F1 and F2 filial generation 1 and 2; L1-L11, litter 1-11.

Table A2

Rat breeding scheme. Generation of heterozygous *Tp53*$^{+/C273X}$ experimental rats (black) rats from heterozygous only or homozygous (*Tp53*$^{C273X/C273X}$) and wild-type (*Tp53*^{wt}) parents. Original *Tp53* alleles are indicated: *Aa*, *Bb*, *Cc*, *Dd*, and *Ee*.

Dd		*Aa*		*Cc*		*Bb*		*Ee*
#1♀ *Tp53* $^{+/C273X}$	X	#3♂ *Tp53* $^{+/C273X}$		#5♀*Tp53* $^{+/C273X}$	X	#2♂ *Tp53* $^{+/C273X}$	X	#6♀*Tp53* $^{+/C273X}$
	#19´♂ AN			**F1, L2:**	#3´ CBCT		#8♀ AN	
	#57♂ AN				#5´ 3×5 Gy VMAT		#11♂ AN	
	#94♀ AN						#13♂ AN	
	#62♂ AN						#20♀ AN	
	#12´♀ CBCT						#83♀ AN	
	#59♂ CBCT						#7♀ CBCT	
	#21´ CBCT						#19♀ CBCT	
	#92♀ CBCT					**F1, L3:**	#75♂ CBCT	
	#96♀ CBCT						#87♀ CBCT	
F1, L1:	#15´♀ 3×5 Gy VMAT						#9♀ 3×5 Gy VMAT	
	#20´♂ 3×5 Gy VMAT						#88♀ 3×5 Gy VMAT	
	#65♂ 3×5 Gy VMAT						#85♀ 3×5 Gy VMAT	
	#71♀ 3×5 Gy VMAT						#10♀ 3×5 Gy APPA	
	#91♂ 3×5 Gy VMAT						#18♀ 3×5 Gy APPA	
	#14´♀ 3×5 Gy APPA						#89♀ 3×5 Gy APPA	
	#16´♂ 3×5 Gy APPA							
	#63♂ 3×5 Gy APPA							
	#69♀ 3×5 Gy APPA							
	#95♀ 3×5 Gy APPA							
	#97♀ 3×5 Gy APPA							
	#18´♂*Tp53* $^{C273X/C273X}$	X			#6´♀*Tp53* ^{wt}			
		#35´´♂ AN						
		#40´´♂ AN						
		#30´´♀ CBCT						
		#34´´♀ CBCT						
		#42´´♂ CBCT						
		F2, L4: #39´´♂ 3×5 Gy APPA						
		#38´´♂ 3×5 Gy VMAT						
		#33´´♀ 3×5 Gy AP/PA						
		#41´´♂ 3×5 Gy APPA						
		#43´´♂ 3×5 Gy APPA						
	#61♂*Tp53* $^{C273X/C273X}$	X			#6´♀*Tp53* ^{wt}			
		F2, L5: #6´´♀: 3×8 Gy VMAT						
		#27´´♂ 3×8 Gy APPA						
	#61♂*Tp53* $^{C273X/C273X}$	X			#72♀*Tp53* ^{wt}			
		#53´´♀ 3×8 Gy VMAT						
		#54´´♀ 3×8 Gy VMAT						
		#56´´♀ 3×8 Gy VMAT						
		#64´´♀ 3×8 Gy VMAT						
		F2, L6: #22´´♂ 3×8 Gy APPA						
		#24´´♂ 3×8 Gy APPA						
		#52´´♀ 3×8 Gy APPA						
		#58´´♀ 3×8 Gy APPA						
		#60´´♀ 3×8 Gy APPA						
	♀#13'*Tp53* ^{wt}				X		#15♂*Tp53* $^{C273X/C273X}$	
		#21´´♀ CBCT						
		#49´´♂ CBCT						
		#26´´♀ 3×5 Gy VMAT						
		F2, L7: #28´´♀ 3×5 Gy VMAT						
		#46´´♂ 3×5 Gy VMAT						
		#48´´♂ 3×5 Gy VMAT						
		#23´´♀ 3×5 Gy APPA						
					X		#79♂*Tp53* $^{C273X/C273X}$	
		#29´´♂ 3×8 Gy VMAT						
		#31´´♂ 3×8 Gy VMAT						
		F2, L8: #37´´♂ 3×8 Gy VMAT						
		#32´´♂ 3×8 Gy APPA						
		#33´´´♂ 3×8 Gy APPA						
	#17'♂*Tp53* $^{C273X/C273X}$				X		#16♀*Tp53* ^{wt}	
		#1´´♀ AN						
		#2´´♀ AN						
		#4´´♀ AN						
		F2, L9: #27´´♂ AN						
		#51´´♂ 3×5 Gy VMAT						
		#50´´♂ 3×5 Gy AP/PA						
	#68♀*Tp53* ^{wt}				X		#81♂*Tp53* $^{C273X/C273X}$	
		#43´´´♂ 3×8 Gy VMAT						
		#86´´♀ 3×8 Gy VMAT						
		F2, L10: #90´´♀ 3×8 Gy VMAT						
		#42´´´♂ 3×8 Gy VMAT						
		#36´´♂ 3×8 Gy APPA						
		#82´´♀ 3×8 Gy APPA						
	#70(90)♀*Tp53* ^{wt}				X			
		#45´´♀ 3×8 Gy VMAT						
		#47´´♀ 3×8 Gy VMAT						
		#98´´♂ 3×8 Gy VMAT						
		F2, L11: #44´´♀ 3×8 Gy APPA						
		#79´´♀ 3×8 Gy APPA						
		#81´´♀ 3×8 Gy APPA						
		#93´´♂ 3×8 Gy APPA						
		#99´´♂ 3×8 Gy APPA						

Abbreviations: F1 and F2, Filial generation 1 and 2; L1-L11, litter 1-11; *Tp53*, *Tumor protein 53*; Gy, Gray; VMAT, volumetric-modulated arc therapy; AP/PA, anterior-posterior/ posterior-anterior; AN, anesthesia only; CBCT, cone-beam CT only.

Table A3

Rat data 2. (**A**) Rat identity and sex (female/male). (**B**) Radiation treatment plan size based on 160 g (small) and 250 g (large) rat planning CTs. (**C**) Used dose delivering technique (VMAT or AP/PA). (**D**) Fraction number and the fraction dose in Gy (Gray). (**E**) The volume (cm^3) affected by index tumors: high dose volume (HDV), bordering HDV (BHDV), low dose volume (LDV), and non-irradiated volume (NIRV); (**F**) the size (cm^3) of volumes in which tumors were found. (**G**) Dose to volume relationships (DVRs) in percent of minimal received doses calculated using Monaco®; (**H**) estimated received total doses in Gy, and (**I**) time to tumor (TTT) from the first treatment fraction (days).

A	B	C	D	E	F	G	H	I
91m	Large	VMAT	3×5 Gy	HDV	0.782	>90%	>13.5 Gy	218
65m	Large	VMAT	3×5 Gy	HDV	0.782	>90%	>13.5 Gy	296
5m	Large	VMAT	3×5 Gy	HDV	0.782	>90%	>13.5 Gy	217
51"m	Large	VMAT	3×5 Gy	BHDV	3.884	50-90%	7.5-13.5 Gy	296
46"m	Large	VMAT	3×5 Gy	HDV	0.782	>90%	>13.5 Gy	298
15'f	Small	VMAT	3×5 Gy	HDV	0.66	>90%	>13.5 Gy	380
28"f	Small	VMAT	3×5 Gy	HDV	0.66	>90%	>13.5 Gy	289
26"f	Small	VMAT	3×5 Gy	HDV	0.66	>90%	>13.5 Gy	191
85f	Small	VMAT	3×5 Gy	LDV	12.394	5-50%	0.75-7.5 Gy	218
88f	Small	VMAT	3×5 Gy	LDV	12.394	5-50%	0.75-7.5 Gy	317
14'f	Small	AP/PA	3×5 Gy	HDV	1.265	>90%	>13.5 Gy	137
50"m	Large	AP/PA	3×5 Gy	HDV	2.465	>90%	>13.5 Gy	256
41"m	Large	AP/PA	3×5 Gy	HDV	2.465	>90%	>13.5 Gy	258
43"m	Large	AP/PA	3×5 Gy	HDV	2.465	>90%	>13.5 Gy	154
95f	Small	AP/PA	3×5 Gy	HDV	1.265	>90%	>13.5 Gy	408
33"f	Small	AP/PA	3×5 Gy	BHDV	3.394	50-90%	7.5-13.5 Gy	381
10f	Small	AP/PA	3×5 Gy	LDV	7.369	5-50%	0.75-7.5 Gy	231
43´´´m	Large	VMAT	3×8 Gy	HDV	0.782	>90%	>21.6 Gy	202
29´´m	Large	VMAT	3×8 Gy	HDV	0.782	>90%	>21.6 Gy	105
64"f	Large	VMAT	3×8 Gy	HDV	0.782	>90%	>21.6 Gy	175
86"f	Small	VMAT	3×8 Gy	HDV	0.66	>90%	>21.6 Gy	143
22´´m	Large	AP/PA	3×8 Gy	HDV	2.465	>90%	>21.6 Gy	102
27´´´m	Large	AP/PA	3×8 Gy	HDV	2.465	>90%	>21.6 Gy	133
93"m	Large	AP/PA	3×8 Gy	HDV	2.465	>90%	>21.6 Gy	135
99"m	Large	AP/PA	3×8 Gy	LDV	12.029	5-50%	1.2-12.0 Gy	135
24´´m	Large	AP/PA	3×8 Gy	LDV	12.029	5-50%	1.2-12.0 Gy	200
82"f	Small	AP/PA	3×8 Gy	HDV	1.265	>90%	>21.6 Gy	189
58"f	Small	AP/PA	3×8 Gy	HDV	1.265	>90%	>21.6 Gy	134
52´´f	Small	AP/PA	3×8 Gy	HDV	1.265	>90%	>21.6 Gy	283
60"f	Small	AP/PA	3×8 Gy	HDV	1.265	>90%	>21.6 Gy	164
81´´f	Small	AP/PA	3×8 Gy	BHDV	3.394	50-90%	12-21.6 Gy	182
44´´f	Small	AP/PA	3×8 Gy	LDV	7.369	5-50%	1.2-12.0 Gy	247

79f	Small	AP/PA	3×8 Gy	LDV	7.369	5-50%	1.2-12.0 Gy	259
38"m	Large	VMAT	3×5 Gy	NIRV	195.55	<5%	<0.75 Gy	269
48"m	Large	VMAT	3×5 Gy	NIRV	195.55	<5%	<0.75 Gy	121
20'm	Large	VMAT	3×5 Gy	NIRV	195.55	<5%	<0.75 Gy	353
71f	Small	VMAT	3×5 Gy	NIRV	127.59	<5%	<0.75 Gy	311
9f	Small	VMAT	3×5 Gy	NIRV	127.59	<5%	<0.75 Gy	337
39"f	Large	AP/PA	3×5 Gy	NIRV	203.13	<5%	<0.75 Gy	247
16'm	Large	AP/PA	3×5 Gy	NIRV	203.13	<5%	<0.75 Gy	293
63m	Large	AP/PA	3×5 Gy	NIRV	203.13	<5%	<0.75 Gy	298
69f	Small	AP/PA	3×5 Gy	NIRV	131.55	<5%	<0.75 Gy	359
23"f	Small	AP/PA	3×5 Gy	NIRV	131.55	<5%	<0.75 Gy	154
18f	Small	AP/PA	3×5 Gy	NIRV	131.55	<5%	<0.75 Gy	288
89f	Small	AP/PA	3×5 Gy	NIRV	131.55	<5%	<0.75 Gy	303
47´´f	Large	VMAT	3×8 Gy	NIRV	195.55	<5%	<1.2 Gy	191
37´´m	Large	VMAT	3×8 Gy	NIRV	195.55	<5%	<1.2 Gy	290
98"m	Large	VMAT	3×8 Gy	NIRV	195.55	<5%	<1.2 Gy	205
31´´m	Large	VMAT	3×8 Gy	NIRV	195.55	<5%	<1.2 Gy	275
42´´´m	Large	VMAT	3×8 Gy	NIRV	195.55	<5%	<1.2 Gy	284
6´´f	Large	VMAT	3×8 Gy	NIRV	195.55	<5%	<1.2 Gy	249
54"f	Small	VMAT	3×8 Gy	NIRV	127.59	<5%	<1.2 Gy	252
90"f	Small	VMAT	3×8 Gy	NIRV	127.59	<5%	<1.2 Gy	189
56"f	Small	VMAT	3×8 Gy	NIRV	127.59	<5%	<1.2 Gy	191
33´´´m	Large	AP/PA	3×8 Gy	NIRV	203.13	<5%	<1.2 Gy	297
32´´m	Large	AP/PA	3×8 Gy	NIRV	203.13	<5%	<1.2 Gy	189
36´´m	Large	AP/PA	3×8 Gy	NIRV	203.13	<5%	<1.2 Gy	135
49"m	–	CBCT	3×0.04 Gy	–	–	–	<0.04 Gy	268
75m	–	CBCT	3×0.04 Gy	–	–	–	<0.04 Gy	431
42"m	–	CBCT	3×0.04 Gy	–	–	–	<0.04 Gy	294
21'm	–	CBCT	3×0.04 Gy	–	–	–	<0.04 Gy	252
3´ m	–	CBCT	3×0.04 Gy	–	–	–	<0.04 Gy	328
59m	–	CBCT	3×0.04 Gy	–	–	–	<0.04 Gy	282
19f	–	CBCT	3×0.04 Gy	–	–	–	<0.04 Gy	128
34"f	–	CBCT	3×0.04 Gy	–	–	–	<0.04 Gy	303
87f	–	CBCT	3×0.04 Gy	–	–	–	<0.04 Gy	267
96f	–	CBCT	3×0.04 Gy	–	–	–	<0.04 Gy	345
92f	–	CBCT	3×0.04 Gy	–	–	–	<0.04 Gy	196
12'f	–	CBCT	3×0.04 Gy	–	–	–	<0.04 Gy	295
7f	–	CBCT	3×0.04 Gy	–	–	–	<0.04 Gy	352
30"f	–	CBCT	3×0.04 Gy	–	–	–	<0.04 Gy	357
11m	–	AN	0	–	–	–	0 Gy	329
35"m	–	AN	0	–	–	–	0 Gy	300
57m	–	AN	0	–	–	–	0 Gy	296
13m	–	AN	0	–	–	–	0 Gy	351

62m	−	AN	0	−	−	−	0 Gy	189
27"m	−	AN	0	−	−	−	0 Gy	242
40"m	−	AN	0	−	−	−	0 Gy	205
8f	−	AN	0	−	−	−	0 Gy	315
2"f	−	AN	0	−	−	−	0 Gy	143
4"f	−	AN	0	−	−	−	0 Gy	387
94f	−	AN	0	−	−	−	0 Gy	417
1"f	−	AN	0	−	−	−	0 Gy	228
20f	−	AN	0	−	−	−	0 Gy	407
53"f	Small	VMAT	3×8 Gy	Sacrificed due to non-tumor causes				179
45´´f	Small	VMAT	3×8 Gy	Sacrificed due to non-tumor causes				164
97f	Small	AP/PA	3×5 Gy	Sacrificed due to non-tumor causes				91
21"f	−	CBCT	3×0.04 Gy	Sacrificed due to non-tumor causes				232
19'm	−	AN	0	Sacrificed due to non-tumor causes				308
83f	−	AN	0	Sacrificed due to non-tumor causes				156

Abbreviations: rat identity and sex (e. g. #1´´f, number 1´´ female), m, male; VMAT, volumetric-modulated arc therapy; AP/PA, anterior-posterior/posterior-anterior irradiation; CBCT, cone-beam computed tomography only controls; AN, anesthesia only controls; Gy, Gray; HDV, high-dose volume; BHDV, bordering high-dose volume; LDV, low-dose volume; NIRV, non-irradiated volume; TTT, time to tumor; 3×5 Gy or 3×8 Gy, three fractions of 5 or 8 Gy.

Table A4

Frequency distribution of tumors in different dose-volumes. The frequency distribution of tumors in different dose-volumes. The incident numbers and total volumes of affected NIRVs, LDVs, BHDVs, and HDVs were summed (based on Monaco Statistics®) and then, ordered by estimated dose levels, and grouped either by prescribed doses (3×5 Gy and 3×8 Gy) or by used irradiation technique (VMAT and AP/PA). The frequency distribution was calculated by dividing of incidence numbers by the summed dose-volumes. An estimate of the sizes of each particular volume, in which an index tumor was developed, bases on the Monaco statistics data and takes into account the particularly prescribed doses, applied irradiation plans (small or large), and used dose delivering modalities represented in Table A3B-D.

Dose Volume	NIRV	LDV	BHDV	HDV
Estimated received dose after 3×5 Gy	<0.75 Gy	0.75-7.5 Gy	7.5-13.5 Gy	13.5-15 Gy
Number of tumors after 3×5 Gy	12	3	2	12
Total volume in cm^3 after 3×5 Gy	1977.42	32.157	10.672	17.65
Distribution (*n* per cm^3) after 3×5 Gy	0.006	0.093	0.187	0.68
Estimated received dose after 3×8 Gy	<1.12 Gy	1.12-12 Gy	12-21.6 Gy	21.6-24 Gy
Number of events after 3×8 Gy	12	4	1	11
Total volume in cm^3 after 3×8 Gy	2165.46	38.796	6.788	16.016
Distribution (*n* per cm^3) after 3×8 Gy	0.0054	0.1	0.147	0.67
Number of events after VMAT	14	2	1	11
Total volume in cm^3 after VMAT	2397.9	24.788	3.884	10.178
Distribution (*n* per cm^3) after VMAT	0.005	0.08	0.257	1.08
Number of events after AP/PA	10	5	2	12
Total volume in cm^3 after AP/PA	1744.98	46.165	13.576	23.29
Distribution (*n* per cm^3) after AP/PA	0.0057	0.108	0.147	0.515

Abbreviations: NIRV, non-irradiated volume; LDV, low-dose volume; BHDV, bordering high-dose volume; HDV, high-dose volume; Gy, Gray.

Table A5

The organ DVRs for 3×5 Gy. Shown are the dose and volume parameter of the small and large irradiation plans for VMAT and AP/PA irradiation (Monaco® statistics).

Structures at risk	Irradiation technique	Volume (cm^3)		D_{min} (Gy)		D_{max} (Gy)	
		Large	Small	Large	Small	Large	Small
PTV	VMAT	0.296	0.296	13.80	13.28	15.99	16.03
	AP/PA	0.296	0.296	12.47	13.02	15.95	15.65
Spine	VMAT	4.14	2.4	0.003	0.007	15.1	14.8
	AP/PA	4.14	2.4	0.09	0.08	16.09	15.06
Heart	VMAT	1.45	1.55	0.72	0.7	14.9	16.03
	AP/PA	1.45	1.55	0.41	0.61	16.2	15.60
Thymus	VMAT	0.39	0.46	0.06	0.04	2.28	11.42
	AP/PA	0.39	0.46	0.23	0.18	6.04	9.58
Sternum	VMAT	0.74	0.54	0.02	0.02	3.27	5.58
	AP/PA	0.74	0.54	0.17	0.09	15.33	13.9
Lung right	VMAT	3.33	1.35	0.24	0.26	15.29	15.53
	AP/PA	3.33	1.35	0.22	0.2	15.85	15.32
Lung left	VMAT	2.81	0.94	0.42	0.28	15.78	15.44
	AP/PA	2.81	0.94	0.24	0.23	15.77	15.65
Chest wall right	VMAT	6.58	5.33	0.015	0.014	10.12	11.9
	AP/PA	6.58	5.33	0.041	0.023	15.6	14.15
Chest wall left	VMAT	6.51	5.21	0.015	0.014	8.57	11.90
	AP/PA	6.51	5.21	0.04	0.03	15.16	14.80
Back muscles right	VMAT	3.62	2.12	0.02	0.008	6.6	4.07
	AP/PA	3.62	2.12	0.014	0.015	14.62	13.32
Back muscles left	VMAT	3.92	2.36	0.03	0.008	6.19	5.17
	AP/PA	3.92	2.36	0.02	0.02	15.12	13.57
Axilla (armpit) right	VMAT	2.14	1.75	0.05	0.02	5.45	6.25
	AP/PA	2.14	1.75	0.09	0.013	2.35	0.63
Axilla (armpit) left	VMAT	2.14	1.77	0.04	0.005	4.85	5.45
	AP/PA	2.14	1.77	0.07	0.0	0.51	0.68
Kidney right	VMAT	1.39	1.21	0.014	0.007	0.14	0.06
	AP/PA	1.39	1.21	0.012	0.0	0.20	0.09
Kidney left	VMAT	1.4	1.21	0.012	0.011	0.11	0.07
	AP/PA	1.4	1.21	0.01	0.0	0.21	0.24
Liver	VMAT	12.59	7.82	0.01	0.06	11.92	12.21
	AP/PA	12.59	7.82	0.02	0.23	14.21	15.65
Intestine	VMAT	1.46	0.68	0.002	0.01	0.04	0.034
	AP/PA	1.46	0.68	0.0	0.07	0.16	0.015
Stomach	VMAT	6.8	4.9	0.014	0.05	0.46	0.69
	AP/PA	6.8	4.9	0.02	0.06	0.76	1.5

Abbreviations: D_{min} and D_{max}, minimal and maximal doses; NIRV, non-irradiated volume; PTV, planning target volume; VMAT, volumetric-modulated arc therapy; AP/PA, anterior-posterior/posterior-anterior beams.

Table A6

The DICOM data list of the rat CT. The original file IDs are listed. SOMATOM Force data were saved on the server of the Department of Clinical Radiology and Nuclear Medicine, Medical Faculty Mannheim of Heidelberg University) and on WD Server (4 TB) #WCC4E2NJO3Y6 (WD® NL B. V. Hoofddorp, the Netherlands) under project number G184-14 (Department of Radiation Oncology of the University Medical Center Mannheim of Heidelberg University).

#91m_VMAT15_1FCTn_17.02.2016	-
#65m_VMAT15_1FCTn_23.12.2015,	#65m_VMAT15_2FCTc_06.04.2016
#51m_VMAT15_1FCTn_08.01.2016,	#51m_VMAT15_FCTc_fin_20.06.2016
#46´´m_VMAT15_1FCTn_08.01.2016	-
#15´L0R2f_VMAT15_1FCTn_17.12.2015,	#15'L0R2.f_VMAT15 fin.-FCTc_04.05.2016
#28´´f_VMAT15_1FCTn_11.03.2016	#28´´f_VMAT15_FCTc_fin_25.5.16
#26´´f_VMAT15_1FCTn_17.02.2016	-
#85f_VMAT15_2FCTn_29.01.2016	#85f_VMAT15_1FCTn_01.03.2016
#88f_VMAT15_1FCTn_29.01.2016	#88´´f_VMAT15_FCTc-fin_08.06.2016
#50´´m_APPA15_1FCTn_08.01.2016	#50´´m_APPA15_2FCTn_23.03.2016
#41´´m_APPA15_1FCTn_05.01.2016	#41´´m_APPA15c_8.4.2016
#43´´m_APPA15_finFCTn_29.12.2016	-
#43´´´m_VMAT24_1FCT_19.4.2016	#43´´´m_VMAT24_2-finFCT_12.6.16
#95f_APPA15_1FCTn_29.01.2016	#95f_APPA15-160 fin. fCTc2´_08.06.16
#33´´f_APPA15_1FCTn_11.03.2016	#33´´m_APPA24_2FCTn.19.8.16
	#33´´f_APPA15_finFCTc_25.8.16
#10f_APPA15_2XFCT_14.12.15	-
#64f_VMAT24_1FCTn_20.4.2016	#64f_VMAT24_2FCTc_fin_09.05.2016
#86´´f_VMAT24_22.4.2016	-
#22´´m_APPA24_1FCTn_19.02.2016	-
#93´´m_APPA24_1FCTc_06.04.2016	#99´´m_APPA24_1FCTn_06.04.2016
#24"m_APPA24_1FCTn_23.03.2016	#24´´m_APPA24_2finFCTc_27.05.2016
#82´´f_APPA24_22.4.2016	#82´´f_APPA24_finFCTc_20.06.2016
#58´´f_APPA24_1finFCTc_29.03.2016	-
#52´´f_APPA24_20.4.2016	#52f_APPA24_finFCTc_25.08.2016_2Recons
#60´´f_APPA24_1FCTn_20.4.2016	-
#81´´f_APPA24_1FCTn_22.4.2016	#81´´f_APPA24_finFCT_13.06.2016
#44´´f_APPA24_1FCTn_13.4.2016	#44´´f_APPA24_2finFCTc_20.07.2016
#38´´m_VMAT15_1FCTn_08.01.2016	#38m_VMAT15_2-2XfinFCTc_28.4.2016
#48m_VMAT15_1FCTn_26.11.2015	-
#20´L0R3m_VMAT15_1FCTn_22.12.2015	-
#71(91)f_VMAT15_1FCTn_23.12.2015	#71(91)f_APPA15_28.4.2016
#9f_VMAT15_1FCTn_17.12.2015	#9f_VMAT15_2FCTc_fin_29.03.2016
#39´´m_APPA15_1FCTn_05.01.2016	-
#16´L2R1m (19)-APPA15_22.12.15	#16´L2R1m_APPA15_1FCTn_02.02.2016
#63m_APPA15_1FCTn_23.12.2015	#63m_APPA15_2FCTc_08.04.2016
#69f_APPA15_1FCTn_23.12.2015	#69f_APPA15_FCTc_15.06.2016
#18f_APPA15_1FCTn_16.02.2016	-
#89´´f_APPA15_1FCTn_29.01.2016	#89´´f_APPA15_2FCTc_25.05.2016
#47´´f_VMAT24_1FCTn_13.04.2016	#47´´f_VMAT24_2FCTc_25.05.2016

#37´´m_VMAT24_19.04.2016	#37´´m_VMAT24_2FCTn_19.8.16, #37´´m_VMAT24_3finFCTc_25.08.2016 /2Recon
#98´´m_VMAT24_19.04.2016	#98m_VMAT24_fin-2XFCTc_15.07.2016
#31´´m_VMAT24_19.4.2016	#31´´m_VMAT24_FCTc2-fin_03.08.2016
#42´´´m_VMAT24_2 X fin. FCTn_19.8.16	-
#6´´f_VMAT15-1FCTn_24_20.04.16	#6´´f_VMAT24_19.8.16_2Recons
#54´´f_VMAT24_20.04.2016	-
#90´´f_VMAT24_22.04.2016	#90f_VMAT24_FCTc-fin_20.06.2016
#56´´f_VMAT24_1FCTn_20.4.2016	#56´´f_VMAT24_2FCTc_25.05.2016
#33´´´m APPA24_fCTc.fin. 25.8.16	-
#32´´m_APPA24_FCTc_09.05.16	-
#36"m_APPA24_1FCTn_23.03.2016	-
#75m_CBCT_1FCTn_05.01.2016	#75m_CBCT_16.9.16_2Recon
#42´´m_CBCT_1finFCTc_T0_27.05.2016	-
#21´´f _CBCT_1FCTn_11.03.2016	#21´´f_CBCT_2FCTc_fin_29.03.2016,
#21´L3R1m _CBCT_1FCTn_22.12.2015	-
#3m_CBCT_1FCTc_I-300_14.03.2016	-
#59m_CBCT_1FCTn_2X_23.12.2015	-
#19´m_CTRL_1FCTn_16.02.2016	-
#34´´f_CBCT_1FCTn_11.03.2016	-
#87f_CBCT_1FCTn_29.01.2016	#87f_CBCT_19. 04.2016
#96f_CBCT_1FCTn_11.03.2016	#96f_CBCT_FCT2n_fin_20.07.2016
#92f_CBCT_1FCTn_29.01.2016	-
#12´R1L0f_CBCT_1FCTn_17.12.2015	#12'R1L0f_CBCT_2FCTn_09.02.2015
#7f_CBCT_1FCTn_17.12.15	#7f_CBCT_1FCTn_13.04.16
#30´´f_CBCT_1FCTn_11.03.2016	-
#11m_CTRL_1FCTn_08.01.2016	#11m_CTRL_2FCTc-I300,0,6ml_14.03.2016
#35´´m_CTRL_1FCTn_08.01.2016	#35´´m_CTRL_2, finFCTn_15.7.16
#57m_CTRL_1FCTn_23.12.2015	#57m_CTRL_2FCTc_06.04.2016
#13´m _CTRL_1FCTn_29.12.2015	#13´m_CTRL_2FCTn_06.04.2016
#62m_CTRL_1FCTn_28.12.2015	-
#27´´m_CTRL_1fCTn_14.03.16	#27´´m_CTRL_1fCTn_4.4.16
#40´´m_CTRL_1FCTn_14.03.2016	#40"m_CTRL_2FCTn_23.03.2016
#8f_CTRL_1FCTn_17.12.2015	#8f_CTRL_2FCTn_01.03.2016
#4´´f_CTRL_1FCTn_14.03.2016	#4f_CTRL_10.10.16_2 recons
#94f_CTRL_1FCTn_14.03.2016	#94f_CTRL_2FCT_16.9.16
#1´´f_CTRL_1FCTn_14.03.2016	-
#20f_CTRL(CBCT)_2FCTc_15.06.2016	-
#53´´f_VMAT24_20.4.2016	-
#45´´f_VMAT24_13.4.2016	-
#83f_CTRL_1FCTn_29.12.2015	-

Abbreviations: rat identity and sex (e. g. #1´´f, number 1´´ female); m, male; VMAT, volumetric-modulated arc therapy; AP/PA, anterior-posterior/posterior-anterior; CBCT, cone-beam CT; CTRL corresponds to AN control group; 1FCT, first ‘Force CT’; fin, final; n, native; c contrast media; date of scanning (date, month, year).

Table A7

Rat data 3. (**A**) Rat identity and sex. (**B**) The organs affected by index tumors and additional tumors (asterisks represented). (**C** – **J**) Tumor entities (C, bone sarcoma; D, soft tissue sarcoma; E, lymphoma; F, malignant mesothelioma; G, carcinoma; H, breast cancer; I, brain tumor; and J, non-determined tumor). (**K**) Loss of *Tp53*$^{+/C273X}$ heterozygosity (LOH). (**L**) Ratio of the A/T peaks on the sequencing chromatogram (LOH determined by ≥ 2 times difference between A and T peaks). (**M**) Inflammation in tumor free lungs (graded by 0, none; 1, rare; 2, moderate; and 3, frequent).

A	B	C	D	E	F	G	H	I	J	K	L	M
91m	Mediastinum to both lungs			1						–	–	
65m	Mediastinum/spine*	1*		1						LOH	>2	
5m	Spine to lungs	1								–	–	
51"m	Mediastinum				1					C273X	0,3	
46"m	Mediastinum/chest wall right*	1*		1						–	–	
15'f	Mediastinum/spine*	1*	1							LOH	>2	
28"f	Mediastinum, lung, chest wall					1				C273X	1	
26"f	Mediastinum		1							–	–	
85f	Chest wall left (rib)	1								–	–	
88f	Chest wall left (rib)	1								C273X	0,3	
14'f	Mediastinum		1							–	–	
50"m	Mediastinum			1						–	–	
41"m	Mediastinum			1						C273X	1	
43"m	Thymus and mediastinum			1						–	–	
95f	Mediastinum/spine*	1*		1						C273X	0,3	
33"f	Bronchus, lung right					1				–	–	
10f	Axilla right		1							LOH	5	
43´´´m	Mediastinum/lungs*			1		1*				LOH	3	
29´´m	Mediastinum (esophagus)		1							–	–	
64"f	Mediastinum, mesothelia				1					LOH	5	
86"f	Mediastinum			1						–	–	
22´´m	Mediastinum (thymus)			1						–	–	
27´´´m	Mediastinum			1						–	–	
93"m	Mediastinum/lung right*		1	1*						LOH	2,5	
99"m	Sternum, lungs	1								LOH	> 6	
24´´m	Spine to lungs	1								–	–	
82"f	Mediastinum			1						C273X	2	
58"f	Esophagus		1							C273X	0,3	
52´´f	Esophagus		1							–	–	
60"f	Mediastinum					1				LOH	2	
81´´f	Thorax, liver (fs)		1							LOH	5	
44´´f	Back muscles		1							LOH	3	
79f	Back muscles		1								–	

38"m	Dorsal muscle left		1							LOH	>10	
48"m	Abdomen								1		−	0
20'm	Pelvic region, bowel								1		−	
71f	Adrenal region right, kidney								1	C273X	0,2	1
9f	Abdomen, pelvis								1	C273X	0,2	2
39"f	Pelvic region								1		−	
16'm	Pelvic region, prostate, bladder					1					−	0
63m	Femur/scapula bones* right (l. m.)	1								LOH	2,5	
69f	Humerus bone right	1									−	0
23"f	Pelvis soft tissue					1				LOH	7	0
18f	lumbar spine bones	1									−	1
89f	Tailbone	1									−	
47´´f	Skull bone	1									−	1
37´´m	Tailbone and soft tissue (l. m.)					1					−	1
98"m	Pelvic region								1	C273X	0,3	2
31´´m	Femur bone left/prostate*	1				1*					−	1
42´´´m	Femur bone left (l. m.), lungs	1				1*				C273X	0,3	0
6´´f	Hind-limb bone, left	1									−	2
54"f	Brain							1			−	1
90"f	Adrenal region right								1	C273X	1,6	1
56"f	Mammae, inguinal						1			C273X	0,2	2
33´´´m	Pelvic region and testes								1	C273X	0,3	0
32´´m	Pelvic region, prostate					1				C273X	0,3	2
36´´m	Hind limb bone (femur), left	1								LOH	2	1
49"m	Dorsal spine, muscles	1									−	2
75m	Overarm bone right	1									−	2
42"m	Bladder, pelvis					1				C273X	-0,3	1
21'm	Femur, right	1								LOH	4	
3´ m	Hind-limb bone, left, (l. m.)	1								LOH	4	0
59m	Hind-limb bone, left	1								LOH	3	
19f	Tongue		1								−	1
34"f	Mandible, bone	1									−	2
87f	Brain							1			−	2
96f	Shoulder right, spine	1									−	2
92f	Pelvic region								1		−	0
12'f	Oviduct right								1	LOH	3	0
7f	Sacral bone, spine (l. m.)	1								LOH	>10	
30"f	Sacrum bone	1									−	2
11m	Jaw, right	1								LOH	3	2
35"m	Skull bone, pelvis*	1				1*					−	1
57m	Scapula, left	1								LOH	>10	2
13m	Abdomen, chest wall, left								1		−	
62m	Intestine, pelvis								1		−	1

27"m	Pelvis, bowel								1		−	3
40"m	Abdomen, pelvis*				1*	1					−	3
8f	Brain							1			−	1
2"f	Skull bone	1									−	1
4"f	Mammae, inguinal left						1				−	1
94f	Mammae, both inguinal areas						1			C273X	0,4	
1"f	Uterus, oviduct, left					1				LOH	>2	0
20f	Abdomen/pancreas*				1*	1				C273X	1	0

Abbreviations: rat identity and sex (e. g. #1´´f, number 1´´ female), m, male; C273X, heterozygous loss of cysteine 273 coding triplet; LOH, loss of heterozygosity; l. m., lung metastasis.

Table A8

Additional tumors.

Additional tumors	Index tumor	Volume	Treatment
BSA	STSA	BHDV-HDV	VMAT 3×5 Gy
BSA	LY	LDV	VMAT 3×5 Gy
BSA	LY	LDV	VMAT 3×5 Gy
BSA	LY	BHDV	AP/PA 3×5 Gy
LY	STSA	LDV-HDV	AP/PA 3×8 Gy
CA	STSA	BHDV	VMAT 3×8 Gy
CA	BSA	NIRV	VMAT 3×8 Gy
CA	BSA	NIRV	VMAT 3×8 Gy
CA	BSA	NIRV	AN 0 Gy
MM	CA	NIRV	AN 0 Gy
MM	CA	NIRV	AN 0 Gy

Abbreviations: BSA, bone sarcoma; LY, lymphoma; CA, carcinoma; MM, malignant mesothelioma; STSA, soft tissue sarcoma; HDV, high-dose volume; BHDV, bordering high-dose volume; HDV, high-dose volume; VMAT, volumetric-modulated arc therapy; AP/PA, anterior-posterior/posterior-anterior beams; AN, anesthesia controls; Gy, Gray; 3×5 Gy or 3×8 Gy, three fractions of 5 or 8 Gy.

Figure A1

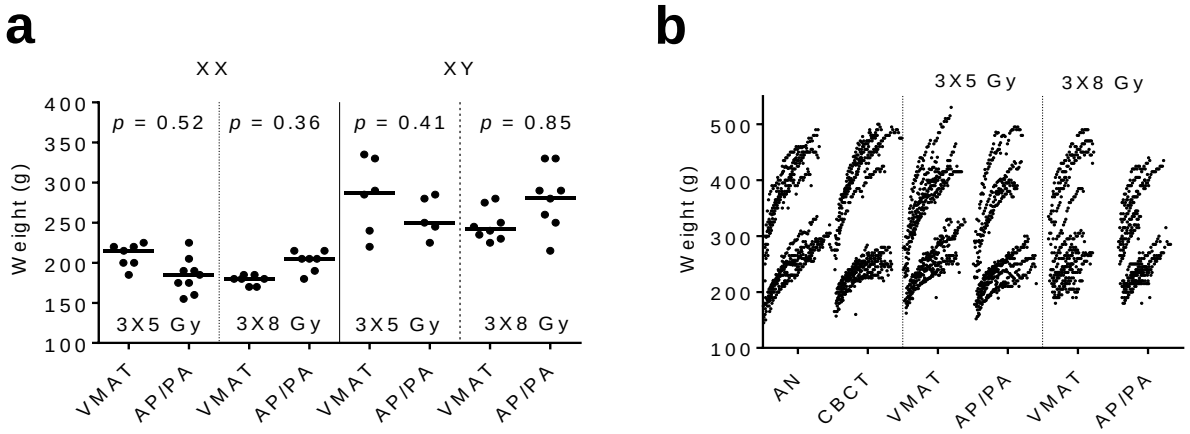

Treatment body size and growth of rats. (**a**) The weight at the treatment of female and male rats was balanced between rats recruiting to VMAT or AP/PA groups (lines indicate the medians). (**b**) No notable difference in growth pattern between groups detected. Each dot represents the weight at every week of life. The lower and upper trails represent females or males respectively. The weight at treatment, weight increments and growth rates are given in Table A1, columns C – F.

Abbreviations: see Figure A2 below.

Figure A2

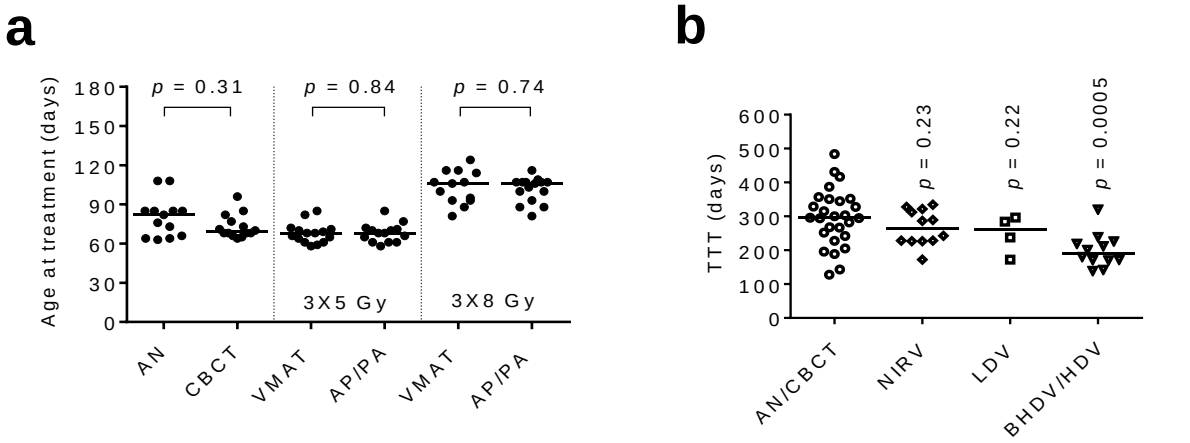

Age at treatment and time to tumor. (**a**) The age at treatment was balanced between rats treated with VMAT and AP/PA, while most 3×8 Gy rats were by median 37.5 days older than rats from other groups (**Table A1**, **column G**). (**b**) Although the TTT in 3 × 8 Gy groups was simulative extended by 37.5 days, it remains significantly decreased for BHDV/HDV tumors. Mann-Whitney test. lines indicate the medians (see also **Table M2**).

Abbreviations: AN, anesthesia only controls; CBCT, cone-beam computed tomography only controls; VMAT, volumetric-modulated arc therapy; AP/PA, anterior-posterior/posterior-anterior beams; Gy, Gray; TTT, time to tumor; NIRV, non-irradiated volume; LDV, low-dose volume; BHDV, bordering high-dose volume; HDV, high dose volume; 3×5 Gy or 3×8 Gy, three fractions of 5 or 8 Gy.

9 CURRICULUM VITAE

PERSONAL DETAILS

Name and first name:	Gomarteli Kaga
Date of birth:	April 24, 1968
Place of birth:	Tiflis, Georgia (‘Tbilisi, Saqartvelo’)
Family status:	Married, three children

ACADEMIC BACKGROUND

1990 – 1997	Biologist (Diploma) Human and animal physiology (major), general biology Faculty of biology Tbilisi State University (TSU) Ilia Tchavtchavadze 1, 0179 Tbilisi, Georgia
2008 – 2012	Dipl.-Biol. (‘Diplom-Biologe’) Cell biology (major), molecular biology, zoology Faculty of chemistry and biosciences Karlsruhe Institute of Technology (KIT) Kaiserstrasse 12, 76131 Karlsruhe, Germany
2015 – 2020	Dr. sc. hum. (‘Doctor scientiarum humanarum’) Radiation therapy (major), cell biology, medical physics Department of radiotherapy and radiation oncology Medical Faculty Mannheim Ruprecht Karl University of Heidelberg Theodor-Kutzer-Ufer 1-3, 68167 Mannheim, Germany

10 ACKNOWLEDGMENTS

My greatest gratitude goes to Prof. Dr. Frederik Wenz and Prof. Dr. Frank Giordano for providing me the opportunity to work on this interesting project, and their guidance, support, and encouragement throughout all the stages of my doctoral research.

I am very grateful to, Dr. Carsten Herskind for supporting me and making accessible the use of all the facilities and equipment in the respective departments whenever it was needed and for scientific support.

My special thank goes to Dr. Jens Fleckenstein for the excellent guidance in planning and carrying out x-ray treatments.

Many Thanks to Dr. Stefanie Kirschner and Dr. Bettina Kraenzlin for their veterinary medicine and animal care support.

I like to express my special thanks to Prof. Dr. Gerhard Glatting for his help in modeling of the study.

My great thank goes to our technical staff members Miriam Bierbaum, Adriana Grbenicek, Victoria Scude, and Petra Prochazka.

I thank the colleagues, Dr. Christian Hoerner, Prof. Dr. Thomas Henzler, Dr. Mathias Meyer, Prof. Dr. Patrick Maier, Prof. Dr. Marlon Veldwijk, Dr. Linda Hartmann, Vladimir Bobu, Barbara Link, and all other participated colleagues and students for the stimulating discussions and for all the interesting time and work we have had together.

And finally, I would like to thank all my family members and friends for being so inspiring over the years.